Mineralogical Magazine, August 2014, Vol. 78(4), pp. 957–1027

The structure hierarchy hypothesis

F. C. HAWTHORNE*

Department of Geological Sciences, University of Manitoba, Winnipeg, MB, R3T 2N2, Canada

[*Received 27 January 2014; Accepted 25 March 2014; Associate Editor: E. Grew*]

ABSTRACT

The structure hierarchy hypothesis states that structures may be ordered hierarchically according to the polymerization of coordination polyhedra of higher bond valence. A mathematical hierarchy is an ordered set of elements where the ordering reflects a natural hierarchical relation between (or arrangement of) the elements. Here, I review the structure hierarchies for the borate, uranyl oxide, phosphate, sulfate, beryllate and oxide-centred Cu, Pb and Hg minerals (plus synthetics where appropriate). Structure hierarchies have two functions: (1) they serve to organize our knowledge of minerals (crystal structures) in a coherent manner; (2) if the basis of the classification involves factors that are related to the mechanistic details of the stability and behaviour of minerals, then the physical, chemical and paragenetic characteristics of minerals should arise as natural consequences of their crystal structures and the interaction of those structures with the environment in which they occur. We may justify the structure hierarchy hypothesis by considering a hypothetical structure-building process whereby higher bond-valence polyhedra polymerize to form the structural unit. The clusters constituting the FBBs (fundamental building blocks) may polymerize to form the following types of structural unit: (1) isolated polyhedra; (2) clusters; (3) chains and ribbons; (4) sheets; and (5) frameworks. The major advantage of this approach to structure hierarchy is the fact that the hypothetical structure-building process outlined above resembles (our ideas of) crystallization from an aqueous solution, whereby complexes in aqueous and hydrothermal solutions condense to form crystal structures, or fragments of linked polyhedra in a magma condense to form a crystal. Although our knowledge of these processes is rather vague from a mechanistic perspective, the foundations of the structure hypothesis give us a framework within which to think about the processes of crystallization and dissolution.

KEYWORDS: Structure hierarchy, crystal structure, sulfates, phosphates, borates, uranyl minerals, beryllates, oxo-centred structures.

Introduction

THE term 'structure hierarchy' has been in use for many years, but has tended to be used intuitively, without any explicit definition or relation to more formal mathematical definitions of hierarchy. This situation has been adequate in the initial stages of the development of hierarchical classifications of minerals as all the factors on which such a classification should be based are not necessarily obvious. However, as outlined below, there has been extensive work on the hierarchical classification of many groups of minerals (here, I use the word 'group' in its colloquial sense) and we now have a good idea of the principal factors that should be involved in such classifications. Hence it now seems an appropriate time to begin consolidating our ideas on structural hierarchy. Here, I will: (1) formalize the idea of structural hierarchy; (2) review several groups of minerals that have been so organized; (3) show how such hierarchies provide a basis for understanding the factors affecting the chemical composition and bond topology of minerals, and provide insight into mechanisms of crystallization.

* E-mail: frank_hawthorne@umanitoba.ca
DOI: 10.1180/minmag.2014.078.4.13

Hierarchies

A mathematical hierarchy is an ordered set of elements in which the ordering reflects a natural hierarchical relation between (or arrangement of) the elements of the set. A partially ordered set (a 'poset') is a set in which, for a pair of elements, one element precedes the other according to some criterion that compares the two elements. Each element is associated with some property; elements with the same property are grouped together (and are often called a class). It is common that such classes (of elements with equivalent properties) are organized in terms of increasing complexity, hence the term 'hierarchy'. Of particular importance in natural objects is the idea of an 'inclusion hierarchy' (or 'nested hierarchy'). Here, at any level in the hierarchy, each element has a parent set above it in the hierarchy. We may illustrate this idea using the polygon hierarchy of Fig. 1*a*. The triangle and the quadrilateral are both polygons and belong to the set of all polygons. We may identify three types of triangles: equilateral triangles, isosceles triangles and scalene triangles, each of which belongs to the set of all triangles. Similarly we may identify various forms of quadrilateral: parallelogram, kite, isosceles trapezoid, trapezoid and trapezium (other more specialized forms are omitted). The square, rectangle, rhombus and rhomboid are various forms of parallelogram. Figure 1*b* indicates how sulfate structures involving octahedrally and tetrahedrally coordinated cations may fit into an inclusion hierarchy in which all sets at one level belong to various (parent) sets at a higher level in the hierarchy (for simplicity, not all observed linkages in sulfate structures are shown here). Inspection of Fig. 1 suggests that an inclusion hierarchy is appropriate for hierarchical classification of mineral structures.

Structural hierarchies

We will define a structure hierarchy as 'a classification of atomic arrangements arranged (ranked) according to their principal constituent cation-polyhedra and the connectivity of those polyhedra'. Later on, we will consider what are suitable 'principal cation-polyhedra'. Ideally, all minerals should be included in a comprehensive structural hierarchy, as Earth processes may involve a wide variety of chemically and structurally different minerals, and it is our eventual intent to arrange mineral hierarchies such that they help in the interpretation of geological processes. Although this final aim is something to keep in mind, at the present state of development, we are focusing on chemically specific groups of minerals (e.g. sulfates, borates, uranyl oxides) and attempting to put in place effective structural hierarchies for these groups. These structure hierarchies have two functions: (1) they serve to organize our knowledge of

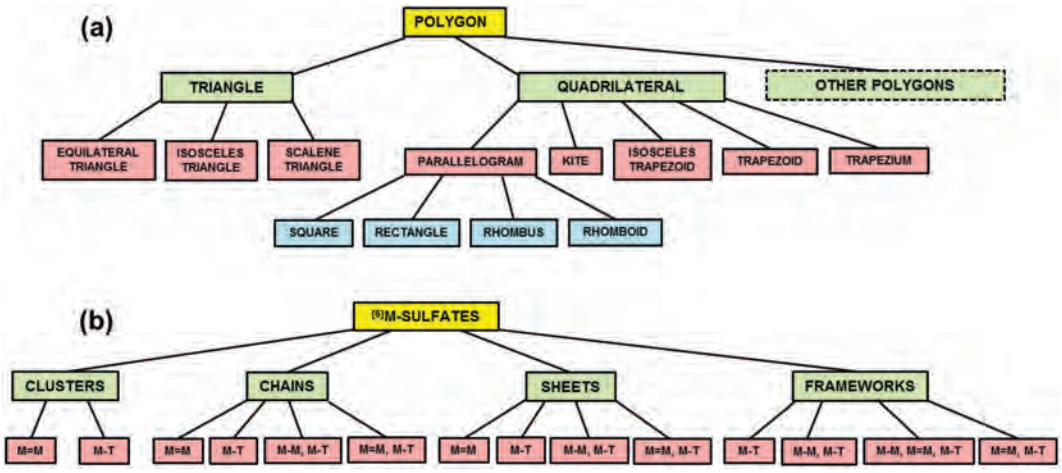

FIG. 1. (*a*) Partial inclusion hierarchy for polygons, focusing on triangles and quadrilaterals; (*b*) partial inclusion hierarchy for sulfate minerals containing octahedrally coordinated cations $^{[6]}$M. Colours indicate equal levels in the hierarchy, lines indicate which sets are included in higher-level sets within the hierarchy.

minerals (crystal structures) in a coherent manner; (2) if the basis of the classification involves factors that are related to the mechanistic details of the stability and behaviour of minerals, then the physical, chemical and paragenetic characteristics of minerals should arise as natural consequences of their crystal structures and the interaction of those structures with the environment in which they occur. Thus adequate structure hierarchies should provide an epistemological basis for understanding the role of minerals in Earth processes (Hawthorne, 1985*a*).

Historical background

Although the first crystal structure was solved in 1913 (Bragg, 1913), confirming the predictions of Barlow (1883, 1898), it wasn't until the late 1920s that the structures of most of the common rock-forming minerals were known. The silicate minerals were of particular interest, both because of their importance in large-scale Earth processes and because of the polymerization of their constituent silicate and aluminosilicate groups. In his seminal work, Bowen (1928) proposed his 'reaction series' which describes the sequence in which silicate minerals crystallize from a parent basaltic liquid: olivine → pyroxene → amphibole → mica → feldspar → quartz. Contemporaneously, Matchatski (1928) proposed classifying the major silicate minerals according to the types of linkage of their constituent silicate and aluminosilicate groups. Bragg (1930) extended this idea to produce the still-familiar neso (ortho-), soro- (pyro-), cyclo- (ring-), ino- (chain-), phyllo- (sheet-), tecto- (framework) silicate classification that we still teach today, and also reviewed the importance of Pauling's rules (Pauling, 1929) with regard to atomic arrangements in silicate minerals. As the number of known mineral structures (particularly silicates) increased, it became apparent that the character of the linkage between the silicate unit and the larger cations depends on the properties of the latter, and Belov (1961) introduced the 'Second Chapter' of silicate crystal chemistry that organizes silicates of large alkali and alkaline-earth cations (e.g. Ca, Ba, Sr). Zoltai (1960) included other tetrahedrally coordinated oxyanions into the Bragg classification, incorporating beryllosilicates and borosilicates and focusing attention on the factors that affect the relative linkage of silicate, beryllate and borate groups in extended polymerizations. Voronkov *et al.* (1973, 1974, 1975) and Sandomirskii and Belov (1984) examined extensively the linkage between different coordination polyhedra in a wide variety of minerals in terms of 'mixed frameworks'. Several other classification criteria for silicate minerals, based on the topological and geometrical characteristics of the silicate and aluminosilicate linkages, were introduced by Liebau (1985).

In terms of hierarchical classification, silicate and aluminosilicate minerals tended to dominate the early and middle parts of the 20th century, presumably because dealing with the polymerization of a single type of polyhedron is simpler than dealing with polymerization of different types of polyhedra. The first non-silicate group of minerals to be classified extensively from a structural perspective was the borates. In borate minerals, B may occur as (Bφ_3) and (Bφ_4) groups ($\varphi = O^{2-}$, OH), and polymerization of these two types of polyhedron is extensive. Edwards and Ross (1960), Ross and Edwards (1967), Christ (1960), Tennyson (1963) and Heller (1970) developed classifications based on the polymerization of these two different types of polyhedra to form a hierarchy of clusters, chains, sheets and frameworks of triangular and tetrahedral borate groups.

For one-dimensional linkages of polyhedra, the terms 'chain' and 'ribbon' are in common use. Generally, the term 'chain' is used for a one-dimensional unit that is narrow in all directions orthogonal to the length of the chain, and the term 'ribbon' is used where the dimensions of the unit orthogonal to the chain are significantly different in different directions. If we are to use specific terms, definitions are desirable. Here, I will define a 'chain' as a one-dimensional linkage of polyhedra that can be broken by deletion/removal of one polyhedron from the linkage (e.g. a pyroxene chain), and a 'ribbon' as a one-dimensional linkage of polyhedra that cannot be broken by deletion/removal of one polyhedron from the linkage (e.g. an amphibole ribbon).

Constraints on the linkage of oxyanions in minerals

The valence-sum rule of bond-valence theory states that the sum of the bond valences at each atom is equal to the magnitude of the atomic valence (Brown, 2002, 2009; Hawthorne, 1994, 2012*a*). This rule exerts considerable constraints on the self-linkage of oxyanions in crystal structures. Consider first the linkage of the

principal oxyanions in silicate and aluminosilicate minerals. As indicated in Fig. 2*a*, where two $(SiO_4)^{4-}$ groups link together, the sum of the incident bond-valences at the linking anion is 2.00 valence units (vu) and hence this linkage is allowed by the valence-sum rule. Where one $(SiO_4)^{4-}$ group and one $(AlO_4)^{5-}$ group link together (Fig. 2*b*), the sum of the incident bond valences at the linking anion is 1.75 vu and this linking anion can accept bonds from other low-valence cations to accord with the valence-sum rule. Consider one $(SiO_4)^{4-}$ and one $(BeO_4)^{6-}$ group (Fig. 2*c*); the sum of the incident bond valences at the linking anion is 1.50 vu, the linking anion can accept bonds from other cations and hence this linkage is allowed by the valence-sum rule.

Next, consider $(CO_3)^{2-}$ groups, $(PO_4)^{3-}$ and $(SO_4)^{2-}$ groups (Fig. 2*d*,*e*,*f*); if these groups were to self-polymerize, the incident bond-valence sums at the linking anions would be 2.67, 2.50 and 3.00 vu, respectively. These linkages are thus forbidden by the valence-sum rule and these oxyanions do not self-polymerize in minerals (with one or two exceptions that form in unusual environments). This is not the case in synthetic compounds, and polyphosphates for example (Corbridge, 1985) are common. In uranyl structures, the uranyl ion and its associated anions form square-, pentagonal- and hexagonal-bipyramids in which the *trans* uranyl bonds have bond valences of ~1.7 vu and the equatorial bonds are ~$(6-2\times1.7)$ / n, where n = 4, 5 and 6: 0.65, 0.52 and 0.43 vu, respectively. Thus, uranyl polyhedra cannot form strong bonds through their uranyl–O anions, but can form strong bonds with all oxyanions and other uranyl polyhedra through their equatorial anions.

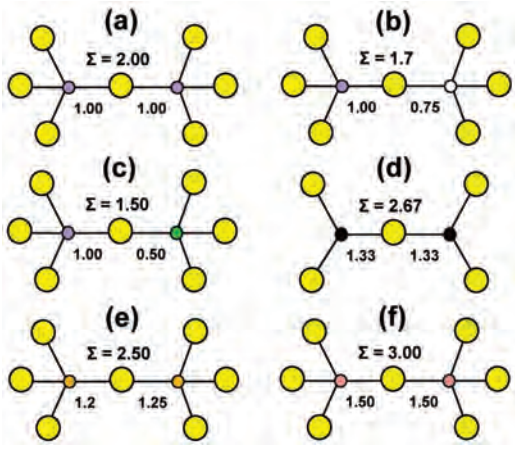

FIG. 2. Linkage of polyhedra and bond valences; (*a*) silicate; (*b*) aluminosilicate; (*c*) beryllosilicate; (*d*) carbonate; (*e*) phosphate; (*f*) sulfate; Si = mauve, Al = white, Be = green, C = black, P = orange, S = salmon pink.

In minerals where the principal oxyanion does not polymerize (or polymerization is rare) (e.g. sulfates, arsenates), classification based on polymerization of the principal oxyanion alone does not work and hierarchical classifications in these groups have been slower to arise. Moore (1973) proposed classifying phosphate minerals according to the polymerization of their constituent divalent-metal octahedra. Furthermore, he showed a relation between paragenesis and structural arrangement in pegmatite phosphate minerals that parallels the relation between Bragg's classification of the common rock-forming silicate minerals and Bowen's reaction series. This correlation between polymerization and paragenesis in two completely different mineral groups (silicates and phosphates) emphasizes the fundamental nature of dimensional polymerization and emphasizes its importance as an appropriate way to organize mineral structures. The problem with proceeding in this way for other groups of minerals based on isolated oxyanion groups [e.g. $(AsO_4)^{3-}$, $(SO_4)^{2-}$] is the fact that the approach of focusing on octahedrally coordinated cations ignores the presence of the principal oxyanion which will, in turn, affect the linkage of octahedra differently according to net charge and size, and this seems to have been a major factor in inhibiting the development of hierarchical classifications for other mineral groups until relatively recently.

Binary structural representation

For many years, many crystal structures of minerals have been illustrated by representing the cation-coordination polyhedra involving strong chemical bonds as polyhedra and weak chemical bonds as lines, and visual recognition of these structures has focused on the part of the structure represented by cation-coordination polyhedra. Hawthorne (1983*a*) took advantage of this type of representation, proposing that the polymerization of these strongly bonded cation-coordination polyhedra be the basis for hierarchical classification. He introduced the idea of Binary Structural Representation: a crystal

structure is split into two components: (1) the 'structural unit', the strongly bonded component of the structure; and (2) the 'interstitial complex', an assemblage of (usually monovalent and divalent) cations, anions and neutral species that weakly bind the structural units together (Hawthorne, 1985*a*). Partitioning of a structure into the structural unit and the interstitial complex is done on the basis of the bond valences involved. Generally, bonds stronger than 0.30 vu belong to the structural unit and bonds weaker than 0.30 vu involve the constituents of the interstitial complex. The cut-off at 0.30 vu is somewhat flexible, depending on the details of a structure, but the value of 0.30 vu is generally applicable. As we consider the polyhedra on the basis of their bond valences, this approach can be applied to all minerals, irrespective of their chemical characteristics (e.g. Hawthorne 1985*a*, 1986, 1990, 1997). Of course, it may also be applied to minerals based on a single oxyanion, e.g. sulfates, phosphates. The division of a structure into its two basic components is illustrated in Fig. 3 for botryogen. We write the chemical formula of the mineral such as to (1) identify these two components and (2) carry as much information as convenient on aspects of the structure: $Mg_2(H_2O)_{10}[Fe_2^{3+}(SO_4)_4(H_2O)_2]_2$; the components of the structural unit are contained within the square brackets, the components of the interstitial complex are outside the square brackets, interstitial (H_2O) bonded directly to interstitial cations occurs before the structural unit, interstitial (H_2O) not bonded directly to interstitial cations (i.e. held in the structure by H bonding only, or occluded) occurs after the structural unit (there is none of this type of interstitial (H_2O) in botryogen).

The structure hierarchy hypothesis

Hawthorne (1983*a*) formally stated the "Structure Hierarchy Hypothesis" as follows: "Structures may be ordered hierarchically according to the polymerization of coordination polyhedra of higher bond-valence." We may consider a hypothetical structure-building process whereby higher bond-valence polyhedra polymerize to form homo- or heteropolyhedral clusters. These clusters may be considered as the 'fundamental building block' (FBB) of the structure (I'm not sure who was the first to use the term "FBB", but it has been in use for a long time). The FBB is repeated, often polymerized, by symmetry to form the structural unit (Hawthorne, 1985*a*). The clusters constituting the FBBs may polymerize to form the following types of structural unit: (1) isolated polyhedra; (2) clusters; (3) chains and ribbons; (4) sheets; and (5) frameworks, as pointed out by Matchatski (1928) and Bragg (1930) for silicates. Hawthorne (1979, 1983*a*, 1985*a*, 1986, 1990) originally referred to assemblages of FBBs linked by strong bonds as (structure) modules. A joint IUCr-IMA Commission (Lima de Faria *et al.*, 1990) required changing "structure module" to "structural unit" and this nomenclature has been adhered to by the author in later publications. However, the term "module" and its various derivatives has since come into fashion and is now in use again.

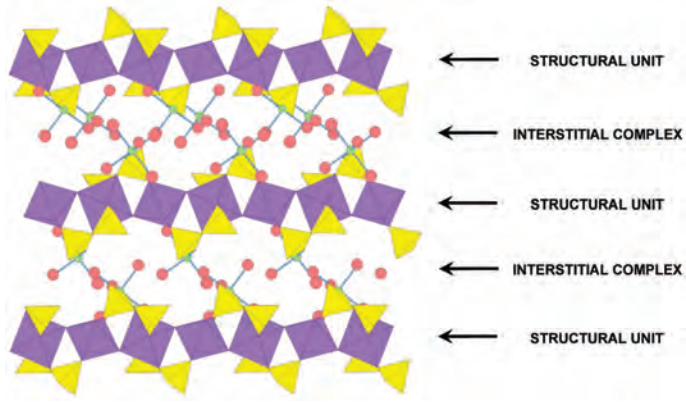

FIG. 3. The crystal structure of botryogen, $Mg_2(H_2O)_{10}[Fe_2^{3+}(SO_4)_4(H_2O)_2]_2$, partitioned into two units, the strongly bonded structural unit (shown as coloured polyhedra) and the weakly bonded interstitial complex (shown as individual atoms and chemical bonds); (SO_4) = yellow, ($Fe^{3+}\varphi_6$) = purple, Mg = green, (H_2O) = orange.

The major advantage of this approach to structure hierarchy is the fact that the hypothetical structure-building process outlined above resembles (our ideas of) crystallization from aqueous solution, whereby complexes in aqueous and hydrothermal solutions condense to form crystal structures, or fragments of linked polyhedra in a magma condense to form a crystal. Although our knowledge of these processes is rather vague from a mechanistic perspective, the foundations of the structure hypothesis give us a mechanism to think about processes of crystallization and dissolution. Note that this approach does not exclude hierarchies based on anion-coordination polyhedra; for example, Filatov *et al.* (1992), Krivovichev (2008) and Krivovichev *et al.* (1998*a*) have developed structural hierarchies based on anion-centred polyhedra, particularly those coordinated by stereoactive lone-pair cations such as Pb^{2+} and Bi^{3+}.

Justification of the structure hypothesis

The structure hypothesis combines the Machatski-Bragg idea of dimensional polymerization of the oxyanion of interest with the approach of Belov (1961) that emphasizes mixed-polyhedron structures. Hawthorne (1983*a*) rationalized the structure hypothesis in the following way. In a crystal structure (or a glass or fluid), the bond-valence requirements of the cations are met predominantly by the formation of coordination polyhedra of anions around those cations. We may thus think of the structure as an array of complex oxyanions that polymerize in order to satisfy the dominant part of their anion bond-valence requirements. In an array of coordination polyhedra, let the bond valences be s_o^i ($i = 1, n$) where $s_o^i > s_o^{i+1}$. According to the valence-sum rule, polymerization can occur where $s_o^1 + s_o^i < |V_{anion}|$ (where V_{anion} is the formal valence of the simple linking anion) and the valence-sum rule is most easily met where $s_o^1 + s_o^i = |V_{anion}|$. These bond-valence requirements can be met most expeditiously by those coordination polyhedra of higher bond valence, subject to the constraint $s_o^1 + s_o^i < |V_{anion}|$, as these linkages come closest to satisfying the valence-sum rule. This argument also suggests a mechanism for the crystallization of minerals, at least from aqueous and hydrothermal solutions, whereby crystallization proceeds by condensation of complex oxyanions in solution (Hawthorne, 1979, 1983*a*); see later section on the crystallization of borate minerals from aqueous solution.

The above justification may be generalized to account for a wider array of mineral structures than that covered by Hawthorne (1983*a*). The argument focuses on the formation of coordination polyhedra of anions around higher-valence cations. However, the specific identification of anions and cations here is not necessary: one may rephrase the argument to cover both the formation of coordination polyhedra of anions around higher-valence cations and the formation of coordination polyhedra of cations around anions. The modification allows natural incorporation of structures that contain higher-valence anions (i.e. O^{2-}, N^{3-}) not associated with an oxyanion. This allows incorporation of that group of structures that Krivovichev and Filatov (1999*a*,*b*) described as containing anion-centred tetrahedra. Moreover, the same mechanism for the crystallization of minerals seems likely, whereby crystallization proceeds by condensation of anion-centred tetrahedra from volcanic gases (Filatov *et al.*, 1992).

The topology of a bond network is the major feature controlling the energy of the structure through expression of the electronic-energy-density of states *via* the method of moments (Burdett *et al.*, 1984; Hawthorne, 1994, 2012*a*). The topology of a bond network is just another way of expressing the polymerization of the coordination polyhedra in a structure. Hence we may recognize an energetic basis for the hierarchical organization of structures according to the details of the polymerization of their principal coordination polyhedra.

Graphical representation of linkage between polyhedra

Many oxygen-based minerals have structures with complex anions involving polymerization of octahedra and tetrahedra. To analyse the connectivity of clusters of octahedra and tetrahedra, Hawthorne (1983*a*) considered clusters of polyhedra from a graph-theoretic perspective. A graph is a mathematical structure that is used to examine pairwise relations between discrete objects, and graph theory is a branch of mathematics that deals with the properties of graphs. Polyhedra are represented by coloured vertices of a labelled graph in which different colours represent different coordination. Linkage is denoted by the presence of an edge or edges between vertices representing linked polyhedra, and the number of edges between two vertices denotes the number of atoms common to both polyhedra. Thus for two

vertices, no edge denotes disconnected polyhedra (Fig. 4*a*), one edge denotes corner sharing between two polyhedra (Fig. 4*b*), two edges denote edge sharing between two polyhedra (Fig. 4*c*) and three edges denotes triangular-face sharing (Fig. 4*d*). In Fig. 4, different polyhedra are denoted by different coloured vertices, respectively. The cluster $[M_2(T\varphi_4)_2\varphi_8]$ and its graphical representation (Fig. 4*e*) shows (M = octahedrally coordinated cation; T = tetrahedrally coordinated cation; φ = unspecified ligand); round brackets and curly brackets denote a polyhedron or a group, e.g. (SO_4), (H_2O); square brackets denote linked polyhedra, e.g. $[M(TO_4)_2\varphi_4]$. Note that in a graphical representation, geometrical information is lost. This is illustrated in Fig. 4*f* which shows two different possible arrangements of the corner-linked cluster $[M(T\varphi_4)_2\varphi_4]$. Both these clusters are described by the same graph; such clusters are called geometrical isomers (Hawthorne, 1983*a*). Information on geometrical isomerism is lost in the graphical representation. It is very useful to represent the FBB (Fundamental Building Block) of a mineral in this graphical fashion as the hierarchical aspects of the classification are immediately grasped from the arrangement of the constituent graphs. This type of graphical representation is used quite commonly to consider the bond topology of complex structures (e.g. Hawthorne, 1983*a*, 1994; Hawthorne *et al.*, 2000; Krivovichev, 2008, 2009; Burns, 1995, 1999, 2005; Burns *et al.*, 1995*a*).

This approach suggests a simple way of both representing linkage of polyhedra in structures and of expressing structure hierarchies in a compact fashion. Let us represent an oxyanion as T and a higher-coordination polyhedra by M. Linkage between the polyhedra can be expressed by connecting the letters by dashes such that the number of dashes represents the numbers of vertices that the polyhedra have in common (Hawthorne, 1985*a*). Thus M M denotes isolated M polyhedra, M−M denotes corner-linked polyhedra, M=M denotes edge-linked polyhedra and M≡M denotes face-linked polyhedra; M T denotes isolated M polyhedra and T oxyanions, M−T denotes corner-linked M polyhedra and T oxyanions, M=T denotes edge-linked M polyhedra and T oxyanions and M≡T denotes face-linked M polyhedra and T oxyanions, etc. In this way, we may organize structural units within a

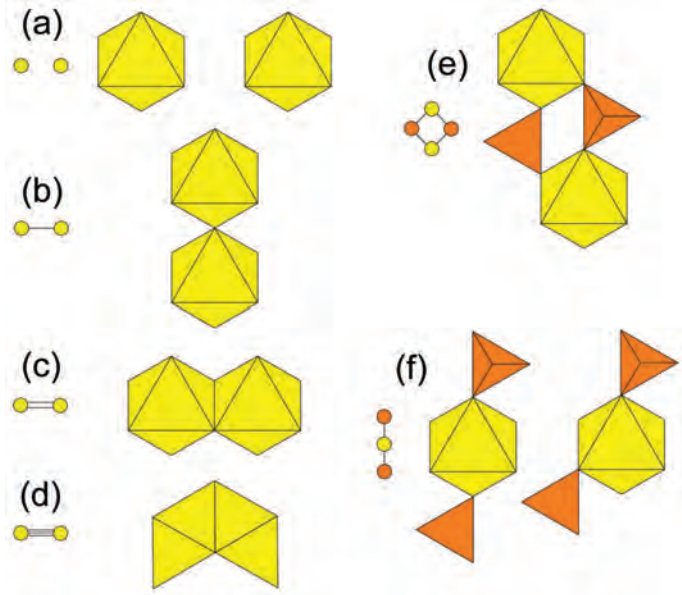

FIG. 4. Graphical representation of polyhedron clusters; octahedra are shown in yellow, M are octahedrally coordinated cations; tetrahedra are shown in orange, T are tetrahedrally coordinated cations. Each cluster of polyhedra is represented by a graph in which the yellow vertices represent octahedra, the orange vertices represent tetrahedra and the edges represent the number of vertices common to pairs of polyhedra: (*a*) $(M\varphi_6)_2$; (*b*) $[M_2\varphi_{11}]$; (*c*) $[M_2\varphi_{10}]$; (*d*) $[M_2\varphi_9]$; (*e*) $[M_2(TO_4)_2\varphi_8]$; (*f*) graphical isomers of $[M(TO_4)_2\varphi_4]$.

specific dimension of polymerization, e.g. within chains or within sheets, as done by Hawthorne *et al.* (2000) for sulfate minerals.

Application of the structure hierarchy hypothesis to specific groups of minerals

Hierarchical classifications have been developed for a range of oxysalt minerals: phosphates, arsenates and vanadates (Kostov and Breskovska, 1989), phosphates (Hawthorne, 1998; Huminicki and Hawthorne, 2002*a*), sulfates (Sabelli and Trosti-Ferroni, 1985; Hawthorne *et al.*, 2000), borates (Burns *et al.*, 1995*a*; Hawthorne *et al.*, 1996; Grice *et al.*, 1999). Hawthorne (1984) used the structure hierarchy hypothesis to classify the aluminofluoride minerals and examined the transition from aluminofluoride minerals to paragenetically related silicate minerals. Other classifications have spanned several traditional chemical groups of minerals. Lima-de-Faria (1978, 1983, 1994) and Hawthorne (1985*a*, 1986, 1990, 1997) have focused on linkage of different types of polyhedra without considering significantly the chemical identities of the principal cations involved. Burns (1999, 2005) and Burns *et al.* (1996) have developed a hierarchical classification for the uranyl oxysalts in which structural coherence is based on the unusual stereochemistry of the $(U^{6+}O_2)^{2+}$ uranyl group. Filatov *et al.* (1992), Krivovichev (2008), Krivovichev and Filatov (1999*a*,*b*) and Krivovichev *et al.* (1998*a*, 2013*b*) have developed a structural hierarchy for anion-centred polyhedra, often involving stereoactive lone-pair cations as coordinating ions.

Next I will briefly review the structure hierarchy developed for the borate minerals (Hawthorne *et al.*, 1996, Grice *et al.*, 1999). It is obviously not feasible to illustrate and discuss all borate minerals here; instead, I will describe a representative cross-section of these structures in order to give a flavour of the information contained in a structural hierarchy. Then I will discuss briefly how we can use this information to interpret the occurrence of minerals, and how we can use the structure hierarchy hypothesis as a basis for developing mechanistic approaches to crystallization and dissolution, and possibly other geochemical processes.

Borate minerals

B^{3+} commonly occurs in triangular and tetrahedral coordination to O (oxygen) and both ($B\varphi_3$) and ($B\varphi_4$) groups ($\varphi = O^{2-}$, OH) are common in borate minerals. The mean bond valences in these oxyanions are 3/3 = 1.00 vu for a ($B\varphi_3$) group and 3/4 = 0.75 vu for a ($B\varphi_4$) group. Consequently, linkage of borate polyhedra produces incident bond-valence sums at the linking anions of 0.75×2 to 1.0×2: 1.5–2.0 vu, and polymerization of borate polyhedra is extensive in borate minerals. Christ and Clark (1977) developed a hierarchical classification that was widely used until the development of the classification of Burns *et al.* (1995*a*), Hawthorne *et al.* (1996) and Grice *et al.* (1999).

B–B graphs and algebraic descriptors

The FBBs of borate structures may be represented as graphs. The vertices of the graphs correspond to B atoms (that are denoted as Δ or □, depending on their coordination number; where the coordination number is not specified, the letter B is used) and the edges of the graph corresponding to B–φ–B linkages (with φ, the linking anion, omitted). The 'algebraic descriptor' of the cluster (Burns *et al.* 1995*a*) has the general form *A*:*B*, where *A* is the number of ($B\varphi_3$) triangles and ($B\varphi_4$) tetrahedra in the cluster, and *B* is a character string that contains the connectivity information for those polyhedra. Isolated polyhedra may be written as *A*:*B* = 1Δ:Δ (Δ = $B\varphi_3$ triangle) or *A*:*B* = 1□:□ (□ = $B\varphi_4$ tetrahedron) (Figs 5*a*,*b*). More than one polyhedron in the descriptor indicates that the polyhedra polymerize by sharing corners: thus 1Δ1□:Δ□ contains one ($B\varphi_3$) triangle and one ($B\varphi_4$) tetrahedron, linked by sharing a corner (Fig. 5*c*). In the B string of the descriptor, adjacent polyhedra are linked, enabling graphical isomers (Hawthorne 1983*a*) to be distinguished, as shown for the clusters Δ2□:□Δ□ (Fig. 5*d*) and Δ2□:Δ□□ (Fig. 5*e*). Rings of polyhedra are denoted by enclosing the polyhedra of the ring by <> in the *B* string: thus a ring of one ($B\varphi_3$) triangle and two ($B\varphi_4$) tetrahedra (Fig. 5*f*) is denoted as 1Δ2□:<Δ2□>. Where rings of polyhedra polymerize, the number of polyhedra common to each ring is denoted by the symbols –, = and ≡ for one, two and three polyhedra, respectively: thus 2Δ2□:<Δ2□>=<Δ2□> consists of two <Δ2□> rings with two polyhedra in common (Fig. 5*g*). Most FBBs in borate minerals do not link through more than two B atoms, but there are exceptions; in **tunellite** (Burns and Hawthorne, 1994*b*), one O atom is bonded to three B atoms. To denote such linkages, [ ] are used to indicate any three- or

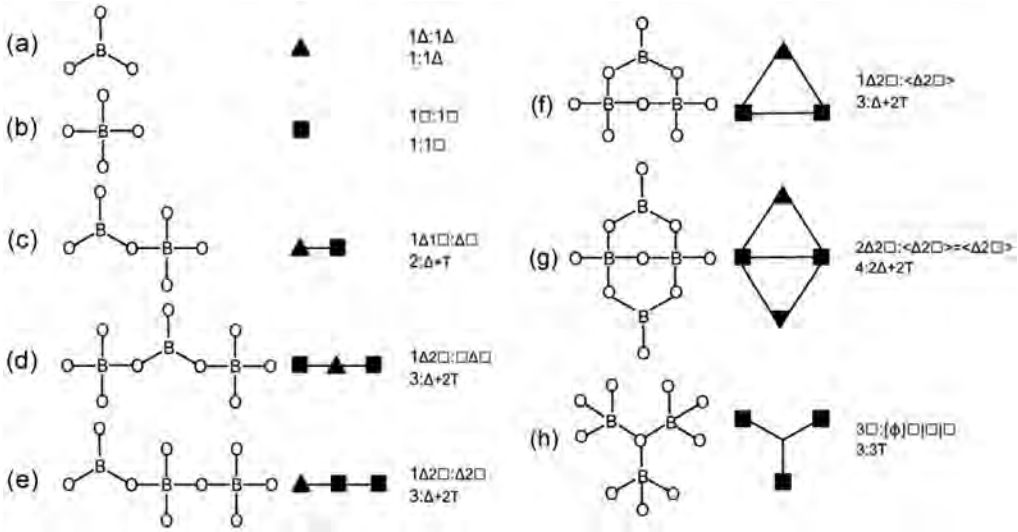

FIG. 5. Examples of borate clusters, their B−B graphs and algebraic descriptors; ▲ = (Bφ$_3$), ■ = (Bφ$_4$). After Burns *et al.* (1995*a*).

higher-connected anion (φ), polyhedron (Δ or □) or ring of polyhedra (e.g. <Δ2□>), and the polyhedra or rings connected to the central linking unit follow the [ ]. In addition, clusters that connect to the central linking unit are separated by the symbol |. Thus 3□:[φ] □|□|□| denotes three (Bφ$_4$) polyhedra linked by a common anion φ (Fig. 5*h*) in which the anion φ links to three separate (Bφ$_4$) tetrahedra. Selected borate minerals and their algebraic descriptors are listed in Table 1.

Such algebraic descriptors are very effective in symbolically representing bond topologies and are extremely useful in fundamental examinations of topologically possible atomic arrangements (e.g. Burns, 1995). However, as yet they have not been used for any other types of structures apart from borate minerals, and it remains to be seen if they will prove as effective in studies of the bond topology of silicates, phosphates, sulfates etc.

Borate structures based on isolated triangles and tetrahedra

The division of the isolated Δ and □ groups into subgroups on the basis of the identity of φ is quite significant from a paragenetic point of view. Most minerals in the φ = O^{2-} subgroup are from metamorphic or igneous (pegmatite) parageneses, whereas most minerals in the φ = $(OH)^-$ subgroup are from sedimentary (usually evaporitic) environments.

FBB = Δ, φ = O^{2-}. These structures contain infinite [Mφ$_4$] chains of edge-sharing octahedra that are cross-linked by (Bφ$_3$) triangles and (Bφ$_4$) tetrahedra, and by octahedra sharing edges and vertices with octahedra of adjacent chains. The [Mφ$_4$] chain has an intrinsic repeat distance of ~3 Å along its length (ignoring any ordering along the length of the chain), and they are known as '3 Å wallpaper structures' (Moore and Araki, 1974*a*). These structures may be idealized as colourings of the plane net 3^6; the structures of selected minerals are shown in Fig. 6. Some quantitative structural relations have been derived (Cooper and Hawthorne, 1998), but no general quantitative description of these structures has yet been developed.

FBB = □, φ = $(OH)^-$: Isolated tetrahedra are linked commonly by alkali and alkaline-earth cations (primarily Na and Ca), and the extended linkage of the structure is provided by the larger polyhedra and by H bonds (e.g. **hexahydroborite**: $Ca[B(OH)_4]_2(H_2O)_2$).

Borate structures based on clusters of triangles and tetrahedra

These structures may be divided into seven sets in which ten of the 12 distinct clusters involve three-membered rings of polyhedra:

(1) 2B; (2) <3B>; (3) <3B>=<3B>; (4) <3B>B;
(5) <3B>−<3B>; (6) [φ]<3B>|<3B>|<3B>|;
(7) {<3B>−<3B>}

TABLE 1. Hierarchy for selected borate minerals.

Name	Polyhedra	Algebraic descriptor	Formula	Fig.	Ref.
Isolated polyhedra					
3 Δ wallpaper structures					
Fluoborite	1Δ	Δ	$Mg_3(BO_3)(F,OH)_3$	6*a*	(1)
Warwickite	1Δ	Δ	$(Mg,Ti,Fe^{3+},Al)_2O(BO_3)$	6*b*	(2)
Ludwigite	1Δ	Δ	$Mg_2FeO_2(BO_3)$	6*c*	(3)
Pinakiolite	1Δ	Δ	$(Mg,Mn^{2+})_2(Mn^{3+},Sb^{3+})O_2(BO_3)$	6*d*	(4)
Karlite	1Δ	Δ	$Mg_7(OH)_4(BO_3)_4Cl$	6*e*	(5)
Wightmanite	1Δ	Δ	$Mg_5(OH)_5(BO_3)O(H_2O)_2$	6*f*	(6)
Other structures					
Hexahydroborite	1□	□	$Ca[B(OH)_4]_2(H_2O)_2$	–	(7)
Clusters					
3Δ wallpaper structures					
Suanite	2Δ	2Δ	$Mg_2[B_2O_5]$	6*g*	(8)
Szaibélyite	2Δ	2Δ	$Mg_2(OH)[B_2O_4(OH)]$	6*h*	(9)
Other structures					
Ameghinite	2Δ1□	<2Δ□>	$Na[B_3O_3(OH)_4]$	7*a*	(10)
Kurnakovite	2Δ	2Δ	$Mg[B_3O_3(OH)_5](H_2O)_5$	7*b*	(11)
Hydrochlorborite	2Δ2□	<Δ2□>Δ	$Ca_2[B_3O_3(OH)_4][BO(OH)_3]Cl(H_2O)_7$	7*c*	(12)
Nifontovite	3□	<3□>	$Ca_3[B_3O_3(OH)_6]_2(H_2O)_2$	7*d*	(13)
Uralborite	4□	<3□>□	$Ca_2[B_4O_4(OH)_8]$	7*e*	(14)
Ulexite	2Δ3□	<Δ2□>–<Δ2□>	$NaCa[B_5O_6(OH)_6](H_2O)_5$	7*f*	(15)
Hungchaoite	2Δ2□	<Δ2□>=<Δ2□>	$Mg[B_4O_5(OH)_4](H_2O)_7$	7*g*	(16)
Ammonioborite	12Δ3□	3(<2Δ□>–<2Δ□>)	$(NH_4)_3[B_{15}O_{20}(OH)_8](H_2O)_4$	7*h*	(17)
Chains and ribbons					
Vimsite	1□	□	$Ca[B_2O_2(OH)_4]$	8*a*	(18)
Calciborite	1Δ2□	<Δ2□>	$Ca[B_2O_4]$	8*b*	(19)
Larderellite	4Δ1□	<2Δ□>–<2Δ□>	$(NH_4)[B_5O_7(OH)_2](H_2O)$	8*c*	(20)
Probertite	2Δ3□	<Δ2□>–<Δ2□>	$NaCa[B_5O_7(OH)_4](H_2O)_3$	8*d*	(21)
Ezcurrite	3Δ2□	<Δ2□>–<2Δ□>	$Na_2[B_5O_7(OH)_3](H_2O)_2$	8*e*	(22)
Kaliborite	3Δ3□	<Δ2□>–<Δ2□>Δ	$KMg_2H[B_7O_8(OH)_5](H_2O)_4$	8*f*	(23)
Kernite	3Δ4□	<Δ2□>–<Δ2□>–<Δ2□>	$Na_2[B_4O_6(OH)_2](H_2O)_3$	8*g*	(24)
Aristarainite	3Δ3□	[φ]<Δ2□>|<Δ2□>|<Δ2□>|	$NaMg[B_6O_8(OH)_4]_2(H_2O)_4$	8*h*	(25)

Sheets					
Biringuccite	3Δ2□	<2Δ□>–<Δ2□>	$Na_2[B_5O_8(OH)](H_2O)$	9*a*	(26)
Tuzlaite	2Δ3□	<Δ2□>–<Δ2□>	$NaCa[B_5O_8(OH)_2](H_2O)_3$	9*b*	(27)
Tunellite	3Δ3□	[φ]<Δ2□>|<Δ2□>|<Δ2□>	$Sr[B_6O_9(OH)_2](H_2O)_3$	9*c*	(28)
Strontioborite	5Δ3□	[φ]<Δ2□>|<Δ2□>|<Δ2□>|2Δ	$Sr[B_8O_{11}(OH)_4]$	9*d*	(29)
Fabianite	2Δ4□	<Δ2□>=<4□>=<Δ2□>	$Ca_2[B_6O_{10}(OH)_2]$	9*e*	(30)
Johachidolite	8□	<6□>=<4□>	$Ca_2Al_2[B_6O_{14}]$	9*f*	(31)
Frameworks					
Diomignite	2Δ2□	<Δ2□>=<Δ2□>	$Li_2[B_4O_6]$	10*a*	(32)
Hilgardite-1*A*	2Δ3□	<Δ2□>–<Δ2□>	$Ca_2[B_5O_9]Cl(H_2O)$	10*b*	(33)
Boracite	1Δ6□	[φ]<3□>|<3□>|<3□>|Δ	$Mg_3[B_7O_{13}]Cl$	10*c*	(34)
Pringleite	7Δ8□	<Δ□·>=<Δ2□>Δ	$Ca_9[B_{20}O_{28}(OH)_{18}][B_6O_6(OH)_6]Cl_4(H_2O)_{13}$	10*d*	(35)
Ruitenbergite	7Δ8□	<Δ□·>=<Δ2□>Δ	$Ca_9[B_{20}O_{28}(OH)_{18}][B_6O_6(OH)_6]Cl_4(H_2O)_{13}$	–	(35)

References: (1) Dal Negro and Tadini (1974): (2) Bigi *et al.* (1991); (3) Bonazzi and Menchetti (1989); (4) Moore and Araki (1974*a*); (5) Bonazzi *et al.* (1986); (6) Moore and Araki (1972*a*); (7) Simonov *et al.* (1976*a*); (8) Takéuchi (1952); (9) Takéuchi and Kudoh (1975); (10) Dal Negro *et al.* (1975); (11) Razmanova et al. (1970), Corazza (1974); (12) Brown and Clark (1978); (13) Simonov *et al.* (1978); (14) Simonov *et al.* (1977); (15) Ghose *et al.* (1978); (16) Wan and Ghose (1977); (17) Merlino and Sartori (1971); (18) Simonov *et al.* (1976*b*); (19) Egorov-Tismenko *et al.* (1980); (20) Merlino and Sartori (1969); (21) Menchetti *et al.* (1982); (22) Cannillo *et al.* (1973); (23) Burns and Hawthorne (1994*a*); (24) Cooper *et al.* (1973); (25) Ghose and Wan (1977); (26) Corazza *et al.* (1974); (27) Bermanec *et al.* (1994); (28) Burns and Hawthorne (1994*b*); (29) Brovkin *et al.* (1975); (30) Konnert *et al.* (1970); (31) Moore and Araki (1972*b*); (32) Krogh-Moe (1962); (33) Burns and Hawthorne (1994*c*); (34) Dowty and Clark (1973); (35) Grice *et al.* (1994).

FBB = 2Δ. There are two 3 Å wallpaper structures in this group. **Suanite** (Table 1, Fig. 6*g*) has 4×1 ribbons of octahedra that are cross-linked by $[B_2O_5]$ groups. **Szaibélyite** (Fig. 6*h*) has 2×1 ribbons of edge-sharing octahedra that link through vertices to form corrugated sheets of octahedra that are cross-linked by $[B_2O_5]$ groups to form a framework.

FBB = <2Δ□>. In **ameghnite**, <2Δ□> clusters (Table 1, Fig. 7*a*) combine with $[Na_2\varphi_{10}]$ dimers into a framework with extensive interstitial H bonding.

FBB = <Δ2□>. The <Δ2□> ring in **kurnakovite** (Table 1, Fig. 7*b*) links to $(Mg\varphi_6)$ octahedra to form chains that link *via* direct H bonding and also by H bonding involving a single interstitial (H_2O) group.

FBB = <Δ2□>□. The <Δ2□> ring in **hydrochloroborite** is decorated by a $(B\varphi_4)$ tetrahedron (Table 1, Fig. 7*c*) and these groups are linked by [8]-coordinated Ca and extensive H bonding.

FBB = <3□>. The <3□> ring in **nifontovite** (Table 1, Fig. 7*d*) cross-links chains of edge-sharing $(Ca\varphi_8)$ polyhedra to form a framework that is further linked by extensive H bonding.

FBB = <3□>□. The <3□> ring in **uralborite** is decorated by a $(B\varphi_4)$ tetrahedron (Table 1, Fig. 7*e*) and is cross-linked by dimers of edge-sharing $(Ca\varphi_8)$ polyhedra to form a framework that is further linked by extensive H bonding.

FBB = <Δ2□>–<Δ2□>. In **ulexite**, <Δ2□>–<Δ2□> clusters (Table 1, Fig. 7*f*) link by corner-sharing to [8]-coordinated Ca and [6]-coordinated Na into a framework with extensive interstitial H bonding.

FBB = <Δ2□>=<Δ2□>. In **hungchaoite**, <Δ2□>=<Δ2□> clusters (Table 1, Fig. 7*g*) link by corner-sharing to $\{Mg(OH)(H_2O)_5\}$ octahedra, forming a (neutral) $Mg[B_4O_5(OH)_4](H_2O)_5$

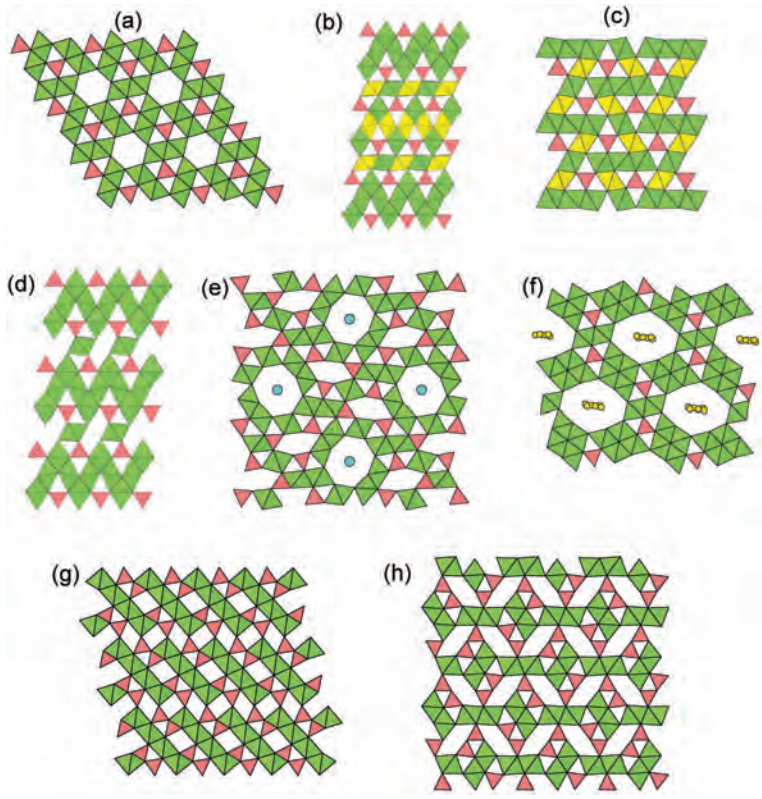

FIG. 6. Selected wallpaper borate structures; (*a*) fluoborite; (*b*) warwickite; (*c*) ludwigite; (*d*) pinakiolite; (*e*) karlite; (*f*) wightmanite; (*g*) suanite; (*h*) szaibélyite. Orange: (BO_3); green: (MgO_6); yellow: (FeO_6); turquoise circles: Cl; yellow circles: (H_2O).

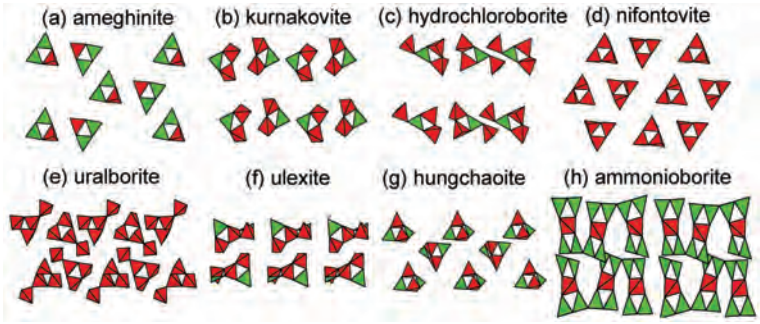

FIG. 7. Selected cluster borate structures; (*a*) ameghinite; (*b*) kurnakovite; (*c*) hydrochlorborite; (*d*) nifontovite; (*e*) uralborite; (*f*) ulexite; (*g*) hungchaoite; (*h*) ammonioborite. Green = ($B\varphi_3$); red = ($B\varphi_4$).

cluster. This cluster links to other identical clusters by H bonding.

FBB = 3{<2Δ□>–<2Δ□>}. In **ammonioborite**, two <2Δ□> rings link through a common □ [($B\varphi_4$) tetrahedron] and the resulting groups link into trimers through sharing triangle vertices (Table 1, Fig. 7*h*). These large clusters link *via* H bonding through interstitial (NH_4) groups.

Borate structures based on chains and ribbons of triangles and tetrahedra

These may be divided into six sets involving seven distinct clusters, all but one of which involve three-member rings of polyhedra:

(1) B; (2) <3B>; (3) <3B>–<3B>;
(4) <3B>–<3B>B; (5) <3B>–<3B>–<3B>;
(6) [φ]<3B>|<3B>|<3B>|

FBB = □. In **vimsite** (Table 1, Fig. 8*a*), ($B\varphi_4$) tetrahedra link by sharing corners to form [$B\varphi_3$] chains that are linked by [8]-coordinated Ca.

FBB = <Δ2□>. In **calciborite** (Table 1, Fig. 8*b*), <Δ2□> rings polymerize to form a chain, each ring sharing two vertices between triangles and tetrahedra of adjacent rings, producing a central chain of ($B\varphi_4$) tetrahedra decorated by ($B\varphi_3$) triangles. These chains are cross-linked *via* chains of $Ca\varphi_8$ polyhedra by sharing corners to form a heteropolyhedral framework.

FBB = <2Δ□>–<2Δ□>. In **larderellite** (Table 1, Fig. 8*c*), two <2Δ□> rings link *via* a ($B\varphi_4$) tetrahedron that is common to each ring. These clusters then link through vertices of ($B\varphi_3$) triangles to form ribbons (Fig. 8*c*) that are cross-linked *via* H bonds involving interstitial (NH_4)

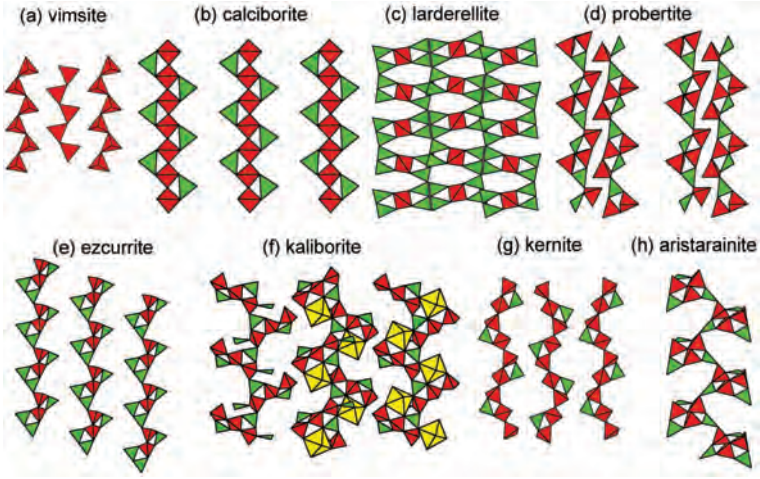

FIG. 8. Selected chain borate structures; (*a*) vimsite; (*b*) calciborite; (*c*) larderellite; (*d*) probertite; (*e*) ezcurrite; (*f*) kaliborite; (*g*) kernite; (*h*) aristarainite. Legend as in Fig. 6, ($Mg\varphi_6$) = yellow.

groups. This ribbon is an extended linkage of the 3{<2Δ□>–<2Δ□>} cluster in **ammonioborite** (Fig. 7*h*).

FBB = <Δ2□>–<Δ2□>. In **probertite** (Table 1, Fig. 8*d*), two <Δ2□> rings link *via* a ($B\varphi_4$) tetrahedron that is common to each ring. The resulting clusters link through vertex sharing between ($B\varphi_3$) triangles and ($B\varphi_4$) tetrahedra to form chains (Fig. 8*d*) that are cross-linked through [9]-coordinated Ca and [6]-coordinated Na, and H bonds involving (OH) and (H_2O) groups.

FBB = <2Δ□>–<Δ2□>. In **ezcurrite** (Table 1, Fig. 8*e*), two different types of three-membered rings link through vertex sharing between ($B\varphi_3$) triangles and ($B\varphi_4$) tetrahedra to form clusters that link *via* vertex sharing between ($B\varphi_3$) triangles and ($B\varphi_4$) tetrahedra to form chains (Fig. 8*e*) that are cross-linked through [6]- and [7]-coordinated Na, and H bonds involving (OH) and (H_2O) groups.

FBB = <Δ2□>–<Δ2□>Δ. In **kaliborite** (Table 1, Fig. 8*f*), two <Δ2□> rings link *via* a ($B\varphi_4$) tetrahedron that is common to each ring and these clusters link by sharing vertices between ($B\varphi_3$) triangles and ($B\varphi_4$) tetrahedra of different clusters to form very convoluted ribbons. The very open interrupted rings apparent in Fig. 8*f* (left) are closed by ($Mg\varphi_6$) octahedra (Fig. 8*f*, right) and the ribbons are cross-linked by [8]-coordinated K and H bonds.

FBB = <Δ2□>–<Δ2□>–<Δ2□>. **Kernite** (Table 1, Fig. 8*g*) has <Δ2□> rings that share vertices with tetrahedra of adjacent rings to form chains that are linked into a continuous structure by Na atoms and a network of H bonds.

FBB = [φ]<Δ2□>|<Δ2□>|<Δ2□>. In **aristarainite** (Table 1, Fig. 8*h*), the FBB has a central anion, denoted as φ, which is shared between three <Δ2□> rings. This FBB links to other FBBs *via* ($B\varphi_3$) and ($B\varphi_4$) groups to form very convoluted chains. ($Na\varphi_5$) polyhedra and a network of H bonds knit these chains into a three-dimensional structure.

Borate structures based on sheets of triangles and tetrahedra

These may be divided into seven sets in which there are eight distinct clusters, all but one of which involve three-membered rings of polyhedra:
(1) <3B>–<3B>; (2) [φ]<3B>|<3B>|<3B>|;
(3) [φ]<3B>|<3B>|<3B>|2B
(4) [φ]<3B>|<3B>|<3B>|–[φ]<3B>|<3B>|<3B>|2B;
(5) <3B>=<4B>=<3B>; (6) <6B>=<4B>;
(7) B<3B>–<3B>–<3B>–<3B>B

FBB = <2Δ□>–<Δ2□>. **Biringuccite** (Table 1, Fig. 9*a*) has an FBB consisting of two linked three-membered rings, <2Δ□>–<Δ2□>, (with the plane of each ring orthogonal to that of the other ring), and this cluster polymerizes to form a [B_5O_8(OH)] sheet. In turn, this sheet is cross-linked into a framework by interstitial Na cations.

FBB = <Δ2□>–<Δ2□>. In **tuzlaite** (Table 1, Fig. 9*b*), two <Δ2□> rings link through a ($B\varphi_4$) tetrahedron that is common to each ring, and these

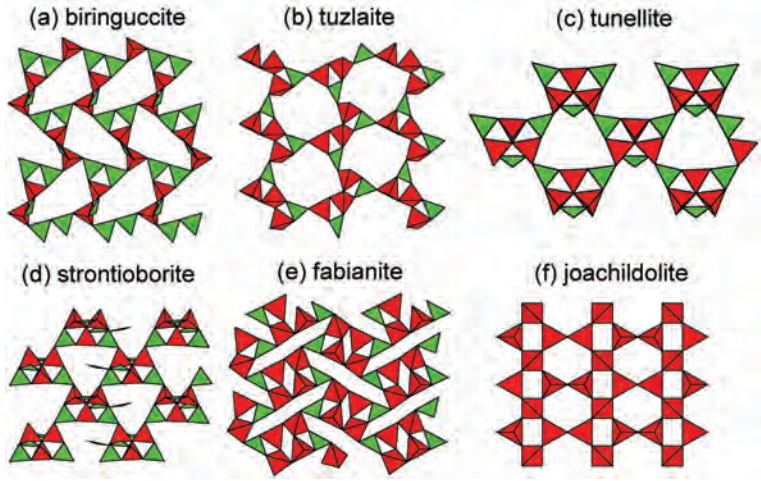

FIG. 9. Selected sheet borate structures; (*a*) biringuccite; (*b*) tuzlaite; (*c*) tunellite; (*d*) strontioborite; (*e*) fabianite; (*f*) joachildite. Legend as in Fig. 6.

clusters link through sharing vertices between ($B\varphi_3$) triangles and ($B\varphi_4$) tetrahedra of different clusters to form open sheets (Fig. 9*b*) that are linked by [8]-coordinated Ca and [7]-coordinated Na.

FBB = [φ]<Δ2□>|<2Δ□>|<2Δ□>|. In **tunellite** (Table 1, Fig. 9*c*), three <2Δ□> rings link through a common vertex, denoted by [φ] in the FBB descriptor (Table 1), to form a cluster involving three triangles and three tetrahedra. Adjacent clusters link to form sheets (Fig. 9*c*) by sharing apical vertices between tetrahedra, and these sheets are cross-linked by [10]-coordinated Sr and a network of H bonds.

FBB = [φ]<Δ2□>|<2Δ□>|<2Δ□>|2Δ. In **strontioborite** (Table 1, Fig. 9*d*), three <2Δ□> rings link through a common vertex to form a cluster involving three triangles and three tetrahedra (as in **tunellite**), and this cluster is decorated by *2*Δ (two corner-shared ($B\varphi_3$) triangles). Adjacent clusters link to form sheets (Fig. 9*d*) by sharing apical vertices between ($B\varphi_3$) triangles and ($B\varphi_4$) tetrahedra of different clusters, and these sheets are cross-linked by [10]-coordinated Sr and a network of H bonds.

FBB = <Δ2□>=<4□>=<Δ2□>. **Fabianite** is rather unusual in containing a four-membered ring of tetrahedra, <4□>. This ring shares two *trans* edges with two three-membered rings, <Δ2□>, and the resulting FBB consists of four tetrahedra and two triangles (Table 1). Adjacent clusters link by sharing vertices of both tetrahedra and triangles to form sheets (Fig. 9*e*) that are cross-linked by chains of ($Ca\varphi_8$) polyhedra.

FBB = <6□>=<4□>. **Joachildite** (Table 1, Fig. 9*f*) consists of a sheet of six-membered and four-membered rings of vertex-sharing ($B\varphi_4$) tetrahedra in which the B atoms occur at the vertices of a $(46^2)_2(4646)$ net (which is the n = 1 member of the $(46^2)_2(4646)(6^3)_{2(n-1)}$ family of plane nets derived by Hawthorne (2012*b*). Adjacent sheets are linked by [6]-coordinated Al and [8]-coordinated Ca.

Borate structures based on frameworks of triangles and tetrahedra

These may be divided into six sets in which there are six distinct clusters, all but one of which involve a three-membered ring of polyhedra:

(1) <3B>; (2) <3B>=<3B>; (3) <3B>–<3B>;
(4) [φ]<3B>|<3B>|<3B>|B; (5) [φ]4B|; (6) <3B>B

FBB = <Δ2□>=<Δ2□>. In **diomignite** (Table 1, Fig. 10*a*), two <Δ2□> rings share an edge through two common ($B\varphi_4$) tetrahedra and these clusters link through sharing vertices between ($B\varphi_3$) triangles and ($B\varphi_4$) tetrahedra of four other clusters to form an open framework (Fig. 10*a*) containing [6]-coordinated Li in its interstices.

FBB = <Δ2□>–<Δ2□>. There are three polymorphs of **hilgardite** and each one has the FBB, <Δ2□>–<Δ2□> (Table 1) consisting of two linked three-membered rings. Each FBB shares polyhedron vertices with adjacent FBBs to form chains that are cross-linked into a framework by sharing corners between ($B\varphi_3$) and ($B\varphi_4$) groups (Fig. 10*b*), and interstitial Ca, Cl and (H_2O) groups occupy the interstices of the framework. Polymorphism arises from different linkages of the two types of stereoisomer of the FBB.

FBB = [φ]<3□>|<3□>|<3□>|Δ. **Boracite** (orthorhombic) has <3□> rings that link by sharing vertices such that one anion, [φ], links to three B cations. An additional Δ further binds the framework and produces <Δ4□> rings (Fig. 10*c*) within the framework, and there is [5]-coordinated Mg in the interstices.

FBB = <Δ□·>=<Δ2□>Δ. **Pringleite** (space group *P*1) and **ruitenbergite** (space group $P2_1$) both have the composition $Ca_9[B_{20}O_{28}(OH)_{18}][B_6O_6(OH)_6]Cl_4(H_2O)_{13}$ and are dimorphs. The FBB of both structures is a 12-membered ring of alternating ($B\varphi_3$) triangles and ($B\varphi_4$) tetrahedra (Fig. 10*d*) that is linked to a decorated three-membered ring of one ($B\varphi_3$) triangle and two ($B\varphi_4$) tetrahedra. The FBBs link directly to form a framework of 12- and three-membered rings (Fig. 10*d*) and polymorphism arises from topological differences in the polymerization of the FBBs.

The relation between the structural unit and the interstitial complex

A structural hierarchy for a group of minerals provides a framework for considering other aspects of their chemical composition and behaviour in geological processes. I will first consider how the chemical composition and bond topology of structural units control aspects of the chemical composition and stereochemical details of the interstitial complex. Above, I described the use of the valence-matching principle to examine constraints on the linkage of oxyanion polyhedra. When examining the aggregate interaction between the structural unit and the interstitial complex for a complicated mineral (e.g. Fig. 3),

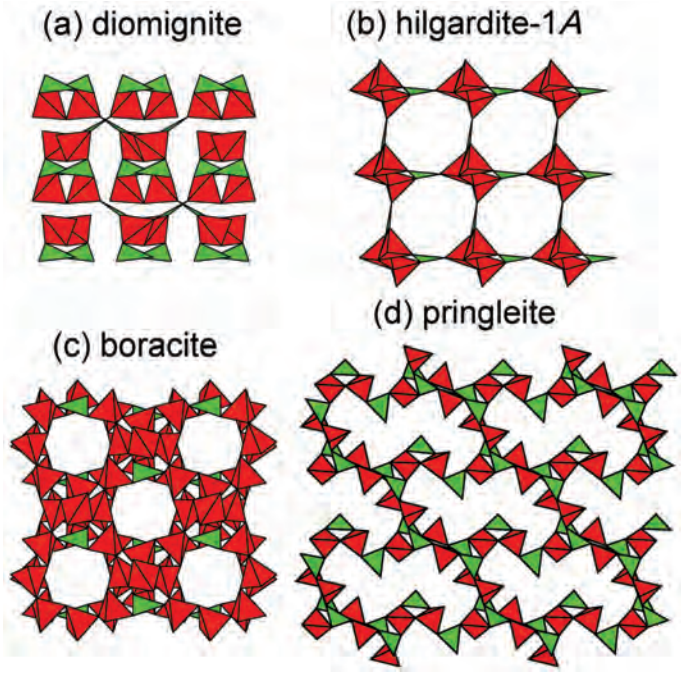

FIG. 10. Selected framework borate structures; (*a*) diomignite; (*b*) hilgardite-1*A*; (*c*) boracite; (*d*) pringleite. Legend as in Fig. 6.

we are no longer dealing with the interaction of (simple) atoms; we are dealing with the interaction of large groups of atoms. Hawthorne and Schindler (2008) introduced a mean-field equivalent of the valence-matching principle, the 'Principle of Correspondence of Lewis Acidity-Basicity', by which one may quantitatively examine the interaction between the structural unit and the interstitial complex. Calculation of the Lewis basicities and Lewis acidities is described in detail by Hawthorne and Schindler (2008).

The chemical formula of a generalized interstitial complex may be written as

$$\{^{[m]}M_a^{+[n]}M_b^{2+[l]}M_c^{3+}(H_2O)_d(H_2O)_e\ {}_{[q]}(OH)_f(H_2O)_g\}^{(a+2b+3c-f)+}$$

where M are interstitial cations of different coordination number ([m], [n] and [l]) and charge, d = the amount of transformer (H_2O) (see Hawthorne, 1985*a*, 1992), e = the amount of non-transformer (H_2O) and g = the amount of (H_2O) not bonded to any interstitial cation (Schindler and Hawthorne 2001*a*). The Lewis acidity of the interstitial complex may be calculated as a function of the variables a to g, l to n and q in the above expression and represented graphically as in Fig. 11*a*: the curved lines show the variation in Lewis acidity (shown on the ordinate) as a function of the number of transformer (H_2O) groups per cation (shown on the abscissa) for interstitial cations of different coordination number and formal charge, with the corresponding coordination numbers and cation charges shown to the left of the curves. Monovalent anions (OH, Cl) may be incorporated as described by Hawthorne and Schindler (2008). Where the range in Lewis basicity of the structural unit overlaps with the Lewis-acidity function, structures of those particular compositions are in accord with the principle of correspondence of Lewis acidity-basicity, and may be stable. Where the properties of the structural unit and interstitial complexes do not overlap, structures of those compositions do not accord with the principle of correspondence of Lewis acidity-basicity, and are not expected to be stable. Hence the principle of correspondence of Lewis acidity-basicity allows us to examine the interaction between the structural unit and interstitial complex as a function of varying chemical composition of each component.

This may be illustrated for the structural unit $[B_4O_5(OH)_4]^{2-}$ that occurs in **borax**: $Na_2(H_2O)_8[B_4O_5(OH)_4]$, **tincalconite**: $Na_2(H_2O)_{2.67}[B_4\ O_5(OH)_4]$ and **hungchaoite**: $Mg(H_2O)_5[B_4O_5(OH)_4](H_2O)_2$. The range in Lewis basicity of the structural unit is 0.17−0.24 vu. (Hawthorne and Schindler, 2008). We may predict the range in chemical composition for possible interstitial complexes for this structural unit by plotting its range in Lewis basicity onto the graph of Lewis acidity (Fig. 11*a*) as shown in Fig. 11*b*. Structures are stable where the Lewis basicity and Lewis acidity functions overlap. Hence interstitial monovalent cations are possible only for coordination numbers [5] and [6] with 0−1 and 0 transformer (H_2O) groups, respectively; **borax** has an interstitial complex $\{^{[6]}Na(H_2O)_0\ ....\}^{+}$ in accord with this. For divalent interstitial cations, $^{[6]}M^{2+}$ is possible with 2−5 transformer (H_2O) groups; **hungchaoite** has an interstitial complex $\{^{[6]}Mg(H_2O)_4\ ....\}^{2+}$. **Tincalconite** has interstitial $^{[5]}Na$ and $^{[6]}Na$; combining the above predictions results in a possible variation of 0−1 plus 0 transformer (H_2O) groups, for a total possible variation of 0−1; the observed value is 0. Many more examples for borates are given by Schindler and Hawthorne (2001*a*,*b*,*c*), and for other mineral groups by Schindler and Hawthorne (2004, 2008) and Schindler *et al.* (2006*a*). What controls the amount of transformer (H_2O) within the ranges indicated is not clear, but it seems reasonable that it is related to the pH of the nascent aqueous solution.

It is apparent from Figs 11*a* and 11*b* that we now have some understanding of what influences the coordination numbers of interstitial cations, as these influence the Lewis acidity of the interstitial complex which is constrained by the Principle of Correspondence of Lewis Acidity-Basicity to be (approximately) equal to the Lewis basicity of the structural unit. Figure 12 compares the coordination numbers of interstitial cations predicted for borate minerals by Schindler and Hawthorne (2001*c*) with the observed values; the coordination numbers, from [4] to [11], are predicted quite accurately.

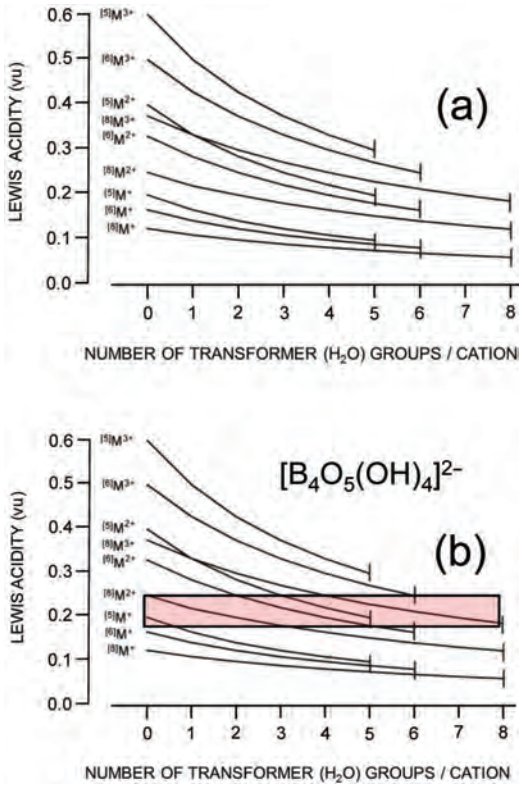

FIG. 11. (*a*) Variation in Lewis acidity of a general interstitial complex as a function of the number of transformer (H_2O) groups for monovalent, divalent and trivalent cations in [5]-, [6]- and [8]-coordination; (*b*) as (*a*) with the range in Lewis basicity of the structural unit $[B_4O_5)(OH)_4]^{2-}$ shown in pink.

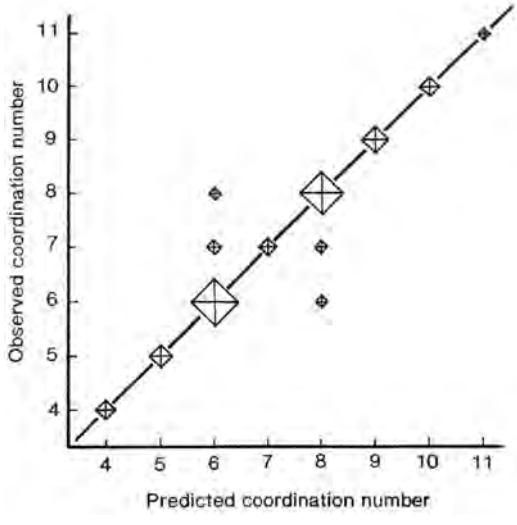

FIG. 12. Observed *vs.* predicted coordination numbers of interstitial cations in borate minerals. From Hawthorne and Schindler (2008).

FIG. 13. The six borate clusters present as FBBs in the structures of all borate minerals. Legend as in Fig. 6.

Crystallization of borate minerals from aqueous solution

The hydroxy-hydrated borate minerals contain the six borate clusters (Fig. 13) embedded within their structures. This observation is remarkable when we realize that we may combine $B(OH)_3$ and $B(OH)_4$ to form many clusters that do not occur in borate minerals (Burns 1995). This observation is also of major significance as these six clusters are also the principal borate complexes occurring in aqueous solution (Fig. 14) (Hawthorne *et al.*, 1996). Thus the principal FBBs of the hydroxy-hydrated borate minerals correspond to the principal aquated-borate species in aqueous solution. In turn, this strongly suggests that clusters condense from solution during crystallization and retain their identity during dissolution.

This process is visually evident for borate minerals containing isolated clusters of borate polyhedra, as the cluster is apparent both visually in the structure itself and in the mineral formula. This situation is illustrated for **inderite** in Fig. 15. The structure of **inderite** is based on the $[B_3O_3(OH)_5]$ cluster (circled in Fig. 15*a*,*b*), and the $[B_3O_3(OH)_5]$ cluster can be identified in the chemical formula of **inderite** (Fig. 15*c*). For chain, sheet and framework structures, crystallization involves polymerization of these FBBs. In **hilgardite**, $Ca_2[B_5O_9]Cl(H_2O)$, a framework-structure borate (Fig. 16), the framework consists of three of the six clusters in Figs 13, 14: $[B_3O_3(OH)_5]$, $B(OH)_4$ and $B(OH)_3$. These clusters polymerize *via* a crystallization reaction (Fig. 16) whereby the clusters polymerize to form the $[B_5O_9]$ framework and release (H_2O) to the solution.

Structural hierarchies for other groups of minerals

When describing the structural hierarchy of the borate minerals above, I also briefly described the interstitial species and some aspects of the bonds that link the adjacent structural units together.

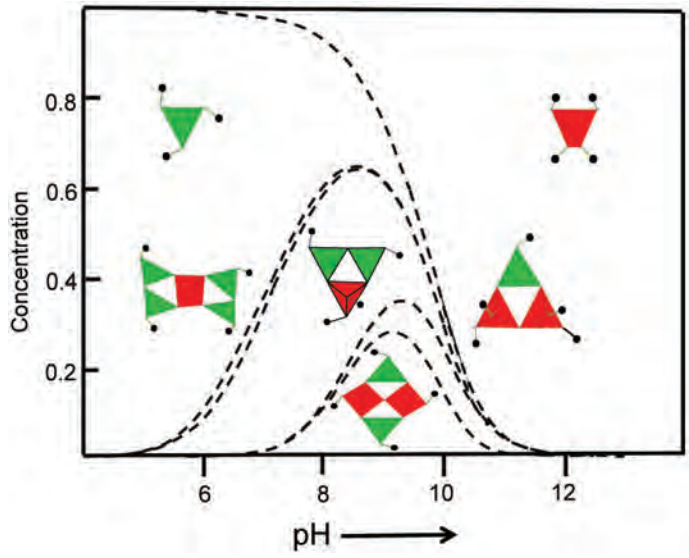

FIG. 14. The distribution of B species as a function of pH in an aqueous solution of 0.40 molar on total $B(OH)_3$; after Christ *et al.* (1967) from the data of Ingri (1963). Legend as in Fig. 6.

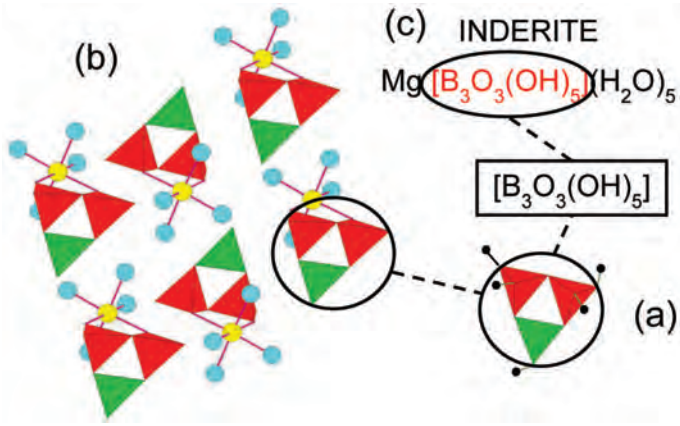

FIG. 15. A sketch of the crystal structure of inderite showing the $[B_3O_3(OH)_5]$ cluster from Fig. 13 and its presence in the crystal structure of inderite and in the chemical formula of inderite (in red); legend as in Fig. 6.

There has been considerable subsequent work on the borate minerals, examining factors that control aspects of the crystal chemistry and chemical composition and attempting to relate the bond topology of the structural units to the borate species present in nascent aqueous borate solutions (Schindler and Hawthorne, 2001*a*,*b*,*c*). There has not been so much work of this type on other classes of minerals, and from this point on I will generally omit details of the interstitial complex and its bond topology. I will focus primarily on the bond topologies of the structural units in each class of structures, and then look for commonalities and differences between them.

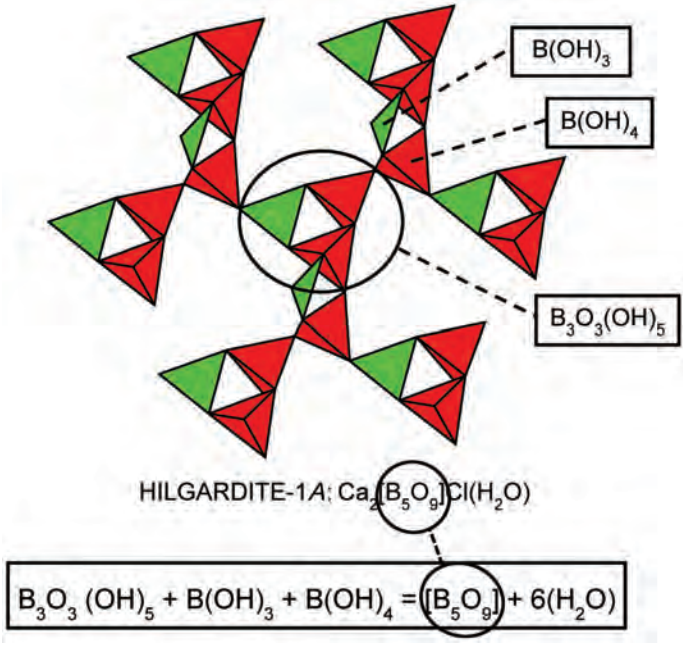

FIG. 16. An oblique view of a fragment of the structure of the framework borate mineral hilgardite, showing how the $[B_5O_9]$ framework is constructed of $[B(OH)_3]$, $[B(OH)_4]$ and $[B_3O_3(OH)_5]$ clusters and how crystallization of the framework can be envisioned as a condensation of these three aqueous species.

Uranyl minerals and compounds

Structural hierarchy for uranyl structures is somewhat different from structure hierachies involving conventional oxysalt constituents as their principal constituent, the U^{6+} cation, generally occurs in crystal structures as the near-linear $(U^{6+}O_2)^{2+}$ group, the uranyl group, which may be considered a complex cation. Burns *et al.* (1997*a*) discussed the crystal chemistry of U^{6+} in an oxide environment. They showed that U^{6+} commonly occurs in [6]-, [7]- and [8]-coordinations: tetragonal bipyramidal (octahedral), pentagonal bipyramidal and hexagonal bipyramidal with the apical O atoms, often labelled as O_{ur} (= O_{uranyl}), at distances of ~1.79 Å (± 0.20 Å) from the central U^{6+} cation, and the equatorial anions at much longer distances (2.1−2.8 Å). Burns *et al.* (1997*a*) also derived accurate bond-valence parameters for U^{6+} in its various coordinations.

Burns *et al.* (1996) and Burns (1999, 2005) presented a structural hierarchy for the rapidly expanding family of uranyl oxides and oxysalts, both minerals and synthetic compounds. Structures are organized into five classes according to the dimensional character of the polymerization: (1) isolated polyhedra; (2) clusters; (3) chains and ribbons; (4) sheets; and (5) frameworks. The $U^{6+}-\varphi_{ur}$ bonds have bond valences generally in the range 1.6−2.0 vu and thus (1) the φ_{ur} anion is constrained to be O^{2-} and I will henceforth write the $U^{6+}-\varphi_{ur}$ bond as $U^{6+}-O_{ur}$; (2) the φ_{ur} anion is only rarely involved in linkage between polyhedra of the structural unit; such linkage commonly involves only the equatorial anions. This is the case in minerals, but linkages involving one $U^{6+}-O_{ur}$ bond and one $U^{6+}-O_{eq}$ bonded to the same anion do occur in synthetic compounds; e.g. Mihalcea *et al.* (2011), Cantos *et al.* (2013), and such linkages are more common in Np^{5+} comppounds; e.g. Cousson *et al.* (1984), Albrecht-Schmitt *et al.* (2003), Krot and Grigoriev (2004).

The $(U^{6+}O_2\varphi_n)$ polyhedra (n = 4−6) thus tend to polymerize by sharing edges, and the majority of uranyl-oxide and uranyl-oxysalt minerals have two-dimensional structural units. The arrangements of equatorial anions within such sheets consist of patterns of squares, pentagons and hexagons that all have a central U^{6+} cation, together with insterstitial polygonal spaces and polygons of anions involving complex anionic groups [e.g. $(CO_3)^{2-}$]. Miller *et al.* (1996) introduced a classification of uranium-oxide-hydrate structures based on the geometrical characteristics of their patterns of equatorial anions, and Burns (1999, 2005) expanded this approach and applied it to O-bearing uranyl structures with sheet-like structural units. Here, I will omit structures with isolated polyhedra only, as our interest here is in the general character of structural polymerization. I will show only a small selection of the known structures, but this will be enough to illustrate the general character of the bond topology of uranyl oxysalts.

Uranyl structures based on clusters of polyhedra

These are illustrated in Fig. 17, together with their graphs, and a selection of the corresponding structures are listed in Table 2. Following on from the isolated polyhedra (monomers), there are two dimers of edge-sharing octahedra and edge-sharing pentagonal bipyramids (Fig. 17*a*), one trimer of edge-sharing pentagonal bipyramids (Fig. 17*b*) and one tetramer of edge-sharing pentagonal bipyramids (Fig. 17*c*). Perhaps other such polymers will be found under different conditions of growth or synthesis. Monomers link to various oxyanions: $(BO_3)^{3-}$, $(CO_3)^{2-}$, $(NO_3)^{1-}$, $(BO_4)^{5-}$, $(SO_4)^{2-}$, $(CrO_4)^{2-}$, $(MoO_4)^{2-}$, $(ClO_4)^{1-}$, and the diversity and difference in Lewis basicity of what is observed suggests that a wider variety of oxyanions may be possible in this group, and that more types of polymerization should be possible with varying pH of conditions of growth or synthesis. The clusters $[(U^{6+}O_2)(ClO_4)_2\varphi_3]^{4-}$ (Fig. 17*d*) and $[(U^{6+}O_2)(TO_4)_4]^{6-}$ (T = Mo^{6+}, Cr^{6+}) (Fig. 17*e*) involve corner sharing between $(U^{6+}O_2\varphi_n)$ polyhedra (n = 5 and 4, respectively) and hexavalent-metal tetrahedal oxyanions. The slightly more complicated $[(U^{6+}O_2)_2(T^{6+}O_4)_8]^{12-}$ cluster (Fig. 17*f*) consists of two pentagonal bipyramids where all equatorial anions link to tetrahedral oxyanion groups, and where the two pentagonal bipyramids are linked by sharing corners with two common tetrahedra.

All clusters described thus far involve corner sharing between the constituent polyhedra. The following two clusters involve both corner sharing and edge sharing. The $[(U^{6+}O_2)(SO_4)_4]^{6-}$ cluster (Fig. 17*g*) consists of a pentagonal bipyramid corner-linked to three sulfate groups and edge-linked to a fourth sulfate group. The $[(U^{6+}O_2)(BO_3)_8(BO_4)_8]^{12-}$ cluster (Fig. 17*l*) consists of a hexagonal bipyramid enveloped by

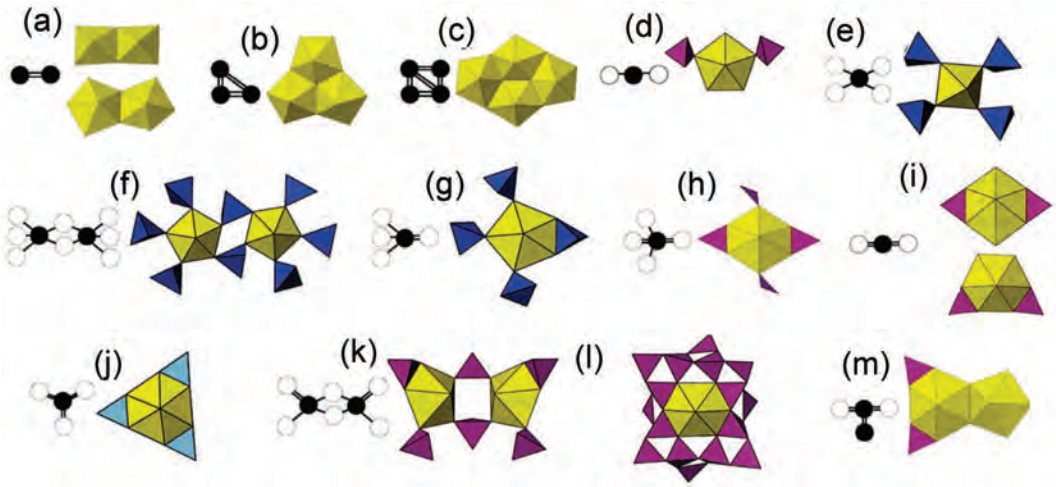

FIG. 17. Selected clusters from uranyl structures; (*a*) dimers of edge-sharing octahedra and pentagonal bipyramids in $K_8[(UO_2)_2O_6]$ and $[(UO_2)(OH)Cl(H_2O)_2]$; (*b*) trimer of edge-sharing pentagonal bipyramids in $[(UO_2)_3O(OH)_3(H_2O)_6](NO_3)(H_2O)_4$; (*c*) tetramer of edge-sharing pentagonal bipyramids in $[(UO_2)_4Cl_2O_2(OH)_2(H_2O)_6](H_2O)_4$; (*d*) cluster of a pentagonal bipyramid and two (ClO_4) tetrahedra in $[(UO_2)(ClO_4)_2(H_2O)_3]$; (*e*) cluster of an octahedron and four (MoO_4) tetrahedra in $Cs_6[(UO_2)(MoO_4)_4]$; (*f*) cluster of two pentagonal bipyramids and eight (MoO_4) tetrahedra in $Na_6[(UO_2)(MoO_4)_4]$; (*g*) cluster of a pentagonal bipyramid and four (SO_4) tetrahedra in $Na_6[(UO_2)(SO_4)_4](H_2O)_2$; (*h*) cluster of a hexagonal bipyramid and four (NO_3) triangles in $Rb_2[(UO_2)(NO_3)_4]$; (*i*) geometrical isomers of a hexagonal bipyramid and two (NO_3) triangles in $[(UO_2)(NO_3)_2](H_2O)_2$ and $[(UO_2)(NO_3)_2(H_2O)_2](H_2O)$; (*j*) cluster of a hexagonal bipyramid and three (CO_3) triangles in liebigite; (*k*) cluster of two pentagonal bipyramids and six (MoO_4) tetrahedra in $K_4[(UO_2)(SO_4)_3]$; (*l*) cluster of a hexagonal bipyramid, eight (BO_4) tetrahedra and eight (BO_3) triangles in $K_6[(UO_2)B_{16}O_{24}(OH)_8](H_2O)_{12}$; (*m*) cluster of a hexagonal bipyramid, a pentagonal bipyramid and two (NO_3) triangles in $[(UO_2)_2(OH)_2(NO_3)_2](H_2O)_4$.

a cluster of eight <Δ2□> borate trimers. Only (BO_4) groups link to the central (($U^{6+}O_2$)O6) group, both by edge sharing and corner sharing, and the ($B\varphi_3$) groups link to the (BO_4) groups by sharing corners. The $[(U^{6+}O_2)_2(BO_4)_6]^{12-}$ cluster (Fig. 17*k*) consists of two pentagonal bipyramids linked by sharing corners with two common (BO_4) groups, with each pentagonal bipyramid also sharing an edge and a corner with two other (BO_4) groups. The most condensed cluster is $[U^{6+}O_2)(CO_3)_3]^{4-}$ (Fig. 17*j*); this cluster is a constituent of several minerals (Table 2) and is a constituent of U^{6+}- and CO_3-bearing aqueous solutions. There are several $(NO_3)^-$-bearing clusters (Fig. 17*h*,*i*) with the (NO_3) groups sharing edges with uranyl hexagonal bipyramids.

Uranyl structures based on chains and ribbons of polyhedra

These are illustrated in Fig. 18, together with their graphs, and a selection of the corresponding structures are listed in Table 2. The simplest chain is the corner-sharing chain of ($U^{6+}O_2\varphi_4$) square bipyramids (Fig. 18*a*) with no additional oxyanions. For chains with uranyl polyhedra linked to oxyanions, there are three broad categories: (1) no linkage between uranyl polyhedra; (2) corner linkage between uranyl polyhedra; and (3) edge linkage between uranyl polyhedra. Within each of these categories, we have additional complexity through different uranyl polyhedra and different oxyanions. There are two types of simple chains involving corner sharing between ($U^{6+}O_2\varphi_n$) polyhedra and tetrahedra in which all meridional vertices of the ($U^{6+}O_2\varphi_n$) polyhedra link to tetrahedral oxyanions (Figs 18*b*,*c*); in these chains, most oxyanion are linked to two ($U^{6+}O_2\varphi_n$) polyhedra. In Fig. 18*d*, we see a ribbon in which all the tetrahedral oxyanions link to three ($U^{6+}O_2\varphi_5$) polyhedra. The remaining two ribbons in this group (where there is no direct linkage between ($U^{6+}O_2\varphi_n$) polyhedra) contain pairs of ($U^{6+}O_2\varphi_5$) polyhedra that are linked through tetrahedral oxyanions and the resulting cluster is linked along the ribbon by triangular-pyramidal oxyanions (Fig. 18*e*,*f*). The chain in Fig. 18*g* consists

TABLE 2. Uranyl structures, structural units and types of polymerization.

Name	Formula unit	Fig.	Ref.
Clusters			
$K_8[(UO_2)_2O_6]$	$[(UO_2)_2O_6]$	17*a*	(1)
$[(UO_2)(OH)Cl(H_2O)_2]$	$[(UO_2)(OH)Cl(H_2O)_2]$	17*a*	(2)
$[(UO_2)_3O(OH)_3(H_2O)_6](NO_3)(H_2O)_4$	$[(UO_2)_3O(OH)_3(H_2O)_6]$	17*b*	(3)
$[(UO_2)_4Cl_2O_2(OH)_2(H_2O)_6](H_2O)_4$	$[(UO_2)_4Cl_2O_2(OH)_2(H_2O)_6]$	17*c*	(4)
$[(UO_2)(ClO_4)_2(H_2O)_3]$	$[(UO_2)(ClO_4)_2(H_2O)_3]$	17*d*	(5)
$Cs_6[(UO_2)(MoO_4)_4]$	$[(UO_2)(MoO_4)_4]$	17*e*	(6)
$Na_6[(UO_2)(MoO_4)_4]$	$[(UO_2)(MoO_4)_4]$	17*f*	(7)
$Na_6[(UO_2)(SO_4)_4](H_2O)_2$	$[(UO_2)(SO_4)_4]$	17*g*	(8)
$Rb_2[(UO_2)(NO_3)_4]$	$[(UO_2)(NO_3)_4]$	17*h*	(9)
$[(UO_2)(NO_3)_2](H_2O)_2$	$[(UO_2)(NO_3)_2]$	17*i*	(10)
$[(UO_2)(NO_3)_2(H_2O)_2](H_2O)$	$[(UO_2)(NO_3)_2(H_2O)_2]$	17*i*	(11)
Liebegite	$[(UO_2)(CO_3)_3]$	17*j*	(12)
$K_4[(UO_2)(SO_4)_3]$	$[(UO_2)(SO_4)_3]$	17*k*	(13)
$K_6[(UO_2)B_{16}O_{24}(OH)_8](H_2O)_{12}$	$[(UO_2)B_{16}O_{24}(OH)_8]$	17*l*	(14)
$[(UO_2)_2(OH)_2(NO_3)_2](H_2O)_4$	$[(UO_2)_2(OH)_2(NO_3)_2]$	17*m*	(15)
Chains and ribbons			
$Na_4[(UO_2)O_3]$	$[(UO_2)O_3]$	18*a*	(1)
Walpurgite	$[(UO_2)(AsO_4)_2]$	18*b*	(16)
$Na_4[(UO_2)(CrO_4)_3]$	$[(UO_2)(CrO_4)_3]$	18*c*	(17)
$[(UO_2)(CrO_4)(H_2O)_2](H_2O)$	$[(UO_2)(CrO_4)(H_2O)_2]$	18*d*	(18)
$K_2[(UO_2)(CrO_4)(IO_3)_2]$	$[(UO_2)(CrO_4)(IO_3)_2]$	18*e*	(19)
$Rb[(UO_2)(CrO_4)(IO_3)(H_2O)]$	$[(UO_2)(CrO_4)(IO_3)(H_2O)]$	18*f*	(19)
$Rb_6[(UO_2)_2O(MoO_4)_4]$	$[(UO_2)_2O(MoO_4)_4]$	18*g*	(20)
$Sr[(UO_2)(SeO_3)_2](H_2O)_2$	$[(UO_2)(SeO_3)_2]$	18*h*	(21)
Parsonsite	$[(UO_2)(PO_4)_2]$	18*i*	(22)
Moctezumite	$[(UO_2)O_3]$	18j	(23)
$[(UO_2)(IO_3)_2]$	$[(UO_2)(IO_3)_2]$	18*k*	(24)
Sheets			
$Cs_2[(UO_2)(SeO_4)_2\ (H_2O)](H_2O)$	$[(UO_2)(SeO_4)_2\ (H_2O)]$	19*b*	(25)
$(NH_4)_2[(UO_2)(SO_4)_2\ (H_2O)](H_2O)$	$[(UO_2)(SO_4)_2\ (H_2O)]$	19*c*	(26)
$Cs_2[(UO_2)(MoO_4)_2]$	$[(UO_2)(MoO_4)_2]$	19*d*	(27)
$Na_2[(UO_2)(MoO_4)_2]$	$[(UO_2)(MoO_4)_2]$	19*e*	(28)
$Mg[(UO_2)_3(MoO_4)_4](H_2O)_8$	$[(UO_2)_3(MoO_4)_4]$	19*f*	(29)
$K_2[(UO_2)_2\ (CrO_4)_3(H_2O)_2](H_2O)_4$	$[(UO_2)_2\ (CrO_4)_3(H_2O)_2]$	19*g*	(30)
$K_4[(UO_2)_3(CrO_4)_5](H_2O)_8$	$[(UO_2)_3(CrO_4)_5]$	19*h*	(30)
Francevillite	$[(UO_2)_2\ (V_2O_8)]$	21*b*	(31)
Ianthanite	$[U_2^{4+}(UO_2)_4O_6(OH)_4(H_2O)_4]$	21*d*	(32)
Iriginite	$[(UO_2)M_2O_7(H_2O)_2]$	21*f*	(33)
Sayrite	$[(UO_2)_5O_6(OH)_2]$	21*h*	(34)
$Pb_3(UO_2)_{11}O_{14}$	$[(UO_2)_{11}O_{14}]$	21*j*	(35)
Curite	$[(UO_2)_8O_8(OH)_6]$	21*l*	(36)
α-UO_3	$[UO_3]$	22*b*	(37)
Rutherfordine	$[(UO_2)(CO_3)]$	22*d*	(38)
$K_2[(UO_2)(W_2O_8)]$	$(UO_2)(W_2O_8)]$	22*f*	(39)
$[(UO_2)(B_2O_3)O]$	$[(UO_2)(B_2O_3)O]$	22*h*	(40)
$Cs[UV_3O_{11}]$	$Cs[UV_3O_{11}]$	22*j*	(41)
$[(UO_2)(Sb_2O_4)]$	$[(UO_2)(Sb_2O_4)]$	22*l*	(42)

Table 2 (*contd.*)

Name	Formula unit	Fig.	Ref.
Frameworks			
$(NH_4)_3(H_2O)_2[(UO_2)_{10}O_{10}(OH)]\{(UO_4)(H_2O)_2\}$	$[(UO_2)_{10}O_{10}(OH)]$	23*a*	(43)
$Pb_2(H_2O)[(UO_2)_{10}UO_{12}(OH)_6(H_2O)_6]$	$[(UO_2)_{10}UO_{12}(OH)_6(H_2O)_6]$	23*b*	(44)
$KNa_3[(UO_2)_2(Si_4O_{10})_2](H_2O)_4$	$[(UO_2)_2(Si_4O_{10})_2]$	23*c*	(45)
Soddyite	$[(UO_2)_2(SiO_4)(H_2O)_2]$	23*d*	(46)
Weeksite	$[(UO_2)_2(Si_5O_{13})]$	23*e*	(47)
$Na_2[(UO_2)(SiO_4)]$	$[(UO_2)(SiO_4)]$	23*f*	(48)
$RbNa[(UO_2)(Si_2O_6)](H_2O)$	$[(UO_2)(Si_2O_6)]$	23*g*	(49)
$[(UO_2)_3(PO_4)_2](H_2O)_4$	$[(UO_2)_3(PO_4)_2]$	23*h*	(50)
$(UO_2)[(UO_2)(AsO_4)]_2(H_2O)_4$	$[(UO_2)_3(AsO_4)_2]$	23*i*	(51)
$(UO_2)[(UO_2)(VO_4)]_2(H_2O)_5$	$[(UO_2)_3(AsO_4)_2]$	23*j*	(52)

References: (1) Wolf and Hoppe (1986); (2) Åberg (1969); (3) Åberg (1978); (4) Åberg (1976); (5) Fischer (2003); (6) Krivovichev and Burns (2002*a*); (7) Krivovichev and Burns (2001*a*); (8) Hayden and Burns (2002); (9) Kapshukov *et al.* (1971); (10) Mueller *et al.* (1971); (11) Shuvalov and Burns (2003); (12) Mereiter (1982*a*); (13) Mikhailov *et al.* (1977); (14) Behm (1985); (15) Perrin (1976); (16) Mereiter (1982*b*); (17) Krivovichev and Burns (2003*a*); (18) Krivovichev and Burns (2003*b*); (19) Sykora *et al.* (2002); (20) Krivovichev and Burns (2002*b*); (21) Almond *et al.* (2002); (22) Locock *et al.* (2005); (23) Swihart *et al.* (1993); (24) Bean *et al.* (2001); (25) Mikhailov *et al.* (2001); (26) Niinistö *et al.* (1978); (27) Krivovichev and Burns (2005); (28) Krivovichev *et al.* (2001); (29) Tabachenko *et al.* (1983); (30) Krivovichev and Burns (2003*c*); (31) Mereiter (1986); (32) Burns *et al.* (1997*b*); (33) Krivovichev and Burns (2000*a*); (34) Piret *et al.* (1983); (35) Ijdo (1993); (36) Li and Burns (2000*a*); (37) Loopstra and Cordfunke (1966); (38) Finch *et al.* (1999); (39) Obbade *et al.* (2003); (40) Gasperin (1987); (41) Duribreux *et al.* (1999); (42) Sykora *et al.* (2004); (43) Li *et al.* (2001*a*); (44) Li and Burns (2000*b*); (45) Burns *et al.* (2000); (46) Demartin *et al.* (1992); (47) Jackson and Burns (2001); (48) Shashkin *et al.* (1974); (49) Wang *et al.* (2002); (50) Locock and Burns (2002*a*); (51) Locock and Burns (2002*b*); (52) Saadi *et al.* (2000).

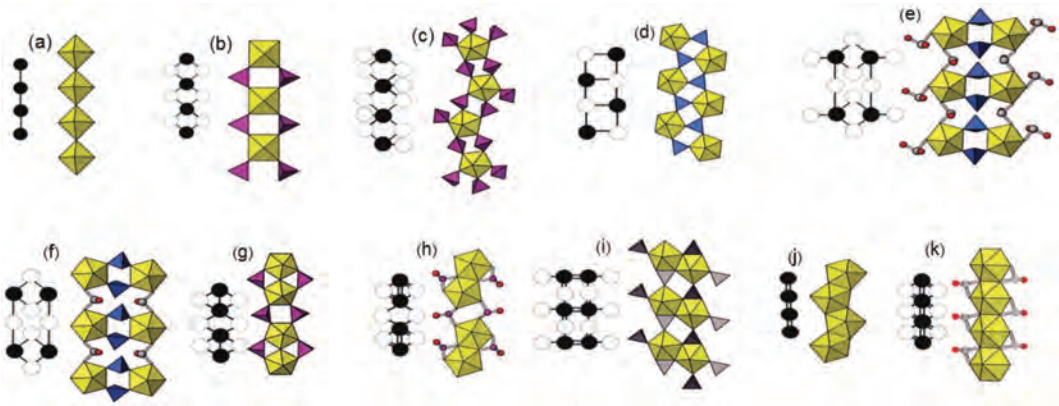

FIG. 18. Selected chains from uranyl structures; (*a*) chain of corner-sharing octahedra in $Na_4[(UO_2)O_3]$; (*b*) chain of corner-sharing octahedra and (AsO_4) tetrahedra in walpurgite; (*c*) chain of corner-sharing pentagonal bipyramids and (CrO_4) tetrahedra in $Na_4[(UO_2)(CrO_4)_3]$; (*d*) ribbon of corner-sharing pentagonal bipyramids and (CrO_4) tetrahedra in $[(UO_2)(CrO_4)(H_2O)_2](H_2O)$; (*e*) ribbon of corner-sharing pentagonal bipyramids, (CrO_4) tetrahedra and (IO_3) triangles in $K_2[(UO_2)(CrO_4)(IO_3)_2]$; (*f*) ribbon of corner-sharing pentagonal bipyramids, (CrO_4) tetrahedra and (IO_3) triangles in $Rb[(UO_2)(CrO_4)(IO_3)(H_2O)]$; (*g*) chain of dimers of corner-sharing pentagonal bipyramids and (MoO_4) tetrahedra in $Rb_6[(UO_2)_2O(MoO_4)_4]$; (*h*) chain of dimers of edge-sharing pentagonal bipyramids and (SeO_3) trigonal pyramids in $Sr[(UO_2)(SeO_3)_2](H_2O)_2$; (*i*) ribbon of dimers of edge-sharing pentagonal bipyramids and (PO_4) tetrahedra in synthetic parsonsite; (*j*) chain of pentagonal bipyramids in moctezumite; (*k*) chain of edge-sharing hexagonal bipyramids and (IO_3) triangles in $[(UO_2)(IO_3)_2]$.

of dimers of corner-sharing ($U^{6+}O_2\varphi_5$) polyhedra decorated by tetrahedral oxyanions that are linked into a chain by sharing corners with other tetrahedral oxyanions, and is intermediate between chains involving isolated ($U^{6+}O_2\varphi_n$) polyhedra and chains involving continuous corner-sharing ($U^{6+}O_2\varphi_n$) polyhedra (which have not been observed as yet). There is one chain and one ribbon involving dimers of edge-sharing ($U^{6+}O_2\varphi_5$) polyhedra linked into chains-ribbons by oxyanion groups. These chains-ribbons involve linkage of dimers through sharing vertices with (TO_3) oxyanions (Fig. 18*h*) and through sharing of both edges and vertices with (TO_3) oxyanions (Fig. 18*i*). There are two chains involving continuous edge sharing between ($U^{6+}O_2\varphi_n$) polyhedra: a simple chain involving ($U^{6+}O_2\varphi_5$) polyhedra (Fig. 18*j*) and the analogous chain decorated by (TO_3) oxyanions sharing edges and corners with the ($U^{6+}O_2\varphi_5$) polyhedra (Fig. 18*k*).

Uranyl structures based on sheets of polyhedra

There are 204 uranyl sheet-structures at last count (Burns, 2005), and their number and complexity preclude comprehensive consideration here. These are considered in two distinct ways by Burns (2005): (1) as connectivities between ($U^{6+}O_2\varphi_n$) polyhedra and other oxyanions (Krivovichev, 2004; Krivovichev and Burns, 2003*b*); and (2) as sheet anion-topologies (Miller *et al.*, 1996).

First, consider corner-sharing connectivities between ($U^{6+}O_2\varphi_n$) polyhedra and other oxyanions. Let us represent the polyhedra of a sheet by a chromatic graph where the coloured vertices represent different polyhedra, and the edges represent corner sharing between those polyhedra. The number of polyhedra which share corners with a polyhedron is defined as the connectedness, **s**, of that polyhedron, and Krivovichev (2004) wrote the resulting graph in terms of the vertices and their connectivity. The example {3.6.3.6} is shown in Fig. 19*a* where the symbol {3.6.3.6} represents the sequence of vertices around each four-membered circuit (closed path) in the graph. Krivovichev (2004) designated {3.6.3.6} as a 'parent graph', and derived 29 subgraphs of {3.6.3.6} that correspond to known uranyl structures (Burns, 2005). A subset of these are illustrated in Fig. 19, together with their graphs and some of the corresponding structures (most of them synthetic compounds) are listed in Table 2.

In $Cs_2[(UO_2)(SeO_4)_2(H_2O)](H_2O)$ (Fig. 19*b*, Table 2), the ratio of ($U^{6+}O_2\varphi_5$) polyhedra to (SeO_4) tetrahedra is 1:2 and each tetrahedron shares two vertices with pentagonal bipyramids. The result is one unshared meridional vertex per pentagonal bipyramid and this must be an (H_2O) group (as required by the valence-sum rule). Several structures in Fig. 19 show an (H_2O) group as a ligand in a pentagonal bipyramid: $(NH_4)_2[(UO_2)(SO_4)_2(H_2O)](H_2O)$, Fig. 19*c*; and $K_2[(UO_2)_2(CrO_4)_3(H_2O)_2](H_2O)_4$, Fig. 19*g*, as indicated by the (H_2O) group within the square brackets of the structural unit in the formulae (Table 2). Other structures have all the vertices of the pentagonal bipyramid linked to tetrahedra: $Cs_2[(UO_2)(MoO_4)_2]$, Fig. 19*d*; $Na_2[(UO_2)(MoO_4)_2]$, Fig. 19*e*; $Mg[(UO_2)_3(MoO_4)_4](H_2O)_8$, Fig. 19*f*; $K_4[(UO_2)_3(CrO_4)_5](H_2O)_8$, Fig. 19*h*, as indicated by the absence of (H_2O) groups within the square brackets of the structural unit in the formulae (Table 2). There is an interesting interplay between the stoichiometry of the major polyhedra in the structural unit and the number of vertices shared between the tetrahedra and the pentagonal bipyramids. In the latter four structures (Fig. 19*d*,*e*,*f*,*h*), all vertices of the pentagonal bipyramids link to tetrahedra. If the ratio of the pentagonal bipyramids to the tetrahedra is n:m, then the number of shared vertices in the sheet is 5n, the number of tetrahedron vertices is 4m and $4m \geqslant 5n$. As n and m are integers, we may derive the connectedness of the tetrahedra with variation in stoichiometry. If n:m = 1:2, the connectedness of the tetrahedra are $^{[2]}T$ and $^{[3]}T$ (Fig. 19*d*,*e*,*f*). If n:m = 3:5, the connectedness of the tetrahedra are $^{[3]}T$ (Fig. 19*h*).

Consider next the representation and classification of sheet uranyl structures as sheet anion-topologies (Miller *et al.*, 1996; Burns *et al.*, 1996). Here, the focus is on the anions of the sheet that form a plane through the centre of the sheet; these anions do not include uranyl O-anions or apical anions of constituent oxyanion groups. Anions belonging to the same coordination polyheda are connected by lines, the anions are then removed from the representation, and the resulting net represents the sheet-anion topology, a two-dimensional tiling of space by triangles, squares, pentagons and hexagons (Burns, 2005). Note that these nets can be quite corrugated, but the linkage between vertices is approximately planar and there is no linkage between adjacent nets. Sheets can be constructed as assemblies of parallel chains; Miller *et al.* (1996) showed that

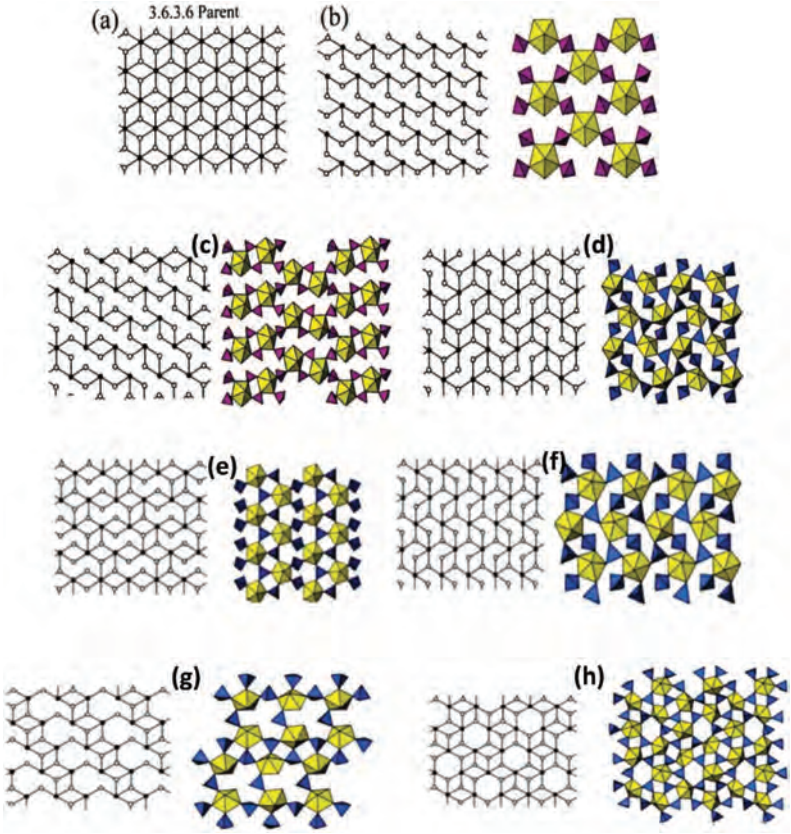

FIG. 19. Selected uranyl-oxysalt sheets based on removing edges from the parent graph {3.6.3.6}: (*a*) the parent graph {3.6.3.6}; (*b*) the sheet in $Cs_2[(UO_2)(SeO_4)_2(H_2O)](H_2O)$, with one unshared meridional vertex per pentagonal bipyramid; (*c*) the sheet in $(NH_4)_2[(UO_2)(SO_4)_2(H_2O)](H_2O)$; (*d*) the sheet in $Cs_2[(UO_2)(MoO_4)_2]$; (*e*) the sheet in $Na_2[(UO_2)(MoO_4)_2]$; (*f*) the sheet in $Mg[(UO_2)_3(MoO_4)_4](H_2O)_8$; (*g*) the sheet in $K_2[(UO_2)_2(CrO_4)_3(H_2O)_2](H_2O)_4$; (*h*) the sheet in $K_4[(UO_2)_3(CrO_4)_5](H_2O)_8$.

sheet-anion topologies can be derived from a small number of chains (Fig. 20*a*), forming chain-stacking sequences. These chains can be assembled orthogonal to their length to form a sheet-anion topology; an example involving triangles, squares and pentagons is shown in Fig. 20*b*. Figure 21 shows selected sheets based on anion topologies containing triangles, squares and pentagons; the corresponding compounds are listed in Table 2. The anion topology of **francevillite** (Fig. 21*a*) forms the basis of 12 structures (Burns, 2005), including **francevillite** (Fig. 21*b*). The pentagons correspond to uranyl pentagonal bipyramids and the squares correspond to square pyramids (e.g. VO_5, NbO_5, CrO_5), the latter forming dimers in which the apical vertices point in different directions relative to the plane of the sheet. The anion topology of Figs 21*c*,*d* corresponds to the structure of β-U_3O_8 and **wyartite** (which contains U^{5+}; Burns and Finch, 1999) and **ianthinite** (which may contain U^{5+}; Burns *et al.*, 1997*b*; Burns, 2005). In the **iriginite** anion topology (Fig. 21*e*), pentagonal bipyramids share edges with dimers of edge-sharing ($M\varphi_6$) octahedra in **iriginite** (Fig. 21*f*). In the **sayrite** anion topology (Fig. 21*g*), uranyl pentagonal bipyramids share edges with uranyl square bipyramids, forming a dense sheet of edge-sharing polyhedra (Fig. 21*h*). The anion topology of Fig. 21*i* is found in synthetic $Pb_3(UO_2)_{11}O_{14}$) (Fig. 21*j*) and its Sr analogue, and is unusual in that some of the pentagonal bipyramids are occupied by Pb^{2+} or Sr. The anion topology of Fig. 21*k* describes a sheet which contains edge-sharing uranyl pentagonal bipyramids and square uranyl bipyramids,

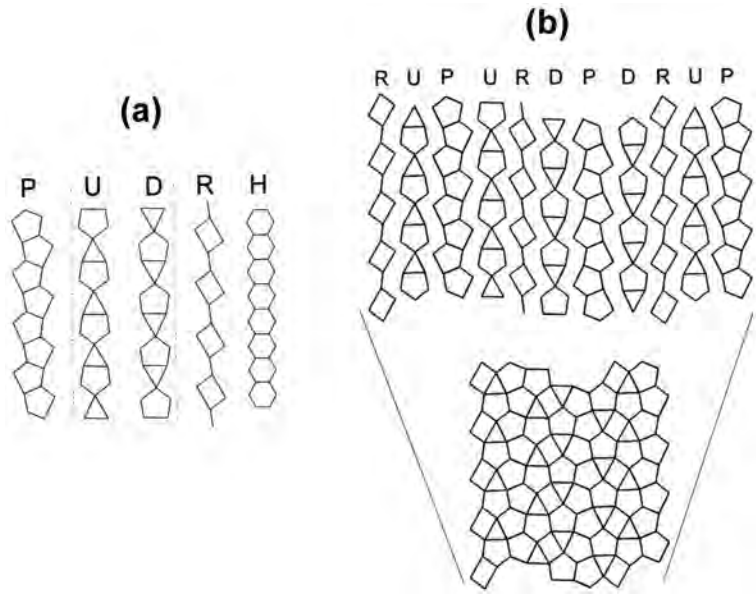

FIG. 20. Construction of sheet anion topologies from simple chains of polygons; (*a*) chain types required; (*b*) construction of a sheet anion topology using a chain-stacking sequence. After Burns (1999).

and the corresponding sheet in **curite** (Fig. 21*l*) shows extensive edge sharing of these polyhedra.

Selected sheets based on anion topologies containing hexagons are shown in Fig. 22; the corresponding compounds are listed in Table 2. The anion topology of Fig. 22*a* forms the basis of 10 structures (Burns, 2005), including α-UO_3 (Fig. 22*b*), a simple sheet in which all meridional edges of the hexagonal bipyramids are shared with each other. The anion topology of Fig. 22*c* corresponds to the structure of **rutherfordine** (Fig. 22*d*) in which each uranyl hexagonal bipyramid shares two edges with (CO_3) groups. The anion topology of Fig. 22*e* corresponds to the structure of four tungstates including $K_2[(UO_2)(W_2O_8)]$ (Fig. 22*f*) in which chains of

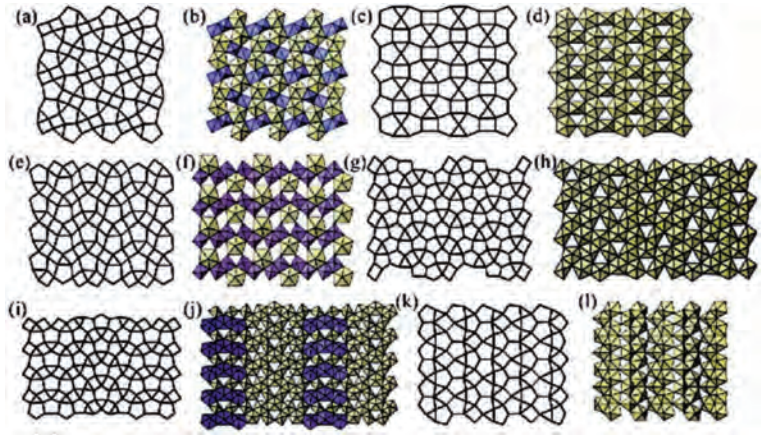

FIG. 21. Selected sheets (of uranyl polyhedra and polyhedra containing other high-valence cations) based on anion topologies that contain triangles, squares and pentagons; (*a*,*b*) topology and sheet in francevillite; (*c*,*d*) topology and sheet in ianthanite; (*e*,*f*) topology and sheet in iriginite; (*g*,*h*) topology and sheet in sayrite; (*i*,*j*) topology and sheet in $Pb_3(UO_2)_{11}O_{14}$; (*k*,*l*) topology and sheet in curite. After Burns (2005).

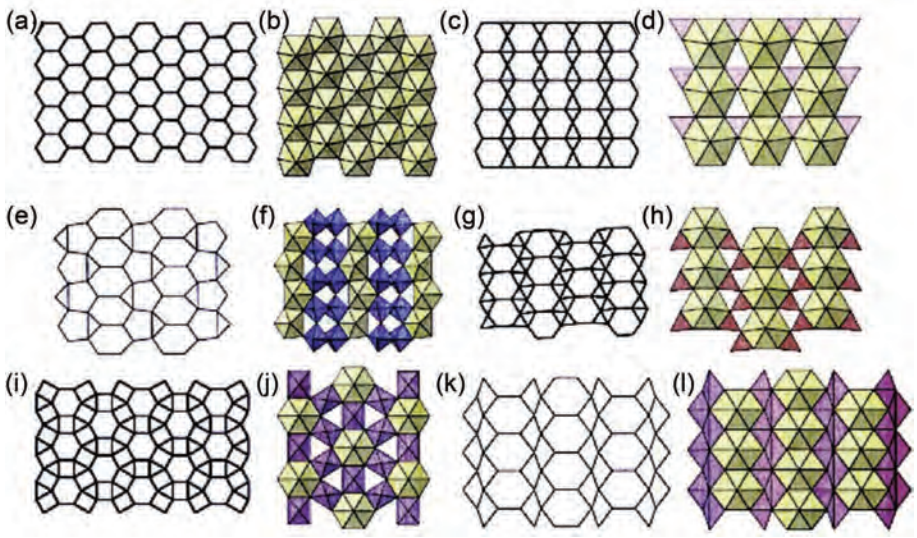

FIG. 22. Selected sheets (of uranyl polyhedra and polyhedra containing other high-valence cations) based on anion topologies that contain hexagons; (*a*,*b*) topology and sheet in α-UO_3; (*c*,*d*) topology and sheet in rutherfordine; (*e*,*f*) topology and sheet in $K_2[(UO_2)(W_2O_8)]$; (*g*,*h*) topology and sheet in $[(UO_2)(B_2O_3)O]$; (*i*,*j*) topology and sheet in $Cs[UV_3O_{11}]$; (*k*,*l*) topology and sheet in $[(UO_2)(Sb_2O_4)]$. From Burns (2005).

edge-sharing pentagonal bipyramids are linked into a sheet by ribbons of vanadate groups. In Fig. 22*g*, the anion topology corresponds to the sheet in $[(UO_2)(B_2O_3O)]$ (Fig. 22*h*) where chains of edge-sharing hexagonal bipyramids are linked into a sheet by chains of corner-sharing (BO_3) groups. The anion topology of Fig. 22*i* forms the basis of three structures (Burns, 2005), including $Cs[UV_3O_{11}]$ (Fig. 22*j*), in which each hexagonal bipyramid shares all meridional edges with vanadate groups and each vanadate group shares edges with two uranyl hexagonal bipyramids. The anion topology of Fig. 22*k* forms the basis of the structure of $[(UO_2)(Sb_2O_4)]$ (Fig. 22*l*), in which chains of edge-sharing hexagonal bipyramids are linked into a sheet by Sb^{3+} cations.

Uranyl sheets are classified in two different ways, depending on the types of polyhedron connectivity that they display. This is not entirely satisfactory from an ideal viewpoint, but the extensive edge-sharing character of several different polyhedra make a single approach rather difficult.

Uranyl structures based on frameworks of polyhedra

These are illustrated in Fig. 23 and a selection of the corresponding structures is listed in Table 2. $(NH_4)_3(H_2O)_2[(UO_2)_{10}O_{10}(OH)]\{(UO_4)(H_2O)_2]\}$ is a framework of uranyl pentagonal bipyramids, square bipyramids and distorted octahedra (Fig. 23*a*); within the framework, there are sheets topologically identical to those in **ianthinite** (Fig. 21*d*), linked by dimers of bipyramids between the sheets. The synthetic compound $Pb_2(H_2O)[(UO_2)_{10}UO_{12}(OH)_6(H_2O)_6]$ consists of dense regions of edge- and vertex-sharing uranyl pentagonal and square bipyramids and a distorted octahedron (Fig. 23*b*) with Pb^{2+} in channels through the framework. $KNa_3[(UO_2)_2(Si_4O_{10})_2](H_2O)_4$ comprises sheets of four-membered rings of tetrahedra linked by sharing tetrahedron vertices (Fig. 23*c*, right), and these sheets are linked by uranyl square bipyramids (Fig. 23*c*, left). **Soddyite**, $[(UO_2)_2(SiO_4)(H_2O)_2]$, contains staggered chains of edge-sharing pentagonal bipyramids (Fig. 23*d*); these chains are cross-linked by silicate tetrahedra and the vertex *trans* to the shared edge is an (H_2O) group. In **weeksite**, $K_2[(UO_2)_2(Si_3O_{13})](H_2O)$ chains of edge-sharing uranyl bipyramids are cross-linked into sheets by chains of silicate tetrahedra (Fig. 23*e*) that also link orthogonally to adjacent sheets to form a framework. In $Na_2[(UO_2)(SiO_4)]$, each ($U^{6+}O_6$) octahedron shares four vertices with silicate tetrahedra to form a framework (Fig. 23*f*), with Na in the interstices. In $RbNa[(UO_2)(Si_2O_6)](H_2O)$,

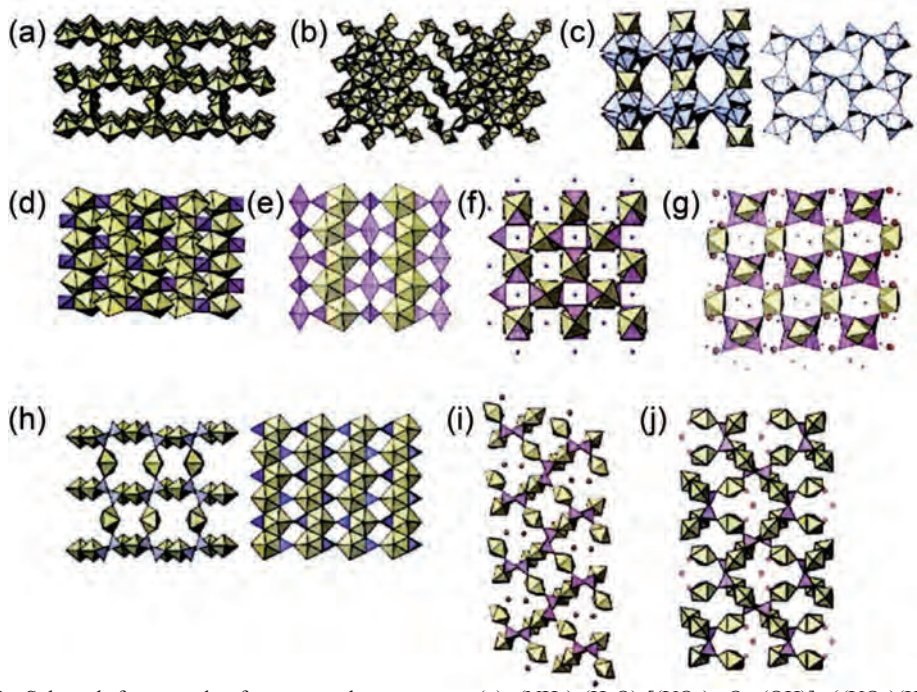

FIG. 23. Selected frameworks from uranyl structures; (*a*) $(NH_4)_3(H_2O)_2[(UO_2)_{10}O_{10}(OH)]$ $\{(UO_4)(H_2O)_2$, a framework of uranyl pentagonal bipyramids, square bipyramids and distorted octahedra; (*b*) $Pb_2(H_2O)[(UO_2)_{10}UO_{12}(OH)_6(H_2O)_6]$, a framework of edge- and vertex-sharing uranyl pentagonal and square bipyramids and a distorted octahedron; (*c*) $KNa_3[(UO_2)_2(Si_4O_{10})_2]$ $(H_2O)_4$ with sheets of four-membered rings of tetrahedra linked by sharing tetrahedron vertices (right), linked by uranyl square bipyramids (left); (*d*) soddyite; (*e*) weeksite; (*f*) $Na_2[(UO_2)(SiO_4)]$ in which each $(U^{6+}O_6)$ octahedron shares four verticies with silicate tetrahedra to form a framework; (*g*) $RbNa[(UO_2)(Si_2O_6)](H_2O)$ in which four-membered rings of silicate tetrahedra form sheets by sharing corners with uranyl square bipyramids; (*h*) $[(UO_2)_3(PO_4)_2](H_2O)_4$ with chains of edge-sharing uranyl pentagonal bipyramids cross-linked into sheets (right) by phosphate tetrahedra; these sheets are linked into a framework by additional uranyl pentagonal bipyramids (left). (*i*) $[(UO_2)_3(AsO_4)_2](H_2O)_4$; (j) $[(UO_2)(UO_2)_3(AsO_4)_2](H_2O)_5$, similar to Fig. 23*i* but with a prominent corrugation in the uranyl-arsenate sheets. After Burns (2005).

four-membered rings of silicate tetrahedra (*cf.* $KNa_3[(UO_2)_2(Si_4O_{10})_2](H_2O)_4$, Fig. 23*c*, right) are linked into sheets by sharing corners with uranyl square bipyramids (Fig. 23*g*), with alkalis in the interstices. $[(UO_2)_3(PO_4)_2](H_2O)_4$ (Fig. 23*h*) contains chains of edge-sharing uranyl pentagonal bipyramids that are cross-linked into sheets (Fig. 23*h*, right) by phosphate tetrahedra; the resulting sheets are linked into a framework by additional uranyl pentagonal bipyramids between the sheets (Fig. 23*h*, left). The structure of $[(UO_2)_3(AsO_4)_2](H_2O)_4$ is very similar, but a change in the unit cell leads to the constituent sheets being inclined (Fig. 23*i*, cf. $[(UO_2)_3(PO_4)_2](H_2O)_4$). $[(UO_2)_3(AsO_4)_2](H_2O)_5$ has a very similar structure, but the additional (H_2O) group leads to a prominent corrugation in the uranyl-arsenate sheets (Fig. 23*j*).

Phosphate minerals

The cation P^{5+} occurs in tetrahedral coordination to O and the mean bond valence in the $(PO_4)^{3-}$ oxyanion is 5/4 = 1.25 vu. Linkage of phosphate groups results in an incident bond valence of 2.50 vu at the linking anion, violating the valence-sum rule, and this linkage is known only in three minerals. However, phosphate may polymerize with tetrahedrally coordinated oxyanions that have mean bond valences $\leqslant 0.75$ vu: (AlO_4), (BO_4), (BeO_4) and (LiO_4) groups. In addition, P−O bonds in specific structural

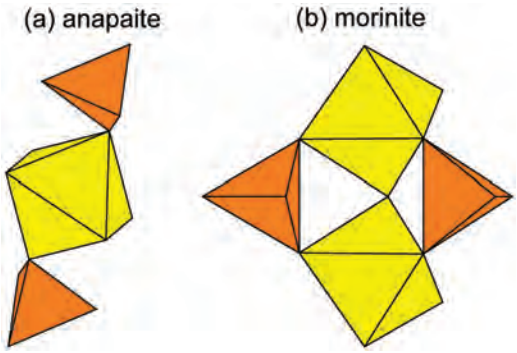

FIG. 24. Selected clusters from phosphate structures; (*a*) anapaite; (*b*) morinite. Orange = ($P\varphi_4$); yellow = ($M\varphi_6$) (M = tetra-, tri- or di-valent cation).

arrangements may have bond valences somewhat less that 1.25 vu, and (PO_4) groups may polymerize with (SiO_4) groups. Phosphate minerals show all of these polymerizations, in accord with the valence-sum rule. Hawthorne (1998) gave a brief hierarchical scheme for the phosphate minerals, and Huminicki and Hawthorne (2002*a*) gave a much more comprehensive scheme that subdivides the phosphate minerals into the following groups: (1) phosphate groups with other tetrahedra; (2) phosphate with divalent- and trivalent-metal octahedra; and (3) phosphate with non-octahedral cation polyhedra. Here I will focus on group (2) as this contains the most numerous and diverse structure types; selected minerals of group (2) are listed in Table 3.

Phosphate structures based on isolated tetrahedra and octahedra

M T linkage. In these minerals, the (PO_4) groups and ($M\varphi_6$) octahedra are linked by H bonding, and hence must involve $M(H_2O)_6$ groups and ($P\varphi_4$) tetrahedra: **strüvite** and **phosphorrösslerite** (Table 3).

Phosphate structures based on clusters of tetrahedra and octahedra

M−T linkage. Linkages of this type are shown in Fig. 24. In the $[M(TO_4)_2\varphi_4]$ cluster in **anapaite**, two (PO_4) groups link to *trans* vertices of an ($Fe^{2+}\varphi_6$) octahedron, where $M = Fe^{2+}$, T = P and $\varphi = (H_2O)$ (Fig. 24*a*). The atomic arrangement in **schertelite** is similar to that in **anapaite** (and also the sulfate minerals **bloedite**, $Na_2[Mg(SO_4)_2(H_2O)_4]$ and **leonite**, $K_2[Mn^{2+}(SO_4)_2(H_2O)_4]$, Hawthorne, 1985*b*).

M−M, M−T linkage. The $[M_2(TO_4)_2\varphi_7]$ cluster in **morinite** consists of two ($Al\varphi_6$) octahedra linked through one vertex to form a dimer and (two pairs of) vertices from each octahedron, *cis* to their common vertex, are linked by (PO_4) groups (Fig. 24*b*). This $[M_2(TO_4)_2\varphi_7]$ cluster is the basis of a short hierarchy of phosphate minerals of higher connectivity: **minyulite**, **olmsteadite**, **hureaulite**, **phosphoferrite**, **kryzhanovskite**, **melonjosephite** and **whitmoreite** (Hawthorne, 1979).

Phosphate structures based on chains and ribbons of tetrahedra and octahedra

M−T linkage. The structural unit of **bøggildite**, a rare phosphate-aluminofluoride mineral, consists of a chain of alternating (PO_4) tetrahedra and (AlO_2F_4) octahedra, decorated by ($AlOF_5$) octahedra linked to the (PO_4) groups (Fig. 25*a*) that are three-connected and point up and down alternately along the length of the chain.

The minerals of the **collinsite** and **fairfieldite** groups are both based on a general $[M(TO_4)_2\varphi_2]$ chain that is formed of alternating ($M^{2+}O_4\{H_2O\}_2$) octahedra and pairs of (PO_4) tetrahedra (Fig. 25*b*), with the (H_2O) groups in a *trans* arrangement about the divalent cation. The repeat distance along the length of the chain is ~5.45 Å, and this is reflected in the *c*-dimensions of these minerals. The two structure types differ in the details of their H bonding.

M−M, M−T linkage. In **childrenite** (and **eosphorite**), ($Al\varphi_6$) octahedra link through pairs of *trans* vertices to form $[Al\varphi_5]$ chains that are decorated by (PO_4) groups that link adjacent octahedra and are arranged in a staggered fashion along the length of the $[M(TO_4)\varphi_3]$ chain (Fig. 25*c*). In **tancoite**, ($Al\varphi_6$) octahedra link through one set of *trans* vertices to form an $[Al\varphi_5]$ chain in which adjacent octahedra are linked by pairs of (PO_4) tetrahedra that point alternately up and down orthogonal to the chain direction, giving rise to an $[Al(PO_4)_2(OH)]$ chain (Fig. 25*d*); topologically identical chains occur in **jahnsite**, **overite** and **sinkankasite**.

M=M, M−T linkage. In **bearthite**, ($Al\varphi_6$) octahedra share one set of *trans* edges with adjacent octahedra to form an $[Al\varphi_4]$ chain. Adjacent octahedra are bridged by (PO_4) tetrahedra to form a decorated chain of the general

TABLE 3. Phosphate minerals, structural units and types of polymerization.

Mineral	Structural unit	Fig.	Ref.
Isolated polyhedra			
Strüvite	$[Mg(H_2O)_6][PO_4]$	–	(1)
Phosphorrösslerite	$[Mg(H_2O)_6][PO_3(OH)]$	–	(2)
Clusters			
Anapaite	$[Fe^{2+}(PO_4)_2(H_2O)_4]$	24*a*	(3)
Schertelite	$[Mg(PO_3\{OH\}_2(H_2O)_4]$	24*a*	(4)
Morinite	$[Al_2(PO_4)_2F_4(OH)(H_2O)_2]$	24*b*	(5)
Chains and ribbons			
Bøggildite	$[Al_2(PO_4)F_9]$	25*a*	(6)
Collinsite	$[Mg(PO_4)_2(H_2O)_2]$	25*b*	(7)
Fairfieldite	$[Mn^{2+}(PO_4)_2(H_2O)_2]$	25*b*	(7)
Childrenite	$[Al(PO_4)(OH)_2(H_2O)]$	25*c*	(8)
Eosphorite	$[Al(PO_4)(OH)_2(H_2O)]$	25*c*	(9)
Tancoite	$[Al(PO_4)_2(OH)]$	25*d*	(10)
Jahnsite	$[Fe^{3+}(PO_4)_2(OH)]_2$	25*d*	(11)
Overite	$[Al(PO_4)_2(OH)]_2$	25*d*	(12)
Sinkankasite	$[Al(PO_3\{OH\})_2(OH)]$	25*d*	(13)
Bearthite	$[Al(PO_4)_2(OH)]$	25*e*	(14)
Brackebuschite	$[Mn^{3+}(VO_4)_2(OH)]$	25*e*	(15)
Vauquelinite	$[Cu^{2+}(PO_4)(CrO_4)(OH)]$	25*e*	(16)
Sheets			
Brianite	$[Mg(PO_4)_2]$	26*a*	(17)
Minyulite	$[Al_2(PO_4)_2F(H_2O)_4]$	26*b*	(18)
Laueite	$[Fe^{+}(PO_4)_2(OH)_2(H_2O)_2]$	26*c*	(19)
Metavauxite	$[Al(PO_4)(OH)(H_2O)]_2$	26*d*	(20)
Montgomeryite	$[MgAl_4(PO_4)_6(OH)_4(H_2O)]$	26*e*	(21)
Mitryaevaite	$[Al_5(PO_4)_2(PO_3\{OH\})_2F_2(OH)_2(H_2O)_8]$	26*f*	(22)
Bermanite	$[Mn^{3+}(PO_4)(OH)]_2$	26*g*	(23)
Ercitite	$[Mn^{3+}(PO_4)(OH)]_2$	26*g*	(24)
Mitridatite	$[Fe^{+}(PO_4)_3O_2]$	26*h*	(25)
Frameworks			
Variscite	$[Al(PO_4)(H_2O)_2]$	27*a*	(26)
Metavariscite	$[Al(PO_4)(H_2O)_2]$	27*b*	(27)
Phosphosiderite	$[Fe^{3+}(PO_4)(H_2O)_2]$	27*b*	(28)
Strengite	$[Fe^{3+}(PO_4)(H_2O)_2]$	27*a*	(28)
Libethenite	$[Cu_2(PO_4)(OH)]$	27*d*	(30)
Palermoite	$[Al(PO_4)(OH)]_4$	27*e*	(31)
Burangaite	$[Fe^{2+}Al_5(PO_4)_4(OH)_6(H_2O)_2]$	27*f*	(32)
Wicksite	$[Fe^{2+}_4\ MgFe^{3+}(PO_4)_6]$	27*g*	(33)
Seamanite	$[Mn^{2+}_3(PO_4)(B\{OH\}_4)(OH)_2]$	27*h*	(34)
Sarcopside	$[Fe^{2+}_3(PO_4)_2]$	–	(35)

(1) Abbona *et al.* (1984); (2) Street and Whitaker (1973); (3) Catti *et al.* (1979); (4) Khan and Baur (1972); (5) Hawthorne (1979); (6) Hawthorne (1982); (7) Herwig and Hawthorne (2006); (8) Giuseppetti and Tadini (1984); (9) Hoyos *et al.* (1993); (10) Hawthorne (1983*b*); (11) Moore and Araki (1974*b*); (12) Moore and Araki (1977*a*); (13) Burns and Hawthorne (1995); (14) Chopin *et al.* (1993); (15) Foley *et al.* (1997); (16) Fanfani and Zanazzi (1968); (17) Moore (1975); (18) Kampf (1977); (19) Moore (1965); (20) Baur and Rama Rao (1967); (21) Fanfani *et al.* (1976); (22) Cahill *et al.* (2001); (23) Kampf and Moore (1976); (24) Cooper *et al.* (2009*a*); (25) Moore and Araki (1977*b*); (26) Kniep *et al.* (1977); (27) Kniep and Mootz (1973); (28) Moore (1966); (29) Guy and Jeffrey (1966); (30) Cordsen (1978); (31) Moore and Araki (1975); (32) Selway *et al.* (1997); (33) Cooper and Hawthorne (1997); (34) Huminicki and Hawthorne (2002*b*); (35) Warner *et al.* (1992).

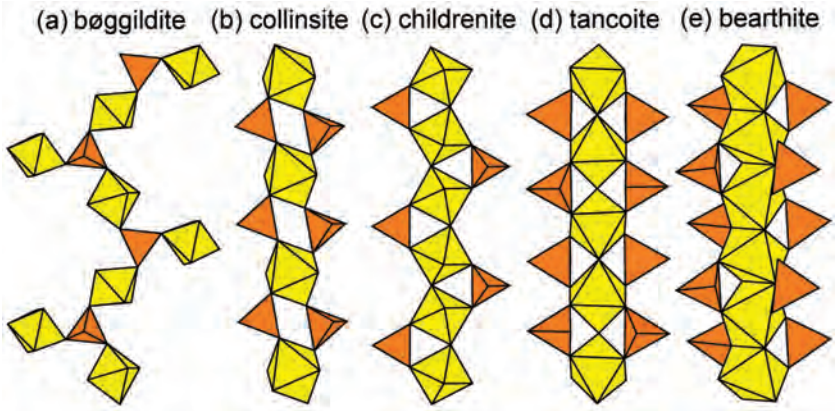

FIG. 25. Selected chains from phosphate structures; (*a*) bøggildite; (*b*) collinsite; (*c*) childrenite; (*d*) tancoite; (*e*) bearthite. Legend as in Fig. 24.

form $[M(TO_4)_2\varphi]$ (Fig. 25*e*) that is also found in the minerals of the **brackebuschite** group and **vauquelinite**.

Phosphate structures based on sheets of tetrahedra and octahedra

M–T linkage. In **brianite**, (PO_4) tetrahedra and (MgO_6) octahedra link to form pinwheel sheets (Fig. 26*a*) linked by interstitial Na and Ca.

M–M, M–T linkage. In **minyulite**, $[Al_2(PO_4)_2F(H_2O)_4O_2]$ clusters (topologically identical to the $[Al_2(PO_4)_2F_4(OH)(H_2O)_2]$ clusters in **morinite** (Fig. 24*b*)) link by sharing vertices between tetrahedra and octahedra (Fig. 26*b*). The minerals of the **laueite** group (Table 3) contain a 7 Å chain (Fig. 25*c*) that meld by sharing one quarter of the flanking (PO_4) vertices with octahedra of adjacent chains to form an $[M_2(PO_4)_2\varphi_4]$ sheet (Fig. 26*c*). A prominent feature of this sheet is the $[M(TO_4)_2\varphi_2]$ chain (Fig. 25*b*) that extends from SE to NW in

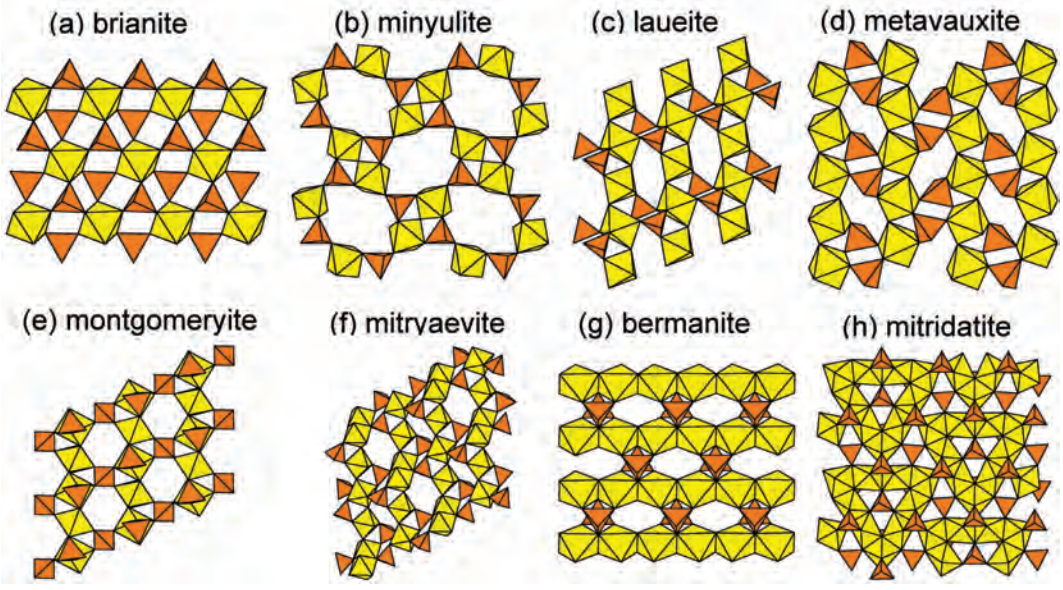

FIG. 26. Selected sheets from phosphate structures; (*a*) brianite; (*b*) minyulite; (*c*) laueite; (*d*) metavauxite; (*e*) montgomeryite; (*f*) mitryaevite; (*g*) bermanite; (*h*) mitridatite. Legend as in Fig. 24.

Fig. 26*c*. Thus we can also think of the **laueite** sheet as composed of $[Fe^{3+}(PO_4)_2O_2]$ chains that are linked by $(Fe^{3+}O_6)$ octahedra. This occurrence of two different types of chain in a sheet or framework structural unit is a common feature, and reflects Nature's parsimony in designing structural arrangements in crystals. In **metavauxite**, topologically identical $[M(TO_4)\varphi_3]$ chains cross-link to form an $[Al(PO_4)(OH)(H_2O)]$ sheet (Fig. 26*d*) that are linked by H bonds emanating from interstitial $(Fe^{2+}\{H_2O\}_6)$ groups. **Montgomeryite** contains 7 Å chains of the form $[M(T\varphi_4)\varphi_2]$ (Fig. 26*e*) in which alternate octahedra are decorated by two tetrahedra that attach to *trans* vertices to give a chain of the form $[M_2(TO_4)_4\varphi_4]$. These chains share flanking (PO_4) groups to form an $[Al_2(PO_4)_3(OH)_2]$ sheet (Fig. 26*e*). **Mitryaevaite** has a very complex sheet that is related to other sheets in this group. The $[M(TO_4)\varphi]$ chain (Fig. 25*c*) is modified by intermittent edge sharing of octahedra, and these chains meld through tetrahedron–octahedron linkages to form a very corrugated sheet.

M=M, M–T linkage. **Bermanite** and **ercitite** contain an $[M(TO_4)\varphi]$ sheet formed from $(M\varphi_6)$ octahedra that share pairs of *trans* edges to form an $[M\varphi_4]$ chain decorated with flanking tetrahedra that link vertices of adjacent octahedra (Fig. 26*g*). These chains link by sharing octahedron vertices to form an $[M(TO_4)\varphi]$ sheet.

M=M, M–M, M–T linkage. The structure of **mitridatite** is of Byzantine complexity. Nonameric triangular rings of edge-sharing $(Fe^{3+}\varphi_6)$ octahedra are centred by a (PO_4) group that shares corners with six of the octahedra (Fig. 26*h*). The corners of each cluster link to the mid-points of the edges of adjacent clusters and the resulting interstices are occupied by (PO_4) tetrahedra.

Phosphate structures based on frameworks of tetrahedra and octahedra

M–T linkage. **Variscite** and **metavariscite** have equal numbers of tetrahedra and octahedra, both polyhedra are four-connected, and hence two vertices of the $(Al\varphi_6)$ octahedron must be one-connected with regard to Al and P. The local bond-valence requirements of the anions at these one-connected vertices require that the anions be (H_2O) groups, as is also the case in the arsenate analogues **scorodite** (Hawthorne, 1976*a*) and **mansfieldite** (Harrison, 2000). In **variscite** (Fig. 27*a*), octahedra and tetrahedra occupy the vertices of a 6^3 net. In **metavariscite**, the tetrahedra and octahedra occupy the vertices of a 4.8^2 plane net (Fig. 27*b*, upper) and the vertices of a very puckered 8^3 net (Fig. 27*b*, lower).

M–M, M–T linkage. **Fluellite** contains a 7 Å chain of the form $[M(TO_4)\varphi_3]$ (Fig. 25*c*) consisting of $(AlF_2\{OH\}(H_2O)_3)$ octahedra linked through pairs of *trans* vertices (= F) and decorated by (PO_4) tetrahedra that link adjacent octahedra along the chain. These chains link into a framework by sharing (PO_4) groups between chains extending in orthogonal directions (Fig. 27*c*).

M=M, M–T linkage. In **libethenite**, a member of the **adamite** group (Hawthorne, 1976*b*), chains of *trans* edge-sharing $(Cu^{2+}\varphi_6)$ octahedra are decorated by (PO_4) tetrahedra to give a chain of the general form $[M_2(TO_4)_2\varphi_4]$ (Fig. 27*d*, upper). These chains link to adjacent chains by sharing octahedron–tetrahedron corners (Fig. 27*d*, lower) to form an open framework with channels containing dimers of edge-sharing $(Cu\varphi_5)$ triangular bipyramids.

M=M, M–M, M–T linkage. In **palermoite**, $[Al_2\varphi_{10}]$ dimers share corners to form an $[Al_2\varphi_8]$ chain that is decorated by (PO_4) tetrahedra to form an $[Al_2(PO_4)\varphi_6]$ chain (Fig. 27*e*, upper). These chains link to form a framework by sharing octahedron–tetrahedron vertices (Fig. 27*e*, lower).

M=M, M–M, M–T linkage. **Burangaite** contains a trimer of face-sharing octahedra (Fig. 27*f*, upper) that is a feature of several basic Fe-phosphate minerals (Moore, 1970). This trimer shares vertices with two $(Al\varphi_6)$ octahedra and two (PO_4) tetrahedra to produce a cluster of the form $[M_5(TO_4)_2\varphi_{18}]$. This cluster polymerizes to form a dense slab of tetrahedra and octahedra that are linked through additional $(Al\varphi_6)$ octahedra into a framework. In **wicksite**, dimers of edge-sharing octahedra are cross-linked into a sheet by sharing corners with (PO_4) tetrahedra (Fig. 27*g*, upper), and these sheets are linked into a framework by sharing corners with additional phosphate groups (Fig. 27*g*, lower). In **seamanite**, chains of $[M_3\varphi_{12}]$ trimers (of octahedra) are decorated by (PO_4) and $(B\varphi_4)$ tetrahedra to form a $[M(B\varphi_4)(PO_4)\varphi_6]$ chain (Fig. 27*h*, upper). These chains condense pairwise by sharing both octahedron–octahedron and octahedron–tetrahedron vertices (Fig. 27*h*, lower) to form columns that link together by sharing vertices between tetrahedra and octahedra.

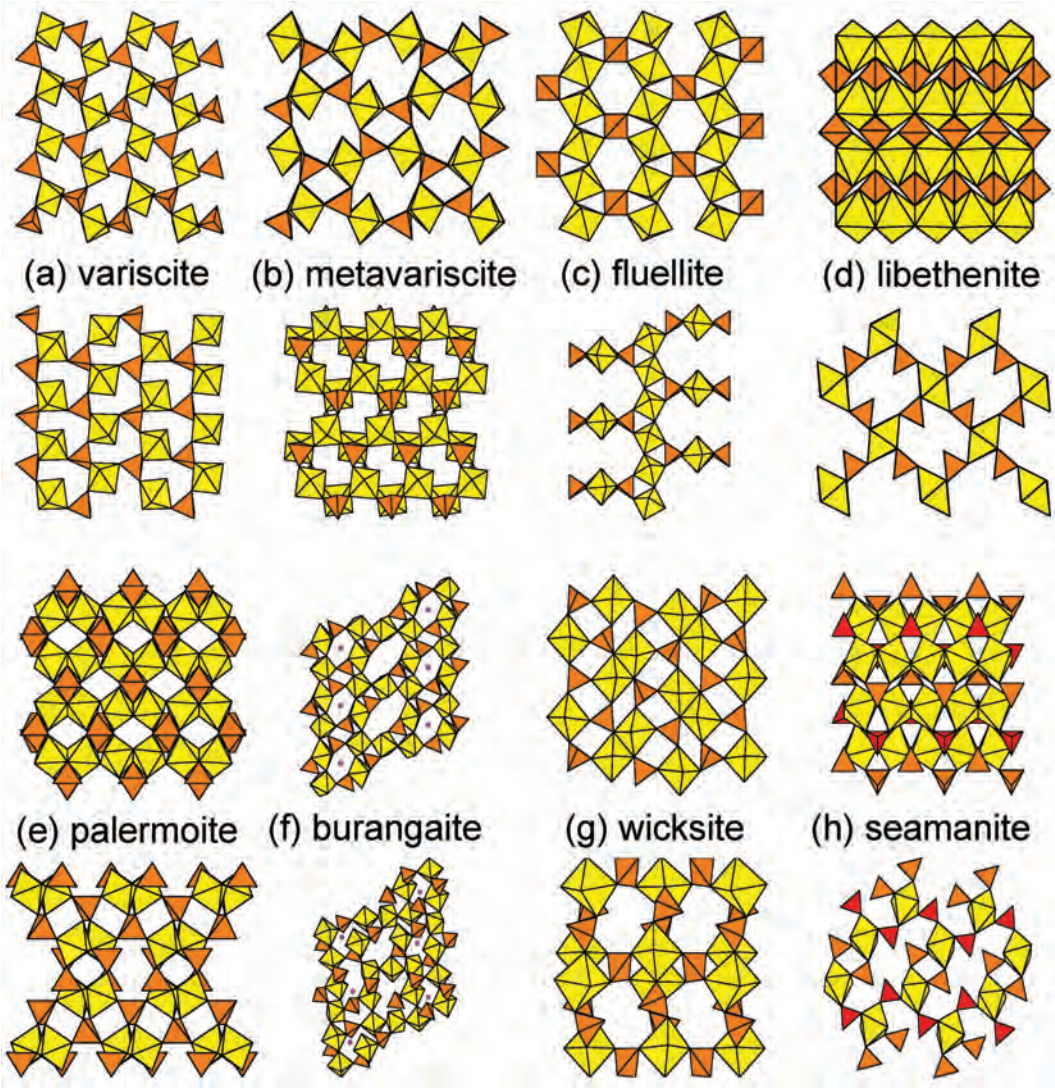

FIG. 27. Selected frameworks from phosphate structures; (*a*) variscite; (*b*) metavariscite; (*c*) fluellite; (*d*) libethenite; (*e*) palermoite; (*f*) burangite; (*g*) wicksite; (*h*) seamanite. Legend as in Fig. 24.

M=M, M=T, M=T linkage. The **triphylite–lithiophyllite**, **sicklerite–ferrisicklerite** and **heterosite–purpurite** series all have the same structural arrangement as olivine. [MO_4] chains of edge-sharing (LiO_6) or (NaO_6) octahedra are decorated by (Fe^{2+},$Mn^{2+}O_6$) or ($\square O_6$) octahedra ($\square$ = vacancy). These decorated chains are linked by sharing octahedron corners with (PO_4) groups to form a fairly dense framework.

Sulfate minerals

The cation S^{6+} occurs in tetrahedral coordination to O [except in thiosulfates, in which S^{6+} is coordinated by a tetrahedron of three O atoms and one S^{2-} anion; e.g. Roberts *et al*. (1999); Cooper and Hawthorne (1999); Cooper *et al.* (2009*b*)]. The mean bond valence in the $(SO_4)^{2-}$ oxyanion is 6/4 = 1.50 vu, and linkage of $(SO_4)^{2-}$ groups does not occur in minerals as the resulting incident bond valence at the linking anions

(1.50 + 1.50 = 3.00 vu) would violate the valence-sum rule. Likewise, the sulfate oxyanion does not polymerize with any of the common oxyanions in minerals [e.g. $(PO_4)^{3-}$, $(AsO_4)^{3-}$, $(VO_4)^{3-}$, $(SiO_4)^{4-}$, $(AlO_4)^{5-}$] because the ideal bond-valence sums incident at the bridging anion would exceed 2 vu significantly. Larger-cation polyhedra have lower mean bond valences and can link to sulfate groups without violating the valence-sum rule, and such linkages constitute the structures of the sulfate minerals. Bokii and Gorogotskaya (1969), Sabelli and Trosti-Ferroni (1985), Rastsvetaeva and Pushcharovskii (1989), Pushcharovsky *et al.* (1998) and Hawthorne *et al.* (2000) have presented classification schemes with various degrees of comprehensiveness. The most recent scheme (Hawthorne *et al.*, 2000) subdivides the sulfate minerals into the following groups: (1) sulfates with divalent- and trivalent-metal octahedra; (2) sulfates with non-octahedral cation polyhedra and Na sulfates; and (3) sulfates with anion-centred tetrahedra. Group (3) will be dealt with later when considering minerals based on anion-centred tetrahedra; here we will focus on group (1) as this contains the most numerous and diverse structure types.

Sulfate structures based on isolated tetrahedra and octahedra

M T linkage. In these minerals, the (SO_4) groups and $(M\varphi_6)$ octahedra are linked by H bonding, and hence must involve $M(H_2O)_6$ groups and (SO_4) tetrahedra. There is a relatively large number of minerals of this type (unlike the phosphates) and there are commonly several mineral species for each structure type.

Sulfate structures based on clusters of tetrahedra and octahedra

M=M linkage. **Creedite** has a $[M_2\varphi_{10}(TO_4)_2]$ cluster (Fig. 28*a*) in which the octahedra form an edge-sharing dimer and the tetrahedra are isolated.

M−T linkage. **Minasragrite** has a simple corner-sharing cluster of a tetrahedron and an octahedron (Fig. 28*b*). The **blödite**-group minerals, the **leonite**-group minerals, **chenite** and related minerals (Table 4) are based on the simple *trans* $[M(T\varphi_4)_2\varphi_4]$ cluster (Fig. 28*c*). The *cis* $[M(T\varphi_4)_2\varphi_4]$ cluster (Fig. 28*d*) occurs in **roemerite**, and is much less common than the analogous *trans* $[M(T\varphi_4)_2\varphi_4]$ cluster (Fig. 28*c*, Table 3). The structure of **ungemachite** is based on the $[M(T\varphi_4)\varphi_6]$ cluster shown in Fig. 28*e*. In his work on **glaserite**-related structures, Moore (1973) called such a cluster a 'pinwheel'. These $[M(TO_4)_6]$ pinwheels are common constituents of more-condensed structures where they link and combine to form sheets and frameworks. The $[M_2(T\varphi_4)_2\varphi_8]$ cluster in **rozenite** (Fig. 28*f*) is the first in the series in Fig. 28 where tetrahedra link between two octahedra. In **coquimbite**, three

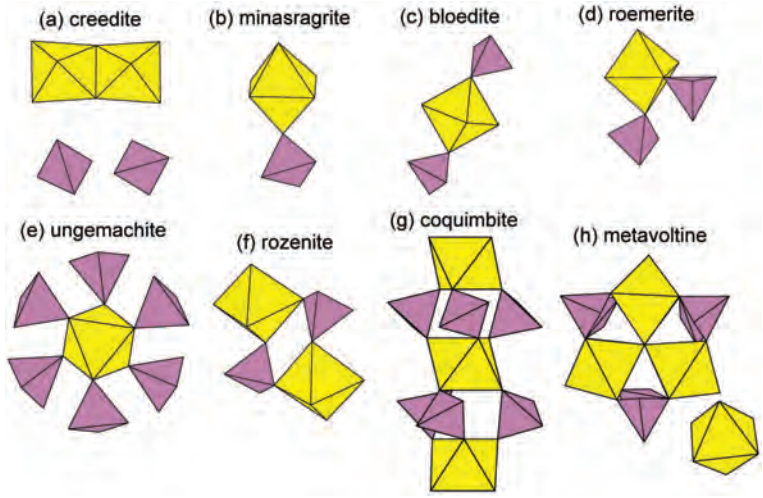

FIG. 28. Selected clusters from sulfate structures; (*a*) creedite; (*b*) minasragrite; (*c*) bloedite; (*d*) roemerite; (*e*) ungemachite; (*f*) rozenite; (*g*) coquimbite; (*h*) metavoltine. Salmon pink = $(S\varphi_4)$; yellow = $(M\varphi_6)$ (M = tetra-, tri- or di-valent cation).

TABLE 4. Structural hierarchy for selected sulfate minerals.

Name	Structural unit	Fig.	Ref.
Clusters			
Creedite	$[Al_2(OH)_2F_8](SO_4)$	28*a*	(1)
Minasragrite	$[V^{4+}O(SO_4)(H_2O)_4]$	28*b*	(2)
Blödite	$[Mg(H_2O)_4(SO_4)_2]$	28*c*	(3)
Leonite	$[Mg(H_2O)_4(SO_4)_2]$	28*c*	(4)
Chenite	$[Cu^{2+}(OH)_4(SO_4)_2]$	28*c*	(5)
Römerite	$[Fe^{3+}(SO_4)_2(H_2O)_4]_2[Fe^{2+}(H_2O)_6]$	28*d*	(6)
Ungemachite	$[Fe^{3+}(SO_4)_6](NO_3)_2$	28*e*	(7)
Rozenite	$[Fe^{2+}(SO_4)(H_2O)_4]$	28*f*	(8)
Coquimbite	$[Fe^{3+}_3(SO_4)_6(H_2O)_6]\{Fe^{3+}(H_2O)_6\}$	28*g*	(9)
Metavoltine	$[Fe^{3+}_3O(SO_4)_6(H_2O)_3]\{Fe^{2+}(H_2O)_6\}$	28*h*	(10)
Chains and ribbons			
Aluminite	$[Al_2(OH)_4(H_2O)_3](SO_4)$	29*a*	(11)
Kroehnkite	$[Cu^{2+}(H_2O)_2(SO_4)_2]$	29*b*	(12)
Krausite	$[Fe^{3+}(H_2O)_2(SO_4)_2]$	29*c*	(13)
Ferrinatrite	$[Fe^{3+}(SO_4)_3]$	29*d*	(14)
Pyracmonite	$[Fe^{3+}(SO_4)_3]$	29*d*	(15)
Aluminopyracmonite	$[Al(SO_4)_3]$	29*d*	(16)
Copiapite	$[Fe^{3+}_2(OH)(H_2O)_4(SO_4)_3]_2$	29*e*	(17)
Butlerite	$[Fe^{3+}(OH)(H_2O)_2(SO_4)]$	29*f*	(18)
Parabutlerite	$[Fe^{3+}(OH)(H_2O)_2(SO_4)]$	29*f*	(19)
Botryogen	$[MgFe^{3+}(OH)(H_2O)_6(SO_4)_2]$	29*g*	(20)
Sideronatrite	$[Fe^{3+}(OH)(SO_4)_2]$	29*h*	(21)
Fibroferrite	$[Fe^{3+}(OH)(H_2O)_2(SO_4)]$	29*i*	(22)
Amarantite	$[Fe^{3+}_2O(H_2O)_4(SO_4)_2]$	29*j*	(23)
Tsumebite	$[Cu^{2+}(OH)(PO_4)(SO_4)]$	29*k*	(24)
Linarite	$[Cu^{2+}(OH)_2(SO_4)]$	29*l*	(25)
Sheets			
Rhomboclase	$[Fe^{3+}(H_2O)_2(SO_4)_2]$	30*a*	(26)
Guildite	$[Cu^{2+}Fe^{3+}(OH)(H_2O)_4(SO_4)_2]$	30*b*	(27)
Slavikite	$[Fe^{3+}_5(H_2O)_6(OH)_6(SO_4)_6][Mg(H_2O)_6]_2(SO_4)$	30*c*	(28)
Alunite	$[Al_3(OH)_6(SO_4)_2]$	30*d*	(29)
Goldichite	$[Fe^{3+}(H_2O)_2(SO_4)_2](H_2O)_2$	30*e*	(30)
Natrochalcite	$[Cu^{2+}_2(OH)(H_2O)(SO_4)_2]$	30*f*	(31)
Wroewolfeite	$[Cu^{2+}_4(OH)_6(H_2O)(SO_4)]$	30*g*	(32)
Gordaite	$[Zn_4(OH)_6Cl(SO_4)]$	30*h*	(33)
Bonattite	$[Cu_{2+}(SO_4)(H_2O)_3]$	31*a*	(34)
Langbeinite	$K_2[Mg_2(SO_4)_3]$	31*b*	(35)
Millosevichite	$[Al_2(SO_4)_3]$	31*c*	(36)
Voltaite	$K_2[Fe^{2+}_5Fe^{3+}_3(H_2O)_{12}(SO_4)_{12}][Al(H_2O)_6]$	31*d*	(37)
Kieserite	$[Mg(SO_4)(H_2O)]$	31*e*	(38)
Sulfoborite	$[Mg_3(OH)F(SO_4)(B(OH)_4)_2]$	31*f*	(39)
Chalcocyanite	$[Cu^{2+}(SO_4)]$	31*g*	(40)
Antlerite	$[Cu^{2+}_3(OH)_4(SO_4)]$	31*h*	(41)

octahedra link through six tetrahedra such that all vertices of the central octahedron link to tetrahedra, and the peripheral tetrahedra each link to three tetrahedra, producing a $[M_3(T\varphi_4)_6\varphi_6]$ cluster (Fig. 28*g*).

M−M, M−T linkage. **Metavoltine** is built from a complex but elegant $[M_3(T\varphi_4)_6\varphi_4]$ cluster (Fig. 28*h*) that also occurs in the structures of Maus's salts (Scordari *et al.*, 1994 and references therein).

Sulfate structures based on chains and ribbons of tetrahedra and octahedra

M=M, M T linkage. **Aluminite** contains a chain of edge-sharing octahedra and isolated tetrahedra (Fig. 29*a*). It is the only example of a chain with polymerized octahedra and isolated tetrahedra, but note that it is the chain analogy of the cluster in **creedite** (Fig. 28*b*).

M−T linkage. The $[M(TO_4)_2\varphi_2]$ chain (Fig. 29*b*) occurs in **kroenkite** and the (phosphate and arsenate) minerals of the **brandtite**, **talmessite** and **fairfieldite** groups (Table 4) (Herwig and Hawthorne, 2006). This chain can be described as being based on the *cis* $[M(TO_4)_2\varphi_4]$ cluster (Fig. 28*d*) polymerized by corner sharing between polyhedra. The $[M(TO_4)_2\varphi]$ ribbon (Fig. 29*c*) occurs in **krausite** and can be considered either as a condensation of two **kroenkite** $[M(TO_4)_2\varphi_2]$ chains (Fig. 29*b*) *via* *M*−*T* linkage or as a condensation of *cis* $[M(TO_4)_2\varphi_4]$ clusters. The $[M(TO_4)_6]$ **ferrinatrite** chain (Fig. 29*d*), also found in **pyracmonite** and **aluminopyracmonite**, consists of octahedra linked to six tetrahedra and polymerized through linkage of each tetrahedron to two octahedra; note that a fragment of this chain occurs as the $[M_3(T\varphi_4)_6\varphi_6]$ cluster (Fig. 28*g*) in **coquimbite**.

M−M, M−T linkage. The $[M_2(TO_4)_3\varphi_4]$ chain (Fig. 29*e*) occurs in **copiapite** and has *M*−*M* dimers flanked by (TO_4) groups forming $[M_2(TO_4)_2\varphi_6]$ clusters (that are present as phosphate clusters in **morinite**, Fig. 24*b*) linked by M−T linkages through (TO_4) groups along the length of the chain. More common are the decorated $[M\varphi_5]$ chains for both sulfate and phosphate structures; these chains have a repeat distance of ~7.1 Å, and Moore (1970) designated them as 7 Å chains. In the $[M_2(TO_4)_2\varphi_6]$ chain in **butlerite** (Fig. 29*f*) and **parabutlerite**, the $[M\varphi_5]$ chain is decorated by staggered tetrahedra that link adjacent octahedra along the length of the

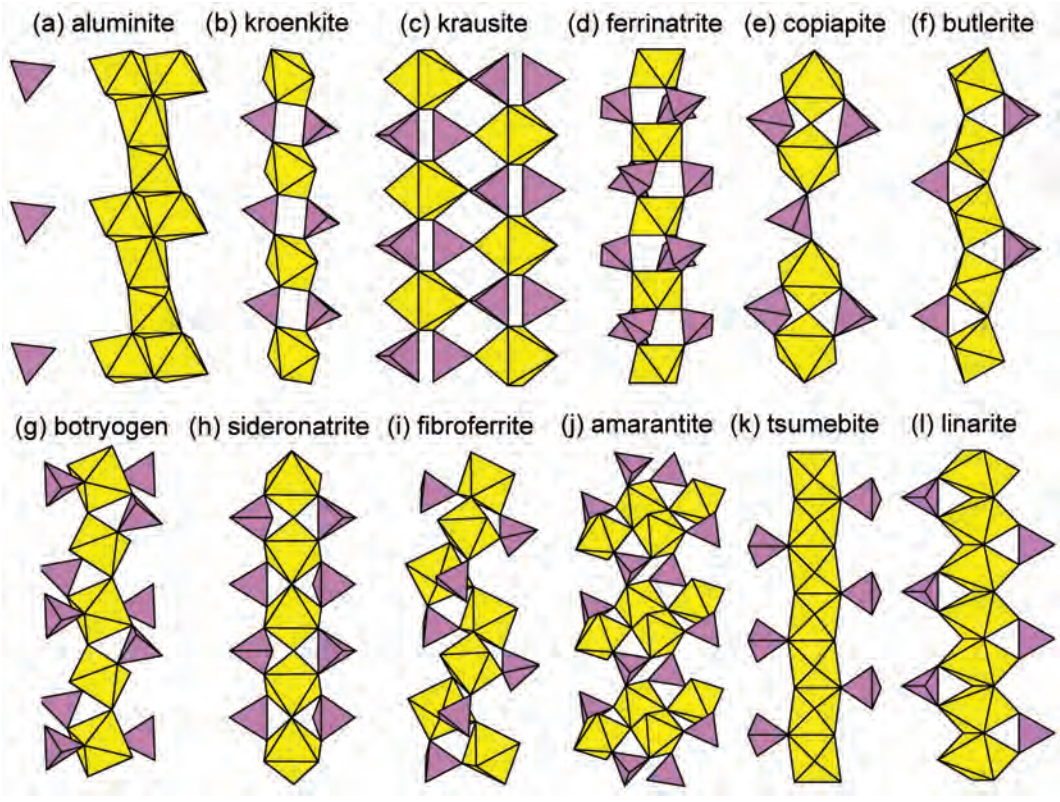

FIG. 29. Selected chains and ribbons from sulfate structures; (*a*) aluminite; (*b*) kroenkite; (*c*) kausite; (*d*) ferrinatrite; (*e*) copiapite; (*f*) butlerite; (*g*) botryogen; (*h*) sideronatrite; (*i*) fibroferrite; (*j*) amarantite; (*k*) tsumebite; (*l*) linarite. Legend as in Fig. 28.

chain. In **botryogen** (Fig. 29*g*), the staggered chain is further decorated by terminal tetrahedra on the octahedron vertices *cis* from those of the bridging tetrahedra: $[M_2(TO_4)_4\varphi_4]$. In **sideronatrite** (Fig. 29*h*), all possible vertices of the octahedra are bridged along the length of the chain by tetrahedra (similar to the arrangement in **tancoite**, Fig. 25*d*): $[M_2(TO_4)_4\varphi_2]$. The $[M\varphi_5]$ chain in **fibroferrite** adds another subtlety to the topology of these chains. The stoichiometry of the **fibroferrite** chain is the same as that of **butlerite**: $[M_2(TO_4)_2\varphi_6]$. However, in **butlerite**, the decorating tetrahedra attach to each octahedron *via trans* vertices (Fig. 29*f*) whereas in **fibroferrite**, the decorating tetrahedra attach to each octahedron *via cis* vertices, imparting a helical character to the chain (Fig. 29*i*).

M−M, M=M, M−T linkage. In **amarantite** (Table 4, Fig. 29*j*), an edge-sharing dimer of octahedra is decorated by sharing each vertex of the shared edge with another octahedron to form a tetramer that is strengthened by tetrahedra sharing *M*−*T* linkages with all four octahedra (Fig. 29*j*). These clusters are linked into ribbons by *M*−*T* linkages.

M=M, M−T linkage. $[M\varphi_4]$ chains are common in both sulfate and phosphate minerals; these chains have a repeat distance of ~6 Å (Lussier and Hawthorne, 2013), and it seems logical to designate them as 6 Å chains. In **tsumebite** (Fig. 29*k*), the $[M_2(TO_4)_2\varphi_6]$ chain is decorated by a staggered arrangement of tetrahedra in which each tetrahedron has a vertex in common with two octahedra (i.e. each tetrahedron links to an anion that is part of a polyhedron edge shared between two octahedra. In **linarite** (Fig. 29*l*), the $[M_2(TO_4)_2\varphi_4]$ chain is decorated by a staggered arrangement of tetrahedra in which each tetrahedron bridges between vertices of adjacent octahedra.

Sulfate structures based on sheets of tetrahedra and octahedra

M−T linkage. In the $[M(TO_4)_2\varphi_2]$ sheet in **rhomboclase** (Fig. 30*a*), each octahedron links to four tetrahedra in the plane of the sheet, and the remaining octahedron vertices are 'tied off' by being (H_2O) groups. In accord with the stoichiometry and the handshaking principle, each tetrahedron links to two octahedra.

M−M, M−T linkage. The $[M_4(TO_4)_4\varphi_{10}]$ sheet (Fig. 30*b*) occurs in **guildite**. The sheet consists of $[M_2(TO_4)_4\varphi_2]$ chains cross-linked into a sheet by *M*−*T* linkage through ($Cu\varphi_6$) octahedra: $[Cu_2 M_2(TO_4)_4\varphi_{10}] = [M_4(TO_4)_4\varphi_{10}]$. In **slavikite** (Fig. 30*c*), **butlerite**-like $[M_2(TO_4)_2\varphi_6]$ chains (Fig. 29*f*) are flexed to form rings involving 12 octahedra, and these rings link in the plane of the sheet through *M*−*M* and *M*−*T* linkage of polyhedra in different rings to form a $[M_5(TO_4)_6\varphi_{12}]$ sheet. In the structures of the minerals of the **alunite** supergroup, $(M^{+},M^{2+})[M_3^{3+}(OH)_6(TO_4)_2]$; [$M^{+}$ = K, Na, Ag^{+}, Tl^{+}, (NH_4), (H_3O); M^{2+} = Ca, Pb^{2+}, Sr, Ba; M^{3+} = Al, Fe^{3+}, Ga; *T* = S, As, P], octahedra occur at the

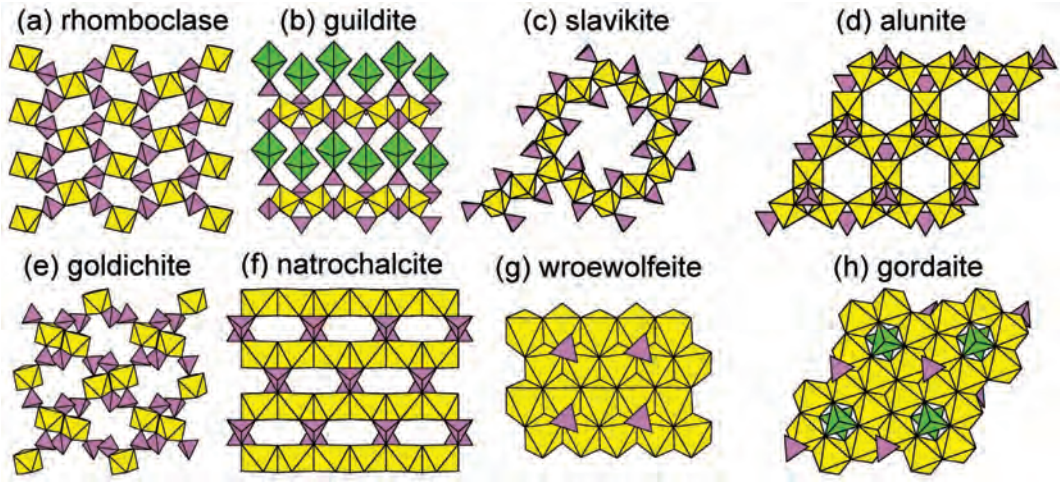

FIG. 30. Selected sheets from sulfate structures; (*a*) rhomboclase; (*b*) guildite; (*c*) slavikite; (*d*) alunite; (*e*) goldichite; (*f*) natrocalcite; (*g*) wroewolfeite; (*h*) gordaite. Legend as in Fig. 10, green = ($Cu\varphi_6$) and ($Zn\varphi_4$) polyhedra.

vertices of a 6^3 plane net, forming six-membered rings with the octahedra linked by sharing corners. At the junction of three six-membered rings is a three-membered ring, and one set of apical vertices of those three octahedra link to a tetrahedron (Fig. 30*d*). In **goldichite** (Fig. 30*e*), a $[M_2(T\varphi_4)_2\varphi_8]$ cluster similar to that in **rozenite** (Fig. 28*f*) links through additional tetrahedra to four other **rozenite**-like clusters by $M-T$ linkage to make a thick slab of the form $[M(TO_4)_2\varphi_2]$.

M=M, M−T linkage. The $[M_2(TO_4)_2\varphi_2]$ sheet in **natrochalcite** (Fig. 30*f*) contains parallel $[M\varphi_4]$ chains of the type occurring in **tsumebite** (Fig. 29*k*) and **linarite** (Fig. 29*l*). Each $[M\varphi_4]$ chain is decorated by a staggered arrangement of tetrahedra in which each tetrahedron bridges between vertices of adjacent octahedra (as in **linarite**), and chains are cross-linked by each tetrahedron linking to an anion of the edge shared between two octahedra of the adjacent chain (as in **tsumebite**). Many minerals consist of **brucite**-like $[M\varphi_2]$ sheets decorated by sulfate groups, e.g. the minerals of the **hydrotalcite** group, ideally $[M^{2+}_6M^{3+}_2(OH)_{16}](TO_n)(H_2O)_m]$ where TO_n = (CO_3) in **hydrotalcite** itself and (SO_4) in many other minerals of this group, and these oxyanions decorate both sides of the **brucite** layer. One-side-decorated sheets occur in the structures of many Cu^{2+} and Zn sulfates (Hawthorne and Schindler, 2000). An example is the structure of **wroewolfeite** (Fig. 30*g*), where the orientational order of Jahn−Teller-distorted $(Cu^{2+}\varphi_6)$ octahedra allows sulfate groups to link to anions of a $[Cu^{2+}\varphi_2]$ sheet. **Gordaite** (Fig. 30*h*) has an interrupted $[M\varphi_2]$ sheet (i.e. some of the M consist of vacancies). Above and below each vacancy, a (TO_4) tetrahedron links to the anions coordinating the vacancy, and small (SO_4) tetrahedra each share an apical anion with the interrupted $[M\varphi_2]$ sheet.

Sulfate structures based on frameworks of tetrahedra and octahedra

M−T linkage. The structure of **bonattite** is based on linear $[M(TO_4)\varphi_4]$ chains that polymerize by corner sharing of polyhedra from adjacent chains. The view in Fig. 31*a* looks like a sheet, but the chains are not parallel; they are skewed with regard to the plane of the projection and link to form a framework. The structures of **langbeinite** (Fig. 31*b*) and **millosevichite** (Fig. 31*c*) are based on the pinwheel cluster of **ungemachite** (Fig. 28*e*) that links both laterally and vertically to form $[M_2(TO_4)_3]$ frameworks. In **voltaite** (Fig. 31*d*), convoluted chains somewhat similar to that in **kroenkite** (Fig. 29*b*) but with an additional $M-T$ linkage form large clusters that link *via* $M-T$ connections to form an open framework.

M−M, M−T linkage. The $[M(T\varphi_4)\varphi]$ framework in **kieserite** (Fig. 31*e*) can be constructed from $[M(T\varphi_4)\varphi_3]$ chains of the type found in **butlerite** (Fig. 29*f*). The chains pack in a *C*-centred array and are cross-linked by sharing corners between octahedra and tetrahedra of adjacent chains. This is a very common arrangement in a wide variety of silicate, phosphate, arsenate, vanadate and sulfate minerals (Hawthorne *et al.*, 2000).

M=M, M−T linkage. In **sulfoborite**, the $[M_3(T\varphi_4)_3\varphi_2]$ framework (Fig. 31*f*) is based on complex sheets of dimers of edge-sharing octahedra that link *via* M−M and M−T linkages to form a framework. The $[M(T\varphi_4)]$ framework of **chalcocyanite** (Fig. 31*g*) is based on **linarite-type** $[M(TO_4)\varphi_2]$ chains cross-linked by the tetrahedral vertices not linked to the central octahedral chain, and strongly resembles the $[M_2(TO_4)_2\varphi_2]$ sheet in **natrochalcite** (Fig. 30*f*). In **antlerite**, double and triple ribbons of edge-sharing octahedra are cross-linked by tetrahedra to form a framework (Fig. 31*h*).

Beryllate minerals

Be^{2+} occurs in tetrahedral coordination to O, and the mean bond valence in the $(BeO_4)^{6-}$ oxyanion is 2/4 = 0.50 vu. This leaves an aggregate bond valence of 1.50 vu that must be contributed through linkage to other cations to satisfy the valence-sum rule. This value (1.50 vu) encompasses all geochemically common oxyanions, from $(BeO_4)^{6-}$ to $(SO_4)^{2-}$, and hence $(BeO_4)^{6-}$ can polymerize with any common oxyanion tetrahedron. There are three general ways in which this bond-valence requirement may be satisfied: (1) the O atom is bonded to three additional Be atoms to produce [4]-coordination by $^{[4]}$Be, with an incident bond valence at the bridging O atom of $4 \times 0.50 = 2.00$ vu, as in **bromellite**, BeO; (2) the O atom can bond to an additional Be atom and one H atom to produce an ideal incident bond-valence arrangement of $2 \times 0.50 + 1.00 = 2.00$ vu, as in **behoite**, $Be(OH)_2$; (3) the O atom bonds to a [4]-coordinated high-valence cation (S^{6+}, As^{5+}, P, Si, Al) with polymerization of tetrahedrally coordinated oxyanions. Most Be minerals consist of $(Be\varphi_4)$

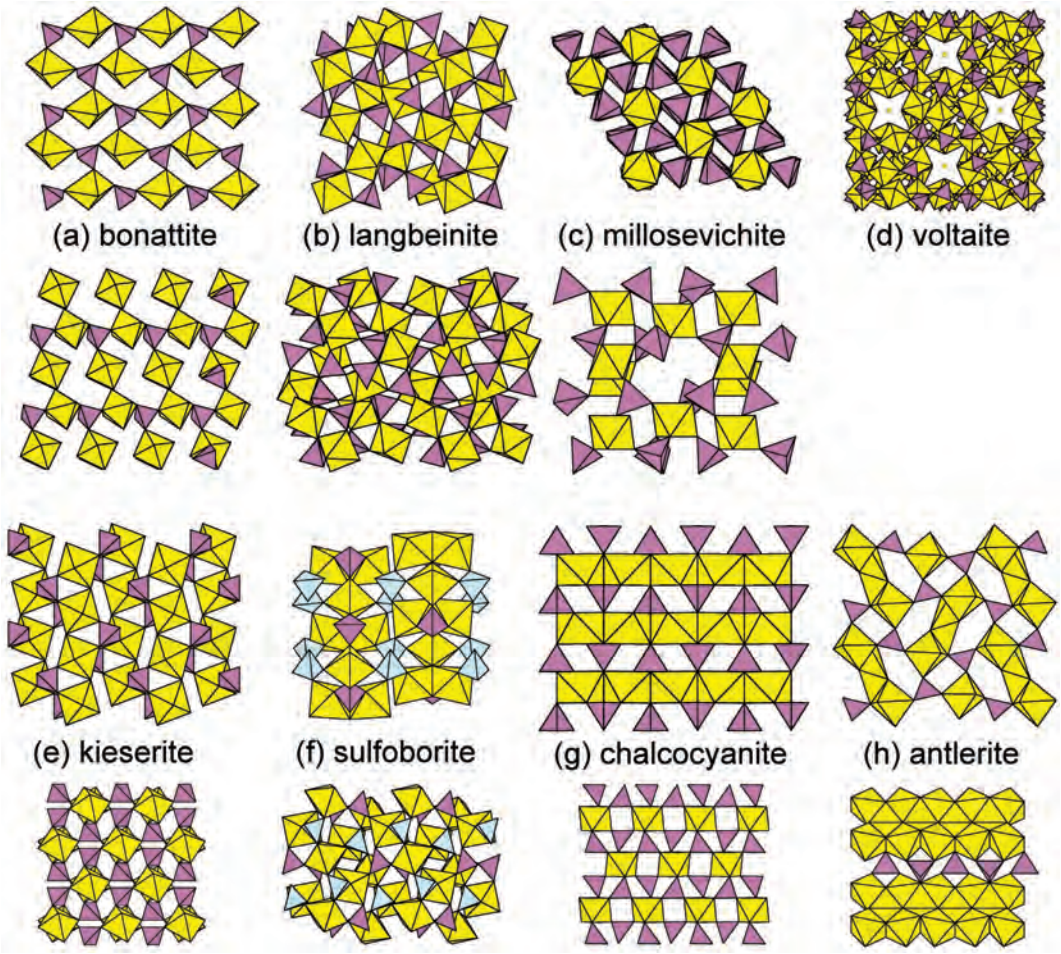

FIG. 31. Selected frameworks from sulfate structures; (*a*) bonattite; (*b*) langbeinite; (*c*) millosevichite; (*d*) voltaite; (*e*) kieserite; (*f*) sulfoborite; (*g*) chalcocyanite; (*h*) antlerite. Legend as in Fig. 10. In general, two views of each structure are shown to illustrate details of the linkage; where only one view is shown, the mineral is cubic.

tetrahedra polymerizing with other ($T\varphi_4$) tetrahedra, and Hawthorne and Huminicki (2002) gave a hierarchical scheme for the beryllate minerals on this basis: (1) isolated polyhedra; (2) clusters; (3) chains and ribbons; (4) sheets; and (5) frameworks. Within each class, structures are arranged in terms of increasing bond valence within the constituent tetrahedra.

Beryllate structures based on isolated tetrahedra

Chrysoberyl, $Al_2[BeO_4]$, is isostructural with **forsterite**, $Mg_2[SiO_4]$; the Be atom occupies the tetrahedron analogous to the (SiO_4) group in **forsterite** (Fig. 32*a*), and Al occupies the octahedrally coordinated *M*1 and *M*2 sites. The overall structure is a close-packed array of O anions with Al and Be occupying the interstices.

Beryllate structures based on clusters of tetrahedra

Gainesite, $Na_2Zr_2[Be(PO_4)_4](H_2O)_{1.5}$, is the only finite-cluster structure (Fig. 32*b*) known so far among the Be minerals. A (BeO_4) tetrahedron links to four (PO_4) tetrahedra to form the pentameric cluster $[BeP_4O_{16}]$ (Fig. 32*b*). These clusters are linked through (ZrO_6) octahedra into a continuous framework that is topologically

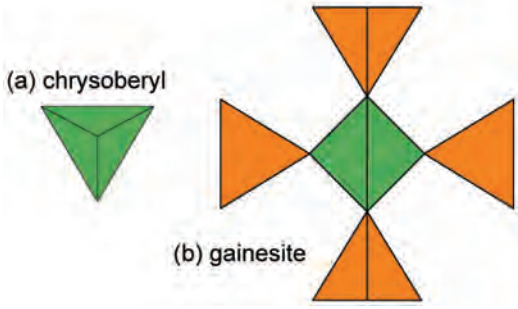

FIG. 32. Isolated tetrahedra and clusters from beryllate structures; (*a*) chrysoberyl; (*b*) gainesite. Green = ($B\varphi_4$); orange = ($P\varphi_4$).

identical to the $[Si_5O_{16}]$ cluster in **zunyite**, $Al_{13}O_4[Si_5O_{16}](OH)_{18}Cl$.

Beryllate structures based on chains and ribbons of tetrahedra

The minerals in this class can be divided into two broad groups based on the (bond valence) linkage involved in the infinite chains: (1) structures with Be–Si (and Si–Si) linkages; (2) structures with Be–P or Be–As linkages. Selected minerals are listed in Table 5. Structures in the first group have no or only minor H bonding, whereas the minerals of the second group have extensive H bonding, although the reason for this is not yet apparent.

Be–Si linkages. **Surinamite**, $(Mg,Fe^{2+})_3Al_3O[BeAlSi_3O_{15}]$, consists of $[T\varphi_3]$ chains of (BeO_4), (AlO_4) and (SiO_4) tetrahedra decorated by (SiO_4) tetrahedra every four tetrahedra along its length (Fig. 33*a*). As with several other chains considered here, the (BeO_4) tetrahedron is three-connected to other tetrahedra. **Sverigeite**, $Na(Mn^{2+},Mg)_2Sn^{4+}[Be_2Si_3O_{12}(OH)]$, has complex chains of corner-sharing $[Be_2SiO_8(OH)]$ three-membered rings and $[Be_2Si_2O_{11}(OH)]$ four-membered rings (Fig. 33*b*). **Euclase**, $Al[BeSiO_4(OH)]$ contains ribbons of (BeO_4) and (SiO_4) tetrahedra (Fig. 33*c*): (BeO_4) tetrahedra link by corner sharing to form a (fully rotated) **pyroxene-like** $[TO_3]$ chain that is decorated on both sides to form a ribbon in which the (BeO_4) tetrahedra are three-connected to (SiO_4) tetrahedra and the (SiO_4) tetrahedra are two-connected to (BeO_4) tetrahedra. In addition, the anion bridging the (BeO_4) tetrahedra also belongs to an (SiO_4) group.

Be–P and Be–As linkages. **Bearsite**, $[Be_2(AsO_4)(OH)](H_2O)_4$, is made up of ribbons of (BeO_4) and (AsO_4) tetrahedra. Two (BeO_4) and one (AsO_4) tetrahedra alternate along the length of a simple $[TO_3]$ chain; two of these chains meld *via* sharing corners such that the (BeO_4) tetrahedra are three-connected and the (AsO_4) tetrahedron is four-connected (Fig. 33*d*). In **fransoletite**, $Ca_3Be_2(PO_4)_2(PO_3OH)_2(H_2O)_4$, one ($BeO_4$) and two ($PO_4$) tetrahedra alternate along the length of a chain (Fig. 33e) in which the (BeO_4) tetrahedron is four-connected and each (PO_4) tetrahedron is two-connected. **Moraesite**, $[Be_2(PO_4)(OH)](H_2O)_4$, has a structure extremely similar to that of **bearsite**, as might be expected by the similarity of the chemical formulae, unit-cell dimensions and space groups ($C2/c$ *vs.* $P2_1/a$): $[Be_2(PO_4)(OH)]$ ribbons extend along the **c** direction (Fig. 33*f*), and are topologically identical to the $[Be_2(AsO_4)(OH)]$ ribbons in **bearsite** (Fig. 33*d*).

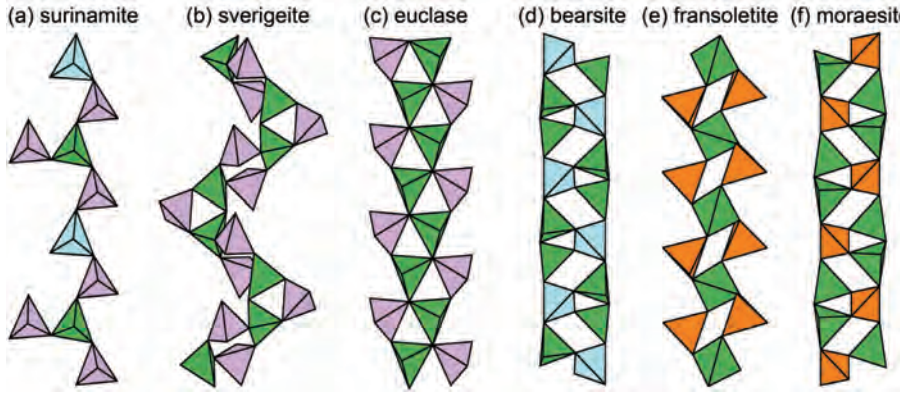

FIG. 33. Selected chains and ribbons from beryllate structures; (*a*) surinamite; (*b*) sverigeite; (*c*) euclase; (*d*) bearsite; (*e*) fransoletite; (*f*) moraesite. Legend as in Fig. 32.

TABLE 5. Structural hierarchy for selected beryllium minerals.

Mineral	Structural unit	Fig.	Ref.
Isolated tetrahedra			
Chrysoberyl	$[BeO_4]$	32*a*	(1)
Clusters			
Gainesite	$[BeP_4O_{16}]$	32*b*	(2)
Chains and ribbons			
Surinamite	$[BeAlSi_3O_{15}]$	33*a*	(3)
Sverigeite	$[Be_2Si_3O_{12}(OH)]$	33*b*	(4)
Euclase	$[BeSiO_4(OH)]$	33*c*	(5)
Bearsite	$[Be_2(AsO_4)(OH)]$	33*d*	(6)
Fransoletite	$[Be_2(PO_4)_2(PO_3OH)_2]$	33*e*	(7)
Moraesite	$[Be_2(PO_4)(OH)]$	33*f*	(8)
Sheets			
Clinobehoite	$[Be(OH)_2]$	–	(9)
Berborite-1T	$[Be_2\{BO_3(OH)\}]$	34*a*	(10)
Berborite-2T	$[Be_2\{BO_3(OH)\}]$	34*a*	(10)
Berborite-2H	$[Be_2\{BO_3(OH)\}]$	34*a*	(10)
Leucophanite	$[Be(Si,Al)_2O_6(O,F)]$	34*b*	(11)
Meliphanite	$[Be(Si,Al)_2O_6(O,OH,F)]$	34*c*	(12)
Hingganite-(Y)	$[Be_2Si_2O_8(OH)_2]$	34*d*	(13)
Bergslagite	$[Be(AsO_4)(OH)]$	34*e*	(14)
Herderite	$[Be(PO_4)F]$	34*f*	(15)
Hydroxylherderite	$[Be(PO_4)OH]$	34*f*	(15)
Semenovite	$[Be_6Si_{14}O_{40}(OH)_4F_4]$	34*g*	(16)
Harstigite	$[Be_4Si_6O_{22}(OH)_2]$	34*h*	(17)
Aminoffite	$[Be_2Si_3O_{10}(OH)_2]$	34*i*	(18)
Samfowlerite	$[(Be_7Zn)Zn_2Si_{14}O_{52}(OH)_6]$	34*j*	(19)
Sørensenite	$[Be_2Si_6O_{18}]$	34*k*	(20)
Ehrleite	$[BeZn(PO_4)_2(PO_3\{OH\})]$	34*l*	(21)
Uralolite	$[Be_4P_3O_{12}(OH)_3]$	34*m*	(22)
Frameworks			
Bromellite	$[BeO]$	35*a*	(23)
Hambergite	$[Be_2(BO_3)(OH)]$	35*b*	(24)
Phenakite	$[Be_2(SiO_4)]$	35*c*	(25)
Hsianghualite	$[Be_3Si_3O_{12}]$	35*d*	(26)
Trimerite	$[Be(SiO_4)]$	35*e*	(27)
Tugtupite	$[Be_2Al_2Si_8O_{24}]$	35*f*	(28)
Bavenite	$[Be_2Al_2Si_9O_{26}(OH)_2]$	35*g*	(29)
Bertrandite	$[Be_4Si_2O_7(OH)_2]$	35*h*	(30)
Leifite	$[Be_2Al_2Si_{16}O_{39}F_2]$	35*i*	(31)
Milarite	$[Be_2AlSi_{12}O_{30}]$	35*j*	(32)
Tiptopite	$[Be_6(PO_4)_6]$	35*k*	(33)
Hurlbutite	$[Be_2(PO_4)_2]$	35*l*	(34)

References: (1) Pilati *et al.* (1993); (2) Moore *et al.* (1983); (3) Moore and Araki (1983); (4) Rouse *et al.* (1989); (5) Hazen *et al.* (1986); (6) Harrison *et al.* (1993); (7) Kampf (1992); (8) Merlino and Pasero (1992); (9) Nadezhina *et al.* (1989); (10) Giuseppetti *et al.* (1990); (11) Grice and Hawthorne (1989); (12) Grice and Hawthorne (2002); (13) Yakubovich *et al.* (1983); (14) Hansen *et al.* (1984); (15) Harlow and Hawthorne (2008); (16) Mazzi *et al.* (1979); (17) Hesse and Stuempel (1986); (18) Coda *et al.* (1967); (19) Rouse *et al.* (1994); (20) Metcalf and Gronbaek (1976); (21) Hawthorne and Grice (1987); (22) Mereiter *et al.* (1994); (23) Hazen and Finger (1986); (24) Burns *et al.* (1995*b*); (25) Tsirel'son *et al.* (1986); (26) Rastsvetaeva *et al.* (1991); (27) Klaska and Jarchow (1977); (28) Hassan and Grundy (1991); (29) Lussier and Hawthorne (2011); (30) Giuseppetti *et al.* (1992); (31) Coda *et al.* (1974); (32) Hawthorne *et al.* (1991); (33) Peacor *et al.* (1987); (34) Bakakin *et al.* (1974).

Beryllate structures based on sheets of tetrahedra

These minerals can be divided into four groups based on the bond valences of the linkages within the infinite sheets: (1) structures with Be–Be linkages; (2) structures with Be–B linkages; (3) structures with Be–Si (and Si–Si) linkages; and (4) structures with Be–As and Be–P linkages.

Be–Be linkages. **Clinobehoite**, $[Be(OH)_2]$, consists of $Be(OH)_4$ tetrahedra linked into sheets by sharing vertices. $(Be\varphi_4)$ tetrahedra share corners to form $[Be\varphi_3]$ chains that resemble almost fully rotated pyroxene chains that are cross-linked into a thick slab by other corner-linked $(Be\varphi_4)$ tetrahedra.

Be–B linkages. **Berborite**, $[Be_2\{BO_3(OH)\}](H_2O)$, has three polytypes, designated 1*T*, 2*T* and 2*H* by Giuseppetti *et al.* (1990). All three structures consist of sheets of corner-sharing (BeO_4) tetrahedra and (BO_3) triangles, and the sheets are identical in all three polymorphs; the structures differ in the relative positioning of adjacent layers in each polytype. The unit cell has a dimer of $(Be\varphi_4)$ tetrahedra surrounded by (BO_3) triangles (Fig. 34*a*), such that the structure in the {001} plane is a 6_3 net of corner-connected $(Be\varphi_4)$ tetrahedra with each hexagonal hole containing a (BO_3) triangle such that the polyhedra define a 3^6 net with adjacent (BeO_4) tetrahedra pointing in opposite directions along *c*; this layer is the first layer in all the polytypes.

Be–Si linkages. In **leucophanite** (Fig. 34*b*), $(Ca,Na)_2[Be(Si,Al)_2O_6(O,F)]$ and **meliphanite** (Fig. 34*c*), $(Ca,Na)_2[Be(Si,Al)_2O_6(O,OH,F)]$, (BeO_4) and (SiO_4) tetrahedra occur at the vertices of a two-dimensional net in which half of the (SiO_4) tetrahedra are two-connected and the rest of the tetrahedra are three-connected. **Hingganite-(Y)**, $Yb_2\square[Be_2Si_2O_8(OH)_2]$, belongs to the **gadolinite–datolite** group. The basic unit of the sheet is a four-membered ring of two (BeO_4) and two (SiO_4) tetrahedra in the sequence [Be–Si–Be–Si]. These rings link by sharing tetrahedral vertices to generate eight-membered rings of alternating (BeO_4) and (SiO_4) tetrahedra (Fig. 34*d*). **Semenovite**, $(RE)_2Fe^{2+}Na_{0-2}(Ca,Na)_8[Be_6Si_{14}O_{40}(OH)_4F_4]$, has ordered $(Be\varphi_4)$ and $(Si\varphi_4)$ tetrahedra occurring at the vertices of a two-dimensional net (Fig. 34*g*). There are two distinct $(Be\varphi_4)$ tetrahedra, both of which are three-connected within the sheet, and five distinct $(Si\varphi_4)$ tetrahedra, one

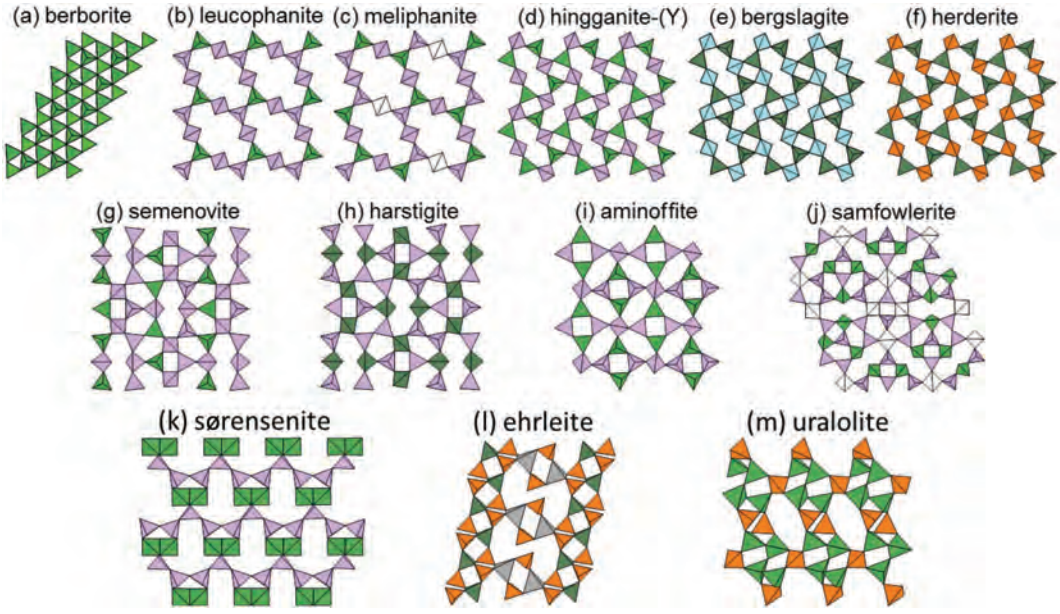

FIG. 34. Selected sheets from beryllate structures; (*a*) berborite; (*b*) leucophanite; (*c*) meliphanite; (*d*) hingganite-(Y); (*e*) bergslagite; (*f*) herderite; (*g*) semenovite; (*h*) harstigite; (*i*) aminoffite; (*j*) samfowlerite; (*k*) sørensenite; (*l*) ehrleite; (*m*) uralolite. Legend as in Fig. 32.

of which is four-connected and four of which are three-connected. The $[Be_6Si_{14}O_{40}F_4]$ sheet in **semenovite** (Fig. 34*g*) is topologically the same as the $[Be_4Si_6O_{22}(OH)_2]$ sheet in **harstigite** (Fig. 34*h*). **Aminoffite**, $Ca_2[Be_2Si_3O_{10}(OH)_2]$, consists of ($Be\varphi_4$) and ($SiO_4$) tetrahedra arranged at the vertices of a two-dimensional net in which four-membered rings of alternating ($Be\varphi_4$) and (SiO_4) tetrahedra are linked by additional (SiO_4) tetrahedra (Fig. 34*i*). The tetrahedra of the ring are three-connected, the linking (SiO_4) tetrahedra are four-connected and the tetrahedra in adjacent four-membered rings point in opposite directions.

Samfowlerite, $Ca_{14}Mn_3^{2+}[(Be_7Zn)Zn_2Si_{14}O_{52}(OH)_6]$, contains ($Be\varphi_4$), ($SiO_4$) and ($Zn\varphi_4$) tetrahedra arranged at the vertices of a two-dimensional net (Fig. 34*j*). Eight-membered rings of tetrahedra [Zn–Si–Be–Si–Zn–Si–Be–Si] link through four-membered [Be–Si–Be–Si] and five-membered rings to form the net; there are two types of five-membered rings: [Zn–Si–Si–Zn–Si] and [Be–Si–Be–Si–Si]. **Sørensenite**, $Na_4Sn^{4+}[Be_2Si_6O_{18}](H_2O)_2$, contains ($BeO_4$) and ($SiO_4$) tetrahedra linked into a sheet in which the (BeO_4) tetrahedra are four-connected and the (SiO_4) tetrahedra are three-connected. Pairs of (BeO_4) tetrahedra share an edge to form a $[Be_2O_6]$ group (Fig. 34*k*) that links to six (SiO_4) tetrahedra, forming a $[Be_2Si_6O_{22}]$ cluster that also occurs in the structures of **eudidymite** and **epididymite**.

Be–P and Be–As linkages. The sheets in **bergslagite** (Fig. 34*e*), Ca[Be(AsO_4)(OH)], and **herderite** (and **hydroxylherderite**) (Fig. 34*f*), Ca[Be(PO_4)F], are topologically identical to that in **hingganite-(Y)** (Fig. 34d) with four-membered rings of alternating ($Be\varphi_4$) and ($T^{5+}O_4$) tetrahedra linked directly by sharing vertices between ($Be\varphi_4$) and ($T^{5+}O_4$) tetrahedra. In **ehrleite**, $Ca_2[BeZn(PO_4)_2(PO_3\{OH\})](H_2O)_4$, there is one distinct (BeO_4) tetrahedron that links to four ($P\varphi_4$) groups (Fig. 34*l*), and one (ZnO_4) tetrahedron that links to four ($P\varphi_4$) groups. Four-membered rings of alternating (ZnO_4), (BeO_4) and (PO_4) tetrahedra link through common (BeO_4) tetrahedra to form chains that are cross-linked into a sheet by (PO_4) groups. **Uralolite**, $Ca_2[Be_4P_3O_{12}(OH)_3]$ $(H_2O)_5$, contains ($Be\varphi_4$) and (PO_4) tetrahedra linked into a sheet (Fig. 34*m*). Eight-membered rings of tetrahedra [P–Be–P–Be–P–Be–P–Be] link through common (PO_4) groups to form chains that link *via* sharing of tetrahedral vertices, forming three-membered [Be–Be–Be] and [Be– Be–P] and four-membered [Be–Be–Be–P] rings.

Beryllate structures based on frameworks of tetrahedra

We may divide these minerals into seven groups based on the linkages involved in the framework: (1) structures with Be–Be linkages; (2) structures with Be–B linkages; (3) structures with Be–Be/Li–Si linkages; (4) structures with Be–Si linkages; (5) structures with Be–Si–Si–Al linkages; (6) structures with Be–Si–Si linkages; and (7) structures with Be–P linkages.

Be–Be linkages. In **bromellite**, [BeO], (BeO_4) tetrahedra occur at the vertices of a 3^6 net, forming three-membered rings of tetrahedra. With only Be and O in the structure, the bond-valence requirements of the anion have to be satisfied solely by Be. As Be–O $\approx$ 0.50 vu, this requires that each O anion be linked to four Be atoms. Hence **bromellite** differs from most of the tetrahedral frameworks in that each tetrahedral vertex has to link to four tetrahedra (Fig. 35*a*), rather than two tetrahedra as is usually the case in these framework structures.

Be–B linkages. **Hambergite**, $[Be_2(BO_3)(OH)]$, consists of a framework of ($Be\varphi_4$) tetrahedra and ($B\varphi_3$) triangles (Fig. 35*b*). The Be:B ratio of 2:1 requires that the structure consist of $[Be_2O_7]$ dimers linked by (BO_3) triangles.

Be–Be and Be–Si linkages. **Phenakite**, $[Be_2(SiO_4)]$, consists of a framework of six-membered rings of tetrahedra connected by four-membered rings of tetrahedra (Fig. 35*c*). One third of the six-membered rings consist solely of (BeO_4) tetrahedra and two thirds consists of alternating (BeO_4) and (SiO_4) tetrahedra, giving a Be:Si ratio of 2:1. The connecting four-membered rings are of two different types: where they connect $[Be_6O_{18}]$ and $[Be_3Si_3O_{18}]$ rings, they consist of three (BeO_4) tetrahedra and one (SiO_4) tetrahedron; where they connect two $[Be_3Si_3O_{18}]$ rings, they consist of two (BeO_4) tetrahedra and two (SiO_4) tetrahedra.

Be–Si linkages. **Hsianghualite**, $Ca_3Li_2[Be_3Si_3O_{12}]F_2$, forms a framework of alternating (BeO_4) and (SiO_4) tetrahedra (Fig. 35*d*). Prominent four-membered rings of (BeO_4) and (SiO_4) tetrahedra are cross-linked to other four-membered rings by tetrahedra that are constituents of other four-membered rings. The result is a four-connected framework that is very similar to the aluminosilicate framework in

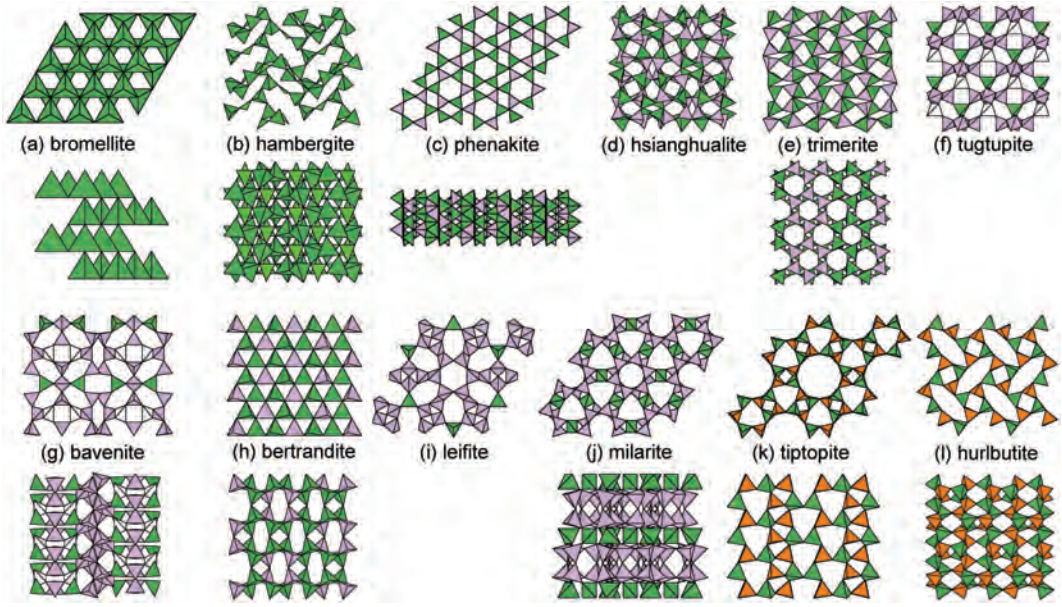

FIG. 35. Selected frameworks from beryllate structures: (*a*) bromellite; (*b*) hambergite; (*c*) phenakite; (*d*) hsianghualite; (*e*) trimerite; (*f*) tugtupite; (*g*) bavenite; (*h*) bertrandite; (*i*) leifite; (*j*) milarite; (*k*) tiptopite; (*l*) hurlbutite. Legend as in Fig. 32.

analcite. **Trimerite**, $CaMn_2^{2+}[Be(SiO_4)]_3$, consists of an ordered framework of four-connected (BeO_4) and (SiO_4) tetrahedra. The tetrahedra occur at the vertices of a 6^3 net (Fig. 35*e*, upper) and point up (*u*) or down (*d*) the **b** direction in the following sequence: [uddudu]. **Trimerite** is topologically isostructural with **beryllonite**, $Na[Be(PO_4)]$.

Be–Si–Si–Al linkages. **Tugtupite**, $Na_8[Be_2Al_2Si_8O_{24}]Cl_2$, is isostructural with **sodalite**, $Na_8[Al_6Si_6O_{24}]Cl_2$. Four-membered rings of (BeO_4), (SiO_4) and (AlO_4) tetrahedra link to six-membered rings of tetrahedra (Fig. 35*f*). Within the four-membered rings, the linkage [Be–Si–Al–Si] does not involve Si–Si linkages. The situation in the six-membered rings is different, as there are two Si–Si linkages involved [Be–Si–Si–Al–Si–Si].

Bavenite, $Ca_4[Be_2Al_2Si_9O_{26}(OH)_2]$, contains four-membered rings of (SiO_4) and (AlO_4) tetrahedra [Al–Si–Al–Si] linked through six-membered rings of (SiO_4) tetrahedra to form chains that are linked through linear [BeO_4–SiO_4–BeO_4] groups (Fig. 35*g*), forming two types of six-membered rings between the chains: [Be–Si–Si–Al–Si–Si] and [Be–Si–Si–Be–Si–Si]. These sheets stack with (AlO_4) tetrahedra as the linking elements between the sheets.

Be–Si–Si linkages. **Bertrandite**, $[Be_4Si_2O_7(OH)_2]$, has the general formula $[T_6\varphi_9] = [T\varphi_{1.5}]$, and the tetrahedra occupy the vertices of a 3^6 net (Fig. 35*h*, upper). The ordering of chemical species over this net is such that the (BeO_4) tetrahedra occupy the vertices of a 6^3 net and the (SiO_4) tetrahedra occupy the interstices of this net. These sheets link through Si–Si and Be–Be linkages (Fig. 35*h*, lower), forming a corrugated 4.6^2 net in which the H atom links to the anion bridging the (BeO_4) tetrahedra. **Leifite**, $Na_6[Be_2Al_2Si_{16}O_{39}F_2](H_2O)_{1.6}$, has six-membered rings of (Si,Al)O_4 tetrahedra linked by $[Si_4O_{11}]$ clusters consisting of an $[Si_2O_7]$ group with two additional tetrahedra sharing corners with both tetrahedra of the $[Si_2O_7]$ group. The six-membered rings occur at the vertices of a plane hexagonal net, and adjacent triplets of hexagonal rings are linked by $[Si_4O_{11}]$ groups (Fig. 35*i*). (BeO_4) tetrahedra occur in large clover-leaf interstices of the aluminosilicate net, linking three different $[Si_4O_{11}]$ groups together. **Milarite**, $KCa_2[Be_2AlSi_{12}O_{30}](H_2O)_x$, is the type structure for a large group of minerals (Hawthorne *et al.*, 1991).

Six-membered rings of (SiO_4) tetrahedra are arranged at the vertices of a hexagonal plane net (Fig. 35*j*, upper) and are linked by (BeO_4) tetrahedra (similar to the linkage by [Si_4O_{11}] groups in **leifite**). These sheets stack (Fig. 35*j*, lower) such that six-membered rings from adjacent sheets share vertices to form an [$Si_{12}O_{30}$] cage (Fig. 35*j*, lower). **Tiptopite**, $K_2(Li_{2.9}Na_{1.7}Ca_{0.7}\square_{0.7})[Be_6(PO_4)_6](OH)_2(H_2O)_4$, is isotypic with the minerals of the **cancrinite** subgroup of the **cancrinite–sodalite** group: $Ca_2Na_6[Al_6(SiO_4)_6(CO_3)_2](H_2O)_2$ for the silicate species. The (BeO_4) and (PO_4) tetrahedra are arranged at the vertices of a corrugated two-dimensional net (Fig. 35*k*) such that all tetrahedra are three-connected. Prominent 12-membered rings are arranged at the vertices of a 3^6 net such that they two-connect four-membered rings and three-connect through six-membered rings. These sheets link in the **c** direction such that all tetrahedra are four-connected. **Hurlbutite** consists of an ordered array of (BeO_4) and (PO_4) tetrahedra in which all tetrahedra are four-connected and there is alternation of (BeO_4) and (PO_4) tetrahedra in the structure. The tetrahedra are arranged at the vertices of a 4.8^2 net (Fig. 35*l*, upper); these sheets link by vertex sharing (Fig. 35*l*, lower). The structure is similar to that of **danburite**, $Ca[B_2(SiO_4)_2]$, but has a different ordering scheme (and space group).

The [Be_2O_6] group

An unusual stereochemical feature of the Be minerals is the presence of the [Be_2O_6] group, a pair of edge-sharing tetrahedra named the maple-tip arrangement by N.V. Belov. Of the oxyanion minerals, only the Be-bearing commonly show this feature. The [Be_2O_6] group occurs in the structures of **sørensenite** (Fig. 34*k*), **eudidymite** and **epididymite**.

Minerals based on anion-centred tetrahedra

Inspection of mineral formulae (at least when written informatively, identifying any oxysalt units in the structure) shows that all O^{2-} ions are associated commonly with the oxysalt units, e.g. **forsterite**: Mg_2SiO_4. However, many minerals have O^{2-} ions that are not associated with oxysalt units, e.g. **dolerophanite**, $Cu_2^{2+}(SO_4)O$ (here, the formula of **dolerophanite** is written in the conventional way, e.g. Back, 2014). Let us consider the structure of **dolerophanite** from the viewpoint of the modified justification of the Structure Hierarchy Hypothesis given above. The bond-valence requirements of S^{6+} are predominantly met by the formation of $S^{6+}-O^{2-}$ bonds to form an $(SO_4)^{2-}$ group with a Lewis-base strength of 0.17 vu (Brown, 2002; Hawthorne, 1994). This leaves Cu^{2+} with a Lewis-acid strength of 0.45 and 0.20 vu, the two distinct values arising because of the Jahn–Teller effect (Jahn and Teller, 1937; Burns and Hawthorne, 1996), and O^{2-} with a very variable Lewis-base strength (from 0 to 2 vu, Hawthorne, 1997). Given the coordination numbers of [6] and [4] for Cu^{2+} and S^{6+}, respectively, there are $6 \times 2 + 4 = 16$ bonds per formula unit. Now consider the requirements of the anions: the Lewis acidity of the $(SO_4)^{2-}$ group is 0.17, and ideally $(SO_4)^{2-}$ requires 16 bonds of strength 0.17 vu; however, this leaves no bonds incident to O^{2-} not bonded to S^{6+}, i.e. it would have a coordination number of [0]. As one conceptually increases the coordination number of O^{2-}, the resulting structure departs increasingly from the valence-matching principle (Brown, 2002; Hawthorne, 1994, 2012*a*). Thus if a structure is possible, it should have the minimum coordination number for O^{2-} consonant with possible $Cu^{2+}-O^{2-}$ bond-valence values. The $O^{2-}-Cu^{2+}$ bond-valence values for [3]-, [4]- and [5]-coordination are 2/3, 2/4 and 2/5 vu; 0.67 vu is too large for a $Cu^{2+}-O^{2-}$ bond, whereas 0.50 and 0.40 vu are both possible. Thus O^{2-} will be [4]-coordinated by Cu^{2+} with a bond valence of 0.50 vu, with much weaker bonds to the $(SO_4)^{2-}$ group. The resulting strongly bonded (OCu_4^{2+}) tetrahedra may polymerize, depending on stoichiometry, and the strongly bonded $(SO_4)^{2-}$ and polymerized (OCu_4^{2+}) units are linked by weaker bonds.

In general, cations in structures with O^{2-} ions that are not associated with oxysalt units must be able to form bonds to O^{2-} of ~0.50 vu, but it is also structurally advantageous (or even required) that these cations form much weaker bonds to other O atoms in the structure. This is most easily done if the relevant cations have strong electronic effects such as Jahn–Teller distortion (e.g. $^{[6]}Cu^{2+}$) or stereoactive lone-pair behaviour (e.g. Pb^{2+}, Bi^{3+}), and such structures commonly contain these cations. Filatov *et al.* (1992), Krivovichev (2004, 2008), Krivovichev and Filatov (1999*a*,*b*), Krivovichev *et al.* (1998*a*, 2013*b*), Magarill *et al.* (2000) and Siidra *et al.* (2008*a*) have looked extensively at these structures and have developed structural hierarchies for both minerals and synthetic compounds based

on the polymerization of (OM_4) tetrahedra (M = cation). Here, our focus will be on Cu^{2+}, Pb^{2+} and Hg minerals, but some synthetic compounds will be included to show the extent of structural variability.

Cu^{2+} minerals and compounds

Selected minerals containing oxo-centred (OCu_4) tetrahedra are listed in Table 6. Their constituent structural units of oxo-centred tetrahedra are shown in Figs 36–39.

Cu^{2+} structures based on clusters of tetrahedra

T–T linkage. **Burnsite** (Table 6) has a $[Cu_7O_2]$ cluster (Fig. 36*a*) consisting of two (OCu_4) tetrahedra linked through a single shared cation. This arrangement also occurs in **fingerite** and **ponomarevite** (Table 6).

T=T linkage. **Fedotovite** (Table 6) has a $[Cu_6O_2]$ cluster (Fig. 36*b*) consisting of two (OCu_4) tetrahedra linked through two shared cations (forming a shared edge); this unit also occurs in **euchlorine** (Table 6). A topologically

TABLE 6. Cu structures containing anion-centered tetrahedra.

Name	Formula	Fig.	Ref.
Clusters			
Starovaite	$KCu^{2+}[(Cu_4^{2+}O)(VO_4)_3]$	–	(1)
Fingerite	$Cu_4^{2+}[(Cu_4^{2+}O)_2(VO_4)_6]$	–	(2)
Ponomarevite	$K_4[Cu_4^{2+}O]Cl_{10}$	–	(3)
Burnsite	$KCd[(Cu_7^{2+}O_2)(SeO_3)_2]Cl_9$	36*a*	(4)
Fedotovite	$K_2[(Cu_3^{2+}O)(SO_4)_3]$	36*b*	(5)
Euchlorine	$NaK[(Cu_3^{2+}O)(SO_4)_3]$	–	(6)
Prewittite	$KPb_{0.5}Cu^{2+}[(PbCu_5^{2+}O_2)Zn(SeO_3)_2]Cl_{10}$	36*c*	(7)
Chains and ribbons			
Cupromolybdite	$[(Cu_3^{2+}O)(MoO_4)_2]$	37*a*	(8)
Vergasovaite	$[(Cu_3^{2+}O)(MoO_4)(SO_4)]$	–	(9)
Chloromenite	$Cu_3^{2+}[(Cu_6^{2+}O_2)(SeO_3)]Cl_6$	–	(10)
Kamchatkite	$K[(Cu_3^{2+}O)(SO_4)_2]Cl$	–	(11)
Stoiberite	$[(Cu_5^{2+}O_2)(VO_4)_2]$	37*b*	(12)
Georgbokiite	α-$[(Cu_5^{2+}O_2)(SeO_3)_2]Cl_2$	37*c*	(13)
Coparsite	$[(Cu_4^{2+}O_2)(AsO_4)]Cl$	37*d*	(14)
Piypite	$K_4[(Cu_4^{2+}O_2)(SO_4)_4]MCl$	–	(15)
Klyuchevskite	$K_3[(Cu_3^{2+}(Fe,Al)O_2)(SO_4)_4]$	37*e*	(16)
Alumoklyuchevskite	$K_3[(Cu_3^{2+}AlO_2)(SO_4)_4]$	–	(17)
Sheets			
Averievite	$[(Cu_5^{2+}O_2)(VO_4)_3](CuCl)$	38*a*	(18)
Dolerophanite	$[(Cu_2^{2+}O)(SO_4)]$	38*b*	(19)
Francisite	$[(Cu_3^{2+}BiO_2)(SeO_3)_2]Cl$	38*c*	(20)
Ilinskite	$Na[(Cu_5^{2+}O_2)(SeO_3)_2]Cl_2$	–	(21)
Nabokoite	$Cu^{2+}[(Cu_6^{2+}TeO_4)(SO_4)_5]Cl$	38*d*	(22)
Frameworks			
Synthetic	$[(Cu_2^{2+}O)(SeO_3)]$-II	–	(23)
Synthetic	$[(Cu_2^{2+}O)(SeO_3)]$-I	–	(23)
Synth Melanothallite	$[(Cu_2^{2+}O)]Cl_2$	39	(24)

References: (1) Pekov *et al.* (2013); (2) Finger (1985); (3) Semenova *et al.* (1989); (4) Burns *et al.* (2002); (5) Starova *et al.* (1991); (6) Scordari and Stasi (1990); (7) Shuvalov *et al.* (2013); (8) Zelenski *et al.* (2012); (9) Berlepsch *et al.* (1999); (10) Krivovichev *et al.* (1998*b*); (11) Varaksina *et al.* (1990); (12) Shannon and Calvo (1973); (13) Krivovichev *et al.* (1999); (14) Starova *et al.* (1998); (15) Effenberger and Zemann (1984); (16) Gorskaya *et al.* (1992); (17) Krivovichev *et al.* (2009*a*); (18) Starova *et al.* (1997); (20) Pring *et al.* (1990); (19) Effenberger (1985); (21) Krivovichev *et al.* (2013*a*); (22) Pertlik and Zemann (1988); (23) Effenberger and Pertlik (1986); (24) Krivovichev *et al.* (2002).

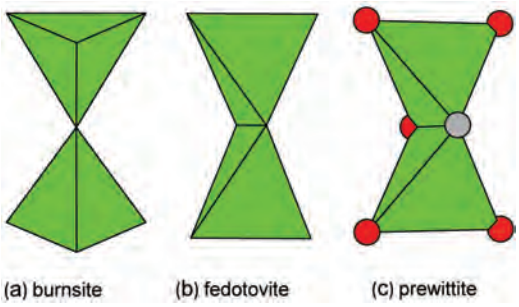

FIG. 36. Selected clusters from oxo-centred Cu structures; (*a*) burnsite; (*b*) fedotovite; (*c*) prewittite. Green = (OCu_4) tetrahedra; where the coordinating cations are all Cu, they are not shown as circles; where there are mixed coordinating cations, Cu is shown as orange circles, Pb^{2+} is shown as grey circles.

similar but topochemically different cluster occurs in the structure of **prewittite**. Two oxo-centred tetrahedra share an edge, but there are two different coordinating cations: five of the cations are Cu^{2+} but the sixth is lone-pair-stereoactive Pb^{2+} (Fig. 36*c*).

Cu^{2+} structures based on chains and ribbons of tetrahedra

T–T linkage. **Cupromolybdite** contains a chain of corner-sharing (OCu_4) tetrahedra: $[O_2Cu_7]$ (Fig. 37*a*). This chain is topologically identical to the pyroxene chain but differs geometrically in that adjacent tetrahedra point in opposite directions orthogonal to the length of the chain. This arrangement also occurs in the structures of **vergasovite**, **chloromenite** and **kamchatkite** (Table 6).

T–T=T linkage. **Stoiberite** (Table 6) is based on a ribbon of tetrahedra with both corner-sharing and edge-sharing linkages (Fig. 37*b*). The unit may be described as dimers of edge-sharing tetrahedra of the form $[O_2Cu_6]$ (topologically identical to the maple-tip $[Be_2O_6]$ dimers in beryllo-silicates, see above) linked into a ribbon by sharing corners with additional (OCu_4) tetrahedra to give a unit of the form $[[O_2Cu_6]Cu_4O_2]] = [Cu_{10}O_4] = 2 \times (Cu_5O_2)$ (Table 6). In **georgbokiite**, $[O_2Cu_6]$ dimers link into a chain by sharing corners (Fig. 37*c*).

T=T linkage. In **coparsite**, (OCu_4) tetrahedra link by sharing edges (Fig. 37*d*) to form a chain of the form $[O_2Cu_4]$. A topologically identical but topochemically different chain occurs in the structures of **klyuchevskite** and **alumoklyuchevskite** (Table 6). In each (OM_4) tetrahedron of the chain, three of the coordinating cations are Cu and one is (Fe,Al) (Fig. 37*e*).

Cu^{2+} structures based on sheets of tetrahedra

T–T linkage. In **averievite** (Table 6), (OCu_4) tetrahedra link by sharing corners (Fig. 38*a*) to form a sheet of six-membered rings of tetrahedra in which adjacent tetrahedra point in different

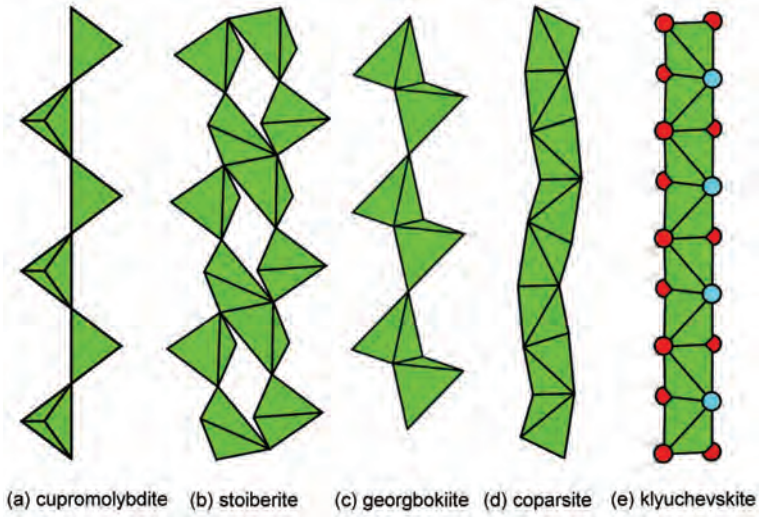

FIG. 37. Selected chains-ribbons from oxo-centred Cu structures; (*a*) cupromolybdite; (*b*) stoiberite; (*c*) georgbokiite; (*d*) coparsite; (*e*) klyuchevskite. Legend as in Fig. 32, blue circles are (Fe,Al).

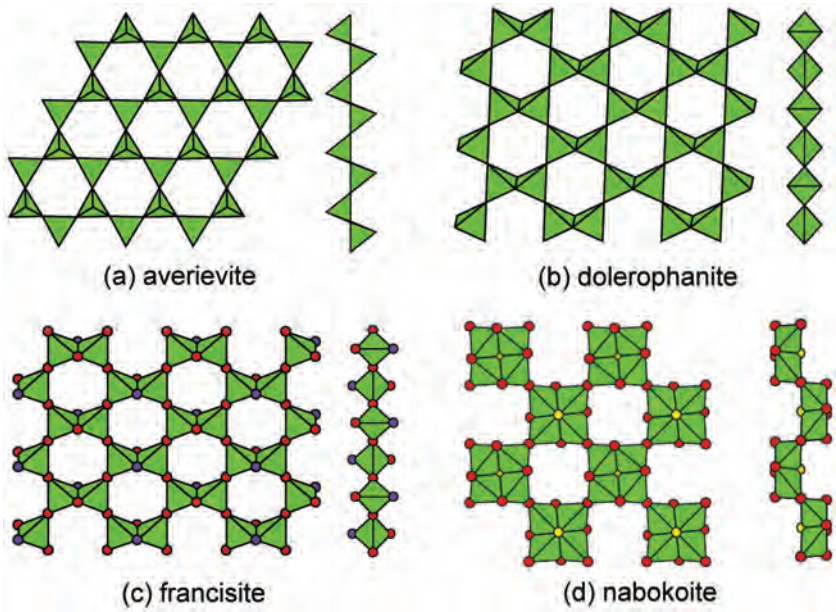

FIG. 38. Selected sheets from oxo-centred Cu structures showing views orthogonal and parallel to the plane of the sheets; (*a*) averievite; (*b*) dolerophanite; (*c*) francisite; (*d*) nabokoite. Legend as in Fig. 36, purple circles are Bi, yellow circles are Te.

directions relative to the plane of the sheet (ududud in the nomenclature of silicate sheets where this arrangement has not been observed).

T−T=T linkage. In **dolerophanite**, edge-sharing dimers of (OCu_4) tetrahedra share corners to form a sheet of six-membered rings of tetrahedra (Fig. 38*b*) in which the sequence of linkage around each six-membered ring is ececec (where e and c indicate edge- and corner-sharing, respectively. The same bond topology occurs in **francisite** (Table 6, Fig. 38*c*), but in each dimer, five of the coordinating cations are Cu and one is Bi. **Nabokoite** has a more complicated linkage (Fig. 38*d*). Four (OM_4) tetrahedra link by sharing edges to form a compact [O_4M_9] tetramer in which the central cation, which links to four O anions, is Te and the peripheral cations are Cu: tetramers link through (OCu_4) corners and adjacent tetramers occur at different levels in the sheet, as is apparent when viewed parallel to the sheet (Fig. 38*d*); the final stoichiometry of the sheet is [O_4TeCu_6].

Cu^{2+} structures based on frameworks of tetrahedra

T−T linkage. A simple completely connected framework occurs in the structure of **melanothallite** (Table 6, Fig. 39) and also in the synthetic compounds [$Cu_2^{2+}O$](SeO_3)-I and [$Cu_2^{2+}O$](SeO_3)-II (Table 6).

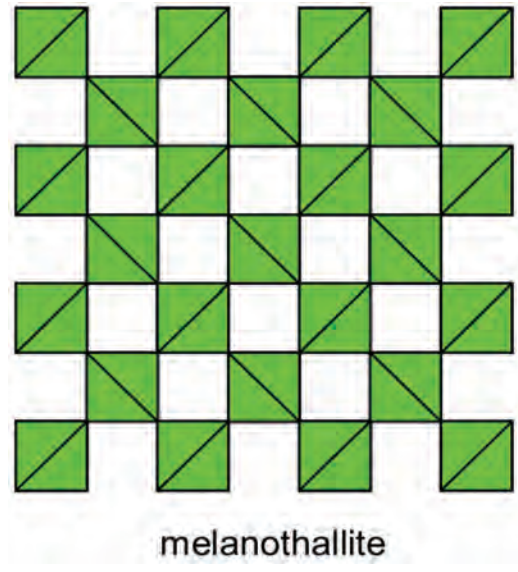

FIG. 39. Framework from oxo-centred Cu structures; melanothallite. Legend as in Fig. 36.

Pb^{2+} minerals and compounds

Selected minerals containing oxo-centred (OPb_4) tetrahedra are listed in Table 7. Their constituent structural units of oxo-centred tetrahedra are shown in Figs 40 to 43.

Pb^{2+} structures based on clusters of tetrahedra

T−T linkage. In synthetic $[Pb_7O_2](Al_8O_{19})$, the pyro-cluster $[Pb_7O_2]$ is formed from two (OPb_4) tetrahedra linked through a single shared vertex (Fig. 40*a*), the minimum possible linkage for a finite cluster. In synthetic $[Pb_3O](UO_5)$, the $[Pb_6O_2]$ cluster is formed from two (OPb_4) tetrahedra linked through a single shared edge (Fig. 40*b*). Synthetic $[Pb_8O_3](BO_3)_2(B_2O_5)$ has a trimer of (OPb_4) tetrahedra linked by sharing edges (Fig. 40*c*) through the *trans* edges of the central tetrahedron. Synthetic $Pb[Pb_8O_4]Br_{10}$ has a tetramer of (OPb_4) tetrahedra linked by sharing edges (Fig. 40*d*) such that there is a vacant

TABLE 7. Pb structures containing anion-centered tetrahedra.

Name	Formula	Fig.	Ref.
Isolated clusters			
Plumbonacrite	$Pb^{2+}[Pb_4^{2+}O](OH)_2(CO_3)$	–	(1)
Synthetic	$Pb^{2+}[Pb_7^{2+}O_2](Al_8O_{19})$	40*a*	(2)
Synthetic	$[Pb_3^{2+}O](UO_5)$	40*b*	(3)
Synthetic	$[Pb_8^{2+}O_3](BO_3)_2(B_2O_5)$	40*c*	(4)
Synthetic	$Pb^{2+}[Pb_8^{2+}O_4]Br_{10}$	40*d*	(5)
Synthetic	$[Pb_{13}^{2+}O_8](OH_6)(NO_3)$	40*e*	(6)
Chains and ribbons			
Phoenicochroite	$[Pb_2^{2+}O](CrO_4)$	–	(7)
Lanarkite	$[Pb_2^{2+}O](SO_4)$	41*a*	(8)
Elyite	$[Pb_2^{2+}O]Cu^{2+}(SO_4)(OH)_4]H_2O$	–	(9)
Sidpietersite	$[Pb_2^{2+}O]_2(OH)_2(SO_3S)$	41*b*	(10)
Chloroxiphite	$Cu^{2+}[Pb_3^{2+}O_2](OH)_2Cl_2$	41*c*	(11)
Plumboselite	$[Pb_3^{2+}O_2](SeO_3)$	–	(12)
Mendipite	$[Pb_3^{2+}O_2]Cl_2$	–	(13)
Damaraite	$[Pb_3^{2+}O_2](OH)Cl$	–	(13)
Sheets			
Litharge	[PbO]	42*a*	(14)
Parkinsonite	$[Pb,Mo,\square)O]_8Cl_2$	42*b*	(15)
Massicot	[PbO]	42*c*	(16)
Thorikosite	$[Pb_3(Sb_{0.6}As_{0.4})O_3](OH)Cl_2$	–	(17)
Asisite	$[Pb_{12}(SiO_4)O_8]Cl_4$	–	(18)
Blixite	$[Pb_8O_5](OH)_2Cl_4$	42*d*	(19)
Kombatite	$[Pb_{14}O_9](VO_4)_2Cl_4$	42*e*	(20)
Symesite	$[Pb_{10}O_7](SO_4)Cl_4(H_2O)$	–	(21)
Mereheadite	$[Pb_{44}O_{24}(OH)_{12}]Pb_3Cl_{25}(BO_3)_2(CO_3)(OH)$	42*f*	(22)
Hereroite	$[Pb_{32}O_{19}(OH)_{12}](AsO_4)_2((Si,Mo,V)O_4)_2Cl_{10}$	42*g*	(23)
Frameworks			
Synthetic	$[Pb_2O]F_2$	43*a*	(24)
Synthetic	$[Pb_{13}O_{10}]Br_6$	43*b*	(25)
Synthetic	$[Pb_{13}O_{10}]Cl_6$	–	(26)

References: (1) Krivovichev and Burns (2000*b*); (2) Ploetz and Muller-Buschbaum (1981); (3) Sterns *et al.* (1986); (4) Yu *et al.* (2012); (5) Keller (1983); (6) Li *et al.* (2001*b*); (7) Williams *et al.* (1970); (8) Sahl (1975); (9) Kolitsch and Giester (2000); (10) Cooper and Hawthorne (1999); (11) Siidra *et al.* (2008*b*); (12) Krivovichev *et al.* (2004); (13) Krivovichev and Burns (2001*b*); (14) Boher *et al.* (1985); (15) Lepore and Welch (2010); (16) Hill (1985); (17) Rouse and Dunn (1985); (18) Welch (2004); (19) Krivovichev and Burns (2006); (20) Cooper and Hawthorne (1994); (21) Welch *et al.* (2000); (22) Krivovichev *et al.* (2009*b*); (23) Siidra *et al.* (2013); (24) Aurivillius (1976); (25) Riebe and Keller (1989); (26) Siidra *et al.* (2007).

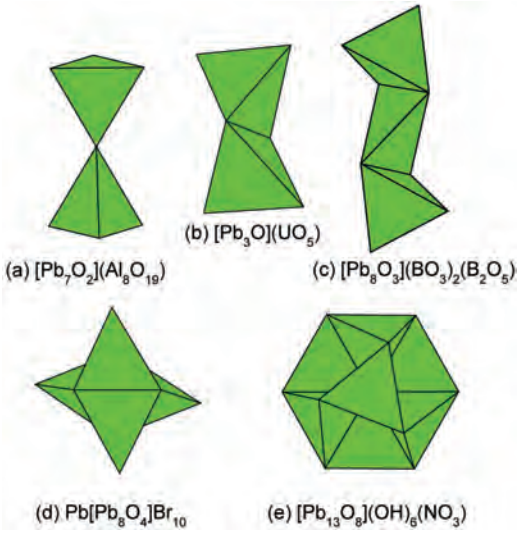

FIG. 40. Selected clusters from oxo-centred Pb structures; (*a*) $[Pb_7O_2](Al_8O_{19})$; (*b*) $[Pb_3O](UO_5)$; (*c*) $[Pb_8O_3](BO_3)_2(B_2O_5)$; (*d*) $Pb[Pb_8O_4]Br_{10}$; (*e*) $[Pb_{13}O_8](OH)_6(NO_3)$. Green = (OPb_4) tetrahedra; where the coordinating cations are all Pb, they are not shown as circles.

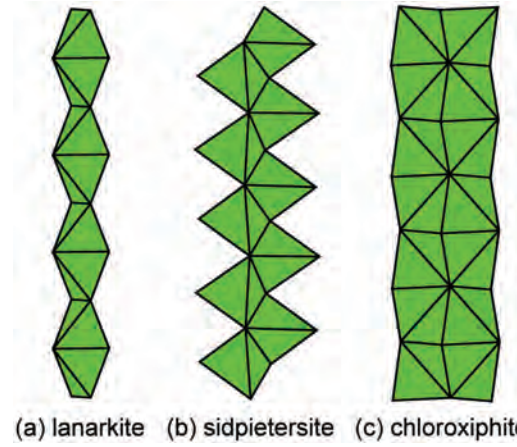

FIG. 41. Selected chains-ribbons from oxo-centred Pb structures; (*a*) lanarkite; (*b*) sidpietersite; (*c*) chloroxiphite. Legend as in Fig. 40.

($\square Pb_4$) tetrahedron in the centre of the cluster. In synthetic $[Pb_{13}O_8](OH)_6(NO_3)$, eight (OPb_4) tetrahedra meet at a single central Pb vertex and share edges with each other to form a very elegant $[O_8Pb_{13}]$ cluster (Fig. 40*e*).

Pb^{2+} structures based on chains and ribbons of tetrahedra

T=T linkage. **Lanarkite** (Table 7) has a chain of edge-sharing (OPb_4) tetrahedra of the form $[OPb_2]$ (Fig. 41*a*).

T=T−T linkage. In **sidpietersite** (Fig. 41*b*), dimers of edge-sharing (OPb_4) tetrahedra share edges with other dimers to form a ribbon of the form $[O_2Pb_4]$ containing Pb in [1]- and [3]-coordination by O. In **chloroxiphite** (Fig. 41*c*), **plumboselite**, **mendipite** and **damaraite** (Table 7), pairs of $[O_2Pb_4]$ chains (as in **lanarkite**, Fig. 41*a*) condense by sharing edges to form a $[O_2Pb_3]$ ribbon containing Pb in [2]- and [4]-coordination by O.

Pb^{2+} structures based on sheets of tetrahedra

T=T−T linkage. **Litharge** may be considered as a parent linkage for many of the structures in this category. In litharge, tetrahedra share edges and vertices to form a dense-packed sheet of (OPb_4) tetrahedra (Fig. 42*a*). **Parkinsonite** has a similar bond topology, but in each tetrahedron, two of the four vertices are occupied in an ordered fashion by Mo (the red spheres in Fig. 42*b*). This is not the case for **thorikosite** (Table 7) in which Pb and (Sb, As) are disordered. **Massicot** also consists of a fairly dense packing of tetrahedra (Fig. 42*c*) but the tetrahedron linkage imparts a modulation to the tetrahedra in the plane of the sheet. The remaining structures of this type shown in Fig. 42*d*−*g* may be considered as vacancy-substituted derivatives of the litharge structure, as developed extensively by Krivovichev (2009, pages 192−201) for both (OPb_4) and (OBi_4) structures.

Pb^{2+} structures based on frameworks of tetrahedra

There are very few of these arrangements involving (OPb_4) tetrahedra, and as we shall see below, those that do occur really struggle to be considered as frameworks.

T=T−T linkage. $[Pb_{13}O_{10}]Br_6$ (Fig. 43) consists of sheets of edge-sharing (OPb_4) tetrahedra that are skew to each other and link into a framework only by sharing a very small number of vertices (corners). Thus the dominant linkages form sheets and the framework character of the structure is weak.

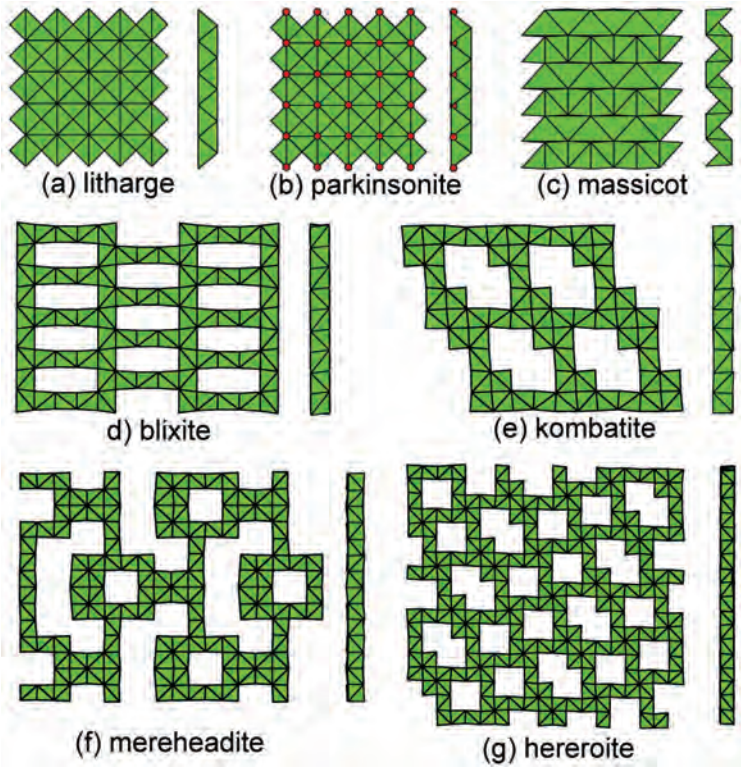

FIG. 42. Selected sheets from oxo-centred Pb structures showing views orthogonal and parallel to the plane of the sheets; (*a*) litharge; (*b*) parkinsonite; (*c*) massicot; (*d*) blixite; (*e*) kombatite; (*f*) mereheadite; (*g*) hereroite. Legend as in Fig. 40, red circles are Mo.

Hg minerals and compounds

Selected minerals containing oxo-centred (OHg_4) and (NHg_4) tetrahedra are listed in Table 8. Their constituent structural units of oxo-centred tetrahedra are shown in Figs 44 to 48.

Hg structures based on clusters of tetrahedra

T−T=T linkage. **Vasilyevite** is intermediate between an isolated-tetrahedron structure and a finite-cluster structure. It contains isolated (OHg_4) tetrahedra and dimers of edge-sharing (OHg_4) tetrahedra (Fig. 44*a*), both of which may be identified in the chemical formula (Table 8) when it is written to reflect the polyhedron linkage: $(OHg_4)[O_2Hg_6]$. In the structure of **deansmithite**, two (OHg_4) tetrahedra share a vertex to form an $[O_2Hg_7]$ pyro-group (Fig. 44*b*). **Poyarkovite** (Fig. 44*c*) contains the edge-sharing (O_2Hg_6) dimer also found in **vasilyevite**.

Hg structures based on chains and ribbons of tetrahedra

T−T=T linkage. **Tedhadleyite** is intermediate between a finite-cluster structure and a chain-ribbon structure. It contains isolated dimers of (OHg_4) tetrahedra: $[O_2Hg_6]$, and chains formed by $[O_2Hg_6]$ dimers linked by sharing one set of *trans* vertices with adjacent dimers: $[O_2Hg_5]$ (Fig. 45*a*) and these linkages are apparent in the way in which the formula of **tedhadleyite** is written (Table 8). Synthetic $Hg_2[Hg_5O_2](PO_4)_2$ (Fig. 45*b*) contains the same chain (formed by $[O_2Hg_6]$ dimers linking by sharing one set of *trans* vertices with adjacent dimers) as in **tedhadleyite**: $[O_2Hg_5]$. In **wattersite** (Fig. 45*c*), $[O_2Hg_6]$ dimers link by sharing the vertices of their shared edges with the two adjacent dimers along the length of the ribbon. Note that the chains in synthetic $Hg_2[Hg_5O_2](PO_4)_2$ (Fig. 45*b*) and the ribbons in **wattersite** (Fig. 45*c*) have the same form: $[O_2Hg_5]$ and are topological isomers. In synthetic $[Hg_2O](CN)_2$ (Fig, 45*d*), $[O_2Hg_6]$

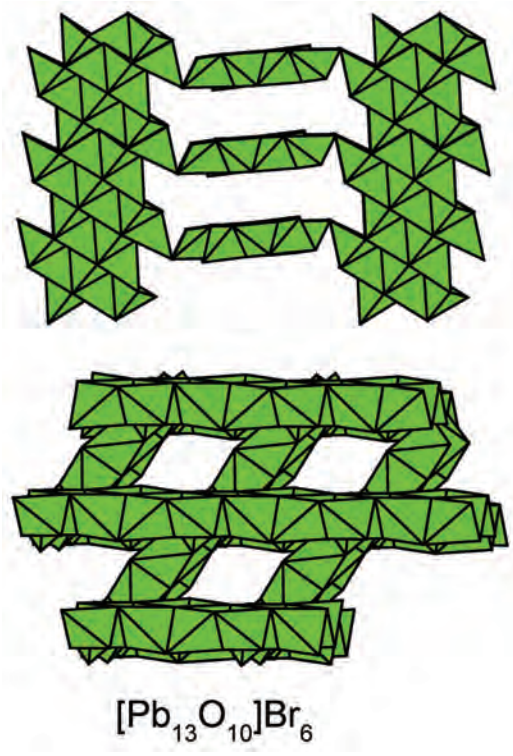

FIG. 43. Selected frameworks from oxo-centred Pb structures showing views from two directions; synthetic $[Pb_{13}O_{10}]Br_6$. Legend as in Fig. 40.

dimers linking by sharing edges with adjacent dimers to give a chain of the form $[O_2Hg_4]$, similar to the $[O_2Pb_4]$ chain in **sidpietersite** (Fig. 41*b*).

Hg structures based on sheets of tetrahedra

T–T=T linkage. In **hanawaltite** (Fig. 46*a*), (OHg_4) tetrahedra and dimers of (OHg_4) tetrahedra, $[O_2Hg_6]$, share vertices to form chains that link laterally by sharing vertices between $[O_2Hg_6]$ dimers to form very open sheets that show prominent modulation in cross-section (Fig. 46*a*). Synthetic $[Hg_2O]I$ consists of $[O_2Hg_6]$ dimers that connect into a sheet by sharing vertices (Fig. 46*b*).

Hg structures based on frameworks of tetrahedra

T–T linkage. **Terlingualite** contains $[O_2Hg_6]$ dimers of (OHg_4) tetrahedra that share vertices to form a fairly open framework that may be envisaged as a condensation of $[O_2Hg_5]$ chains (Fig. 45*b*) *via* sharing of single vertices (Fig. 47*a*). In $[Hg_3O_2]Cl_2$, $[O_2Hg_6]$ dimers link by sharing edges (cf. Fig. 45*d*) and the resulting chains link through the remaining free vertices and edges to chains adjacent in the two directions orthogonal to their length (Fig. 47*b*). In **pinchite** (Table 8), double chains of edge- and vertex-sharing (OHg_4) tetrahedra link by sharing vertices to form sheets (Fig. 47*c*, upper) that then link through sharing vertices to form a framework (Fig. 47*c*, lower).

A simple completely connected framework of N-centred tetrahedra, (NHg_4), occurs in the structures of **mosesite** and **kleinite** (Table 8). In **mosesite** (Fig. 48*a*), all tetrahedra share each of their vertices with one other tetrahedron to form a **cristobalite-like** framework (Krivovichev *et al.*, 2013*b*). In **kleinite**, all (NHg_4) tetrahedra share each of their vertices with one other tetrahedron to form a **tridymite-like** framework (Fig. 48*b*). In **comancheite** (Fig. 48*c*), (NHg_4) tetrahedra link to form an interrupted framework in which some of the Hg atoms are only [1]-coordinated by N atoms; thus although the upper view of the structure in Fig. 48*a* is suggestive of the tetrahedra lying at the vertices of a 6^3 net, this impression is illusory. The tetrahedra link through

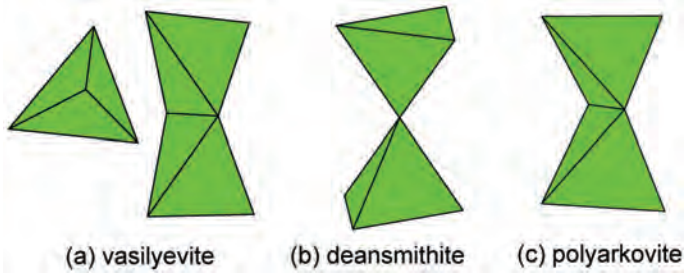

FIG. 44. Selected clusters from oxo-centred Hg structures; (*a*) vasilyevite; (*b*) deansmithite; (*c*) poyarkovite. Green = (OHg_4) tetrahedra.

TABLE 8. Hg structures containing anion-centered tetrahedra.

Name	Formula	Fig.	Ref.
Isolated tetrahedra and clusters			
Vasilyevite	$[Hg_4^{+}O]_2[Hg_6^{+}O_2]_2I_3(Br,Cl)_3(CO_3)$	44*a*	(1)
Deansmithite	$(Hg_2^{+}Hg_1^{2+})[Hg_2^{+}Hg_5^{2+}O_2](CrO_4)_2S_4$	44*b*	(2)
Poyarkovite	$Hg_3^{+}OCl$	44*c*	(3)
Chains and ribbons			
Synthetic	$[Hg_2^{+}Hg_3^{2+}O_2](CrO_4)_2$	–	(4)
Tedhadleyite	$[Hg_5^{+}Hg^{2+}O_2][Hg_5^{+}O_2]I_2(Cl,Br)_2$	45*a*	(5)
Synthetic	$Hg_2^{2+}[Hg_4^{+}Hg^{2+}O_2](PO_4)_2$	45*b*	(6)
Wattersite	$[Hg_4^{+}Hg^{2+}O_2](CrO_4)$	45*c*	(7)
Synthetic	$[Hg_2^{2+}O](CN)_2$	45*d*	(8)
Sheets			
Synthetic	$[Hg^{+}Hg_3^{2+}O_2]_2(OH)(NO_3)_5$	–	(9)
Synthetic	$[Zn_2Hg_2^{2+}O_2](SeO_4)_2(H_2O)$	–	(10)
Hanawaltite	$[Hg_4^{+}Hg^{2+}O_3]Cl_2$	46*a*	(11)
Synthetic	$[Hg^{+}Hg^{2+}O]I$	46*b*	(12)
Frameworks			
Terlinguaite	$[Hg_2^{2+}O]Cl_2$	47*a*	(13)
–	$[Hg_3^{2+}O_2]Cl_2$	47*b*	(14)
Pinchite	$[Hg_5^{2+}O_4]Cl_2$	47*c*	(15)
Mosesite	$[Hg_2^{2+}N](Cl,(SO_4),(CO_3),H_2O)$	48*a*	(16)
Kleinite	$[Hg_2^{2+}N](SO_4)_{0.25}Cl_{0.5})(H_2O)_{0.5}$	48*b*	(17)
Comancheite	$[Hg_{55}^{2+}N_{24}](OH,NH_2)_4(Cl,Br)_{34}$	48*c*	(18)

References: (1) Cooper and Hawthorne (2003); (2) Symanski and Groat (1997); (3) Vasil'ev *et al.* (1999); (4) Weil and Stoeger (2006); (5) Cooper and Hawthorne (2009); (6) Weil and Glaum (2001); (7) Groat *et al.* (1995); (8) Aurivillius (1965); (9) Weil (2005); (10) Weil (2004); (11) Grice (1999); (12) Stålhandske *et al.* (1985); (13) Aurivillius and Folkmarson (1968); (14) Weil (2001); (15) Hawthorne *et al.* (1994); (16) Switzer *et al.* (1953); (17) Giester *et al.* (1996); (18) Cooper *et al.* (2013).

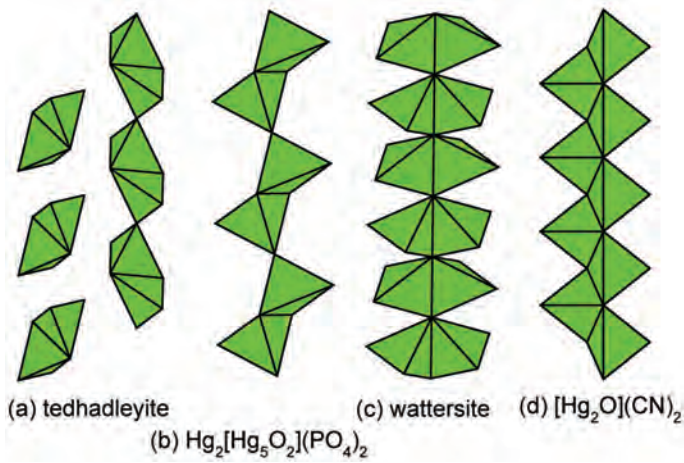

FIG. 45. Selected chains-ribbons from oxo-centred Hg structures; (*a*) tedhadleyite; (*b*) synthetic $Hg_2[Hg_5O_2](PO_4)_2$; (*c*) wattersite; (*d*) synthetic $[Hg_2O](CN)_2$. Legend as in Fig. 44.

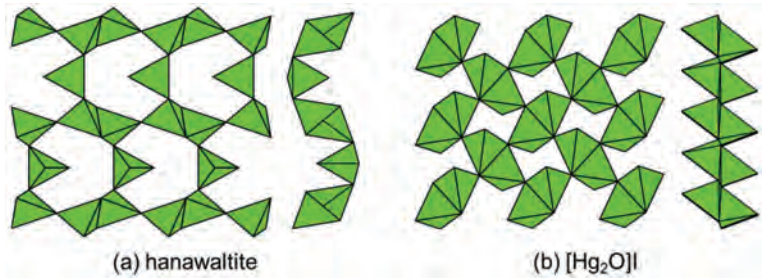

FIG. 46. Selected sheets from oxo-centred Hg structures; (*a*) hanawaltite; (*b*) synthetic $[Hg_2O]I$. Legend as in Fig. 44.

sharing corners orthogonal to the plane of Fig. 48*a* (see Fig. 48*b*).

Chemical composition and bond topology

It is apparent from the overview of structure hierarchies for different general groups of oxysalts given above (i.e. borates, beryllates, phosphates, sulfates, uranyl oxides and oxysalts, and anion-centred Cu, Pb and Hg oxides, nitrides and oxysalts) that there is a strong relation between bond topology and chemical composition. Prior to discussing the bond-topological details of the various hierarchies, I discussed the valence-sum rule (Brown, 2002, 2009; Hawthorne 1994, 2012*a*) as a constraint on the self-linkage of oxyanions in crystal structures. The details of this argument are summarized in Fig. 2 where we see that (1) in some groups of minerals (e.g. sulfates, carbonates), self-polymerization of the principal anionic group cannot occur; (2) in some groups (e.g. phosphates), self-polymerization of the principal anionic group can occur but is extremely limited; and (3) in some groups, self-polymerization of the principal anionic group is extremely common (e.g. silicates, beryllates and beryllosilicates). This constraint is well known (see discussion in Hawthorne, 2006). It is apparent from inspection of Figs 6–48 that there are marked similarities and differences between bond topology (polyhedron linkage) of structural units and the chemical compositions of the principal polyhedra, similarities and differences that are different from those expressed in Fig. 2.

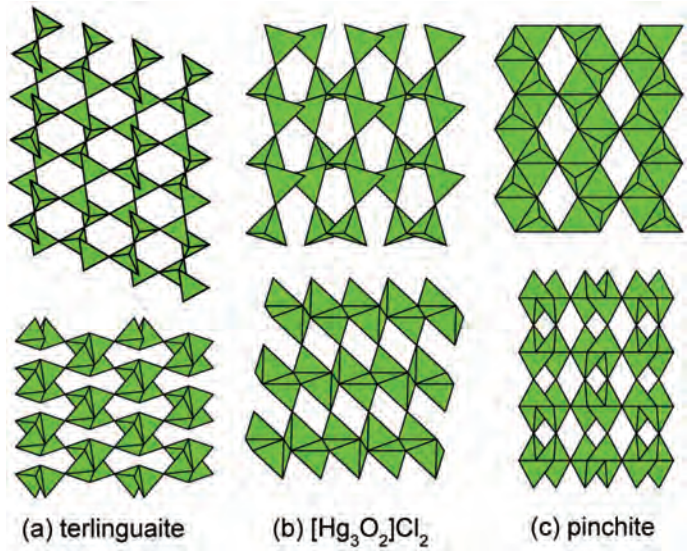

FIG. 47. Selected frameworks from oxo-centred (green) Hg structures; (*a*) terlinguaite; (*b*) synthetic $[Hg_3O_2]Cl_2$.; (*c*) pinchite.

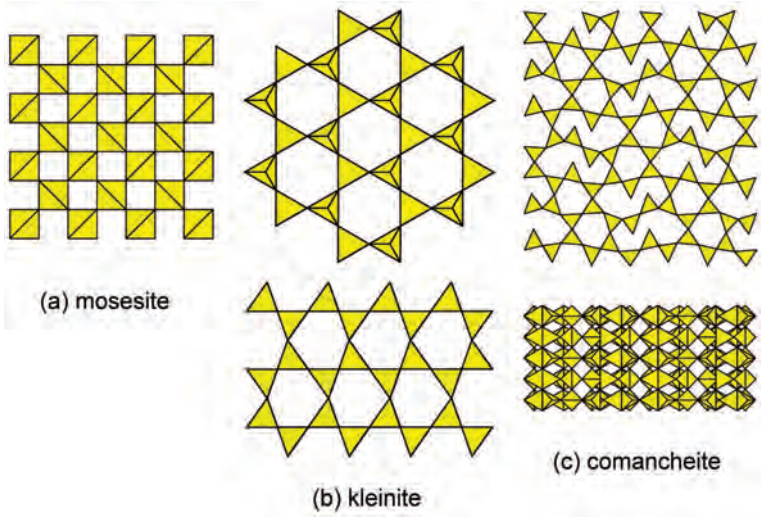

FIG. 48. Selected frameworks from nitride-centred (yellow) Hg structures; (*a*) mosesite; (*b*) kleinite; (*c*) comancheite.

However, before we look at some of these differences, it is necessary to clarify the relation between bond topology and chemical composition. The chemical constituents of the structural unit (e.g. Fe^{3+} and S^{6+} or Be and Si) are, to a major extent, imposed by the chemical composition of the system in which the structure crystallized. On the other hand, there are also bond-topological constraints on the chemical composition of a structural unit: for example, there is no polymerization between phosphate and sulfate groups, even in systems containing both P_2O_5 and SO_3, as such compositions contravene the valence-sum rule and cannot occur. Thus even at this very crude level, we can identify two very distinct constraints on chemical composition of structural units:

(1) the constituents of the structural unit must occur in the chemical system under consideration;

(2) the linkage of the constituents of the structural unit cannot contravene the valence-sum rule.

These constraints seem very obvious, but they emphasize an important point: The chemical composition of the structural unit is not completely dictated either by the chemical composition of the system or by the details of the bond topology. Points (1) and (2) provide constraints under which a structural unit crystallizes, and the resulting arrangement is constrained by both conditions.

Detailed analysis of the similarities and differences in bond topology between the various groups of minerals is obviously premature while a detailed structure hierarchy is not available for the (alumino-)silicate minerals. However, some preliminary observations may be made here:

(3) Vertices shared between tetrahedra tend to be [2]-coordinated as constrained by the valence-sum rule. In beryllates, such vertices may be [3]-coordinated as in **euclase** (Fig. 33*c*) where anions along the chain are coordinated by 2 Be and Si (in accord with the valence-sum rule) or even [4]-coordinated, as in **bromellite** (Table 5, Fig. 35*a*), where we can also consider the structure in terms of anion-centred polyhedra. In borates, vertices may be [3]-coordinated as in **aristarainite** (Fig. 8*h*) and **tunellite** (Fig. 9*c*). However, even in borates and beryllates, [2]-coordinated vertices shared between tetrahedra are far more common than [3]-coordinated vertices. In structures with anion-centred tetrahedra, (cation) vertices may be more highly coordinated, for example [3]-coordinated in **stoiberite** (Fig. 37*b*) and **sidpietersite** (Fig. 41*b*), and [4]-coordinated in **nabokite** (Fig. 38*d*) and **wattersite** (Fig. 45*c*).

(4) For groups in which the principal polyhedra are topologically similar (e.g. sulfates and phosphates), there are strong similarities in bond topologies of structural units. Thus we find topologically similar chains in the phosphate and sulfate minerals **collinsite** (Fig. 25*b*) and **kroenkite** (Fig. 29*b*), **childrenite** (Fig. 25*c*) and **butlerite** (Fig. 29*f*), **tancoite** (Fig. 25*d*) and

sideronatrite (Fig. 29*h*). Similarly, the cluster $[M(TO_4)_2\varphi_4]$ occurs in the phosphate mineral **anapaite** (Fig. 24*a*) and the sulfate mineral **bloedite** (Fig. 28*c*). However, despite these similarities, there are marked differences between the cluster and chain-ribbon groups in phosphates and sulfates. In phosphate minerals, there is only a small number of clusters (Fig. 24) whereas in sulfate minerals, there is a much larger number (Fig. 28) and many are of much greater complexity. The situation is similar with the chain-ribbon structures: In phosphate minerals, there is a smaller number of chains (Fig. 25) whereas in sulfate minerals, there is a much larger number (Fig. 29) and again many of the chains in the sulfates are of much greater complexity.

(5) In borate minerals, three-membered rings of tetrahedra and triangles are extremely common (see Burns 1995). In beryllate minerals, three-membered rings of tetrahedra (with various central cations) are common (Figs 33–35). In silicate minerals, three-membered rings of tetrahedra are less common.

(6) In sulfates and phosphates, edge sharing between tetrahedra does not occur (except in fibrous SiO_2). In beryllates, edge sharing between tetrahedra is uncommon but does occur in the form of $[Be_2O_6]$ dimers. In structures with anion-centred tetrahedra, edge sharing between tetrahedra is very common (Figs 36–47).

Undoubtedly the development of structural hierarchies for other groups of structures will reveal more of these contrasts and parallels. For example, edge sharing is common between [5]-coordinated cations as diverse as Cu^{2+} and As^{5+}, and polymerization *via* this linkage is an important factor in the bond topology of these structures (e.g. Evans and Hughes, 1990; Cooper *et al.*, 2013).

Quantitative relations between chemical composition and bond topology

The chemical composition of the structural unit may be simply derived from the bond topology by counting the types and numbers of atoms. However, the reverse is not true; the bond topology cannot be derived from the chemical composition. There is significant information on bond topology contained in the chemical composition, but it is commonly not easy to extract and there has not been much work on this issue. The development of structure hierarchies and the concomitant writing of chemical formulae to reflect the constituent bond topology will greatly promote our understanding in this area.

M–T graphs

As noted above, we may represent FBBs and their linkage by graphs in which the T vertices represent tetrahedra and the M vertices represent octahedra; this was done by Hawthorne *et al.* (2000) for the sulfate minerals, and for oxysalts in general by Krivovichev (2008). It is desirable that such a system be applied to all groups of minerals, as similarities in bond topology and hierarchy will be emphasized by such a representation.

What affects dimensional polymerization?

The arrangement of structures into groups based on the dimensional polymerization of their coordination polyhedra of higher bond valence raises the question of what affects such polymerization. This question was addressed by Hawthorne (1983*a*, 1992), and we may summarize the important details as follows: The dimensional polymerization of a structural unit is affected intimately by its bonding interactions with the interstitial complex. Polymerization in a particular direction may be terminated by the incidence of one strong bond at the peripheral anion; all other bonds to that anion are weak. Such weak bonds involve either ions of the interstitial complex or ions (usually H) from adjacent structural units. Thus dimensional polymerization may be limited by (1) the incidence of several weak bonds at peripheral anions of the structural unit, or (2) the occurrence of $(OH)^-$ and $(H_2O)^o$ as peripheral anions of the structural unit (Hawthorne, 1985*a*, 1986, 1990, 1992, 1994, 1997).

Such control of the dimensional polymerization of the structural unit will also affect its Lewis basicity (Hawthorne and Schindler, 2008). The Principle of Correspondence of Lewis acidity-basicity states that "stable structures will form when the Lewis-acid strength of the interstitial complex closely matches the Lewis-base strength of the structural unit". This is the mean-field equivalent of the valence-matching principle, and allows quantitative assessment of this interaction. Schindler and Hawthorne (2001*a*,*b*, 2004, 2008) and Schindler *et al.* (2000, 2006*a*) have used this principle to make quantitative predictions about possible chemical compositions and crystal-chemical features of interstitial complexes in

borate, vanadate, sulfate and uranyl-oxysalt minerals. There has been broad recognition of the relation between the degree of dimensional polymerization and the amount of $(OH)^-$ and $(H_2O)^o$ in the constituent minerals (e.g. Hawthorne, 1985*a*, 1986, 1990; Krivovichev, 2008) and the analogous effect has more recently been recognized in inorganic chemistry (e.g. Tulsky and Long, 2001) involving a much wider array of ligands. However, there has been little work done on the relation between the details of the bond topology of the structural unit and the amount of H in hydroxy–hydrate systems (but see Hawthorne and Sokolova, 2012). A much better understanding of this issue is desirable, particularly for minerals, as H plays a major role in controlling the diversity and distribution of mineral species within the Earth.

Surface–fluid interactions

With regard to the Structure Hypothesis and its use of bond-valence theory, one should also recognize that it provides a systematic framework for examining interactions between solid surfaces and fluids to which they are exposed. Bickmore (2013) and Bickmore *et al.* (2004*a*,*b*, 2006) have used bond-valence theory to look at surface–solution interactions primarily in sheet silicates, and Schindler *et al.* (2004*a*,*b*) and Hawthorne and Schindler (2014) have extended the Principle of Correspondence of Lewis acidity-basicity to look at surface interactions between complex oxysalt minerals and aqueous solutions. These interactions may be dissolution, crystallization or adsorption, and provide a framework not only for theoretical examination of associated mechanisms, but also a means to interpret experimental measurements (e.g. Schindler *et al.*, 2006*b*,*c*, 2007*a*,*b*, 2009, 2011).

Coda

Here, I have formalized the idea of structure hierarchy and briefly reviewed the structure hierarchy of several groups of minerals that have been so organized. The basic intent of the Structure Hierarchy Hypothesis is to bring a coherent approach to the organization of our knowledge of the structure of minerals, and together with bond-topology theory and bond-valence theory, provide a basis for understanding the factors affecting the chemical composition and bond topology of minerals, and provide insight into mechanisms of crystallization and dissolution.

Acknowledgements

This work was supported by a Canada Research Chair in Crystallography and Mineralogy and by a Natural Sciences and Engineering Research Council of Canada Discovery grant to FCH.

References

Abbona, F., Calleri, M. and Ivaldi, G. (1984) Synthetic struvite, $MgNH_4PO_4{\cdot}6H_2O$: correct polarity and surface features of some complementary forms. *Acta Crystallographica*, **B40**, 223–227.

Åberg, M. (1969) The crystal structure of $[(UO_2)_2(OH)_2Cl_2(H_2O)_4]$. *Acta Chemica Scandinavica*, **23**, 791–810.

Åberg, M. (1976) The crystal structure of $[(UO_2)_4Cl_2O_2(OH)_2(H_2O)_6]{\cdot}4H_2O$ a compound containing a tetranuclear aqua-chlorohydroxooxo complex of uranyl(VI). *Acta Chemica Scandinavica*, **A30**, 507–514.

Åberg, M. (1978) The crystal structure of hexaaqua-tri-μ-hydroxo-μ_3-oxo-triuranyl(VI)nitrate tetrahydrate, $[(UO_2)_3O(OH)_3(H_2O)_6]NO_3{\cdot}4H_2O$. *Acta Chemica Scandinavica*, **A32**, 101–107.

Adiwidjaja, G., Friese, K., Klaska, K.-H. and Schlüter, J. (1997) The crystal structure of gordaite $NaZn_4SO_4(OH)_6Cl_6(H_2O)$. *Zeitschrift für Kristallographie*, **212**, 704–707.

Albrecht-Schmitt, T.E., Almond, P.M. and Sykora, R.E. (2003) Cation–cation interactions in neptunyl(V) compounds: Hydrothermal preparation and structural characterization of $NpO_2(IO_3)$ and α- and β-$AgNpO_2(SeO_3)$. *Inorganic Chemistry*, **42**, 3788–3795.

Almond, P.M., Talley, C.E., Gibbs, S.M., Peper, S.M. and Albrecht-Schmitt, T.E. (2002) Variable dimensionality and new uranium oxide topologies in the alkaline-earth metal uranyl selenites $AE[(UO_2)(SeO_3)_2]$ (AE = Ca, Ba) and $Sr[(UO_2)(SeO_3)_2]{\cdot}2H_2O$. *Journal of Solid State Chemistry*, **154**, 358–366.

Aurivillius, K. (1965) The structural chemistry of inorganic mercury (II) compounds. *Arkiv for Kemi*, **23**, 205–211.

Aurivillius, B. (1976) A case of mimetic twinning: the crystal structure of Pb_2OFX (X= Cl, Br and I). *Chemica Scripta*, **10**, 156–163.

Aurivillius, K. and Folkmarson, L. (1968) The crystal structure of terlinguaite $Hg_4O_2Cl_2$. *Acta Chemica Scandinavica*, **22**, 2529–2540.

Bachmann, H.-G. and Zemann, J. (1961) Die Kristallstruktur von Linarit, $PbCuSO_4(OH)_2$. *Acta*

Crystallographica, **14**, 747–751.

Back, M.E. (2014) *Fleischer's Glossary of Mineral Species 2008*. The Mineralogical Record, Tucson, Arizona, USA.

Bakakin, V.V., Rylov, G.M. and Alekseev, V.I. (1974) Refinement of the crystal structure of hurlbutite $CaBe_2P_2O_8$. *Kristallografiya*, **19**, 1283–1285 [in Russian].

Barlow, W. (1883) Probable nature of the internal symmetry in crystals. *Nature*, **29**, 186–188.

Barlow, W. (1898) Geometrische Untersuchung über eine mechanische Ursache der Homogenität der Struktur und der Symmetrie; mit besonderer Anwendung auf Kristallization und chemische Verbindung. *Zeitschrift für Kristallographie*, **29**, 433–461.

Baur, W.H. (1960) Die Kristallstruktur von $FeSO_4{\cdot}4H_2O$. *Naturwissenschaften*, **47**, 467.

Baur, W.H. and Rama Rao, B. (1967) The crystal structure of metavauxite. *Naturwissenschaften*, **54**, 561.

Bean, A.C., Peper, S.M. and Albrecht-Schmitt, T.E. (2001) Structural relationships, interconversion, and optical properties of the uranyl iodates, $UO_2(IO_3)_2$ and $UO_2(IO_3)_2(H_2O)$: a comparison of reactions under mild and supercritical conditions. *Chemistry of Materials*, **13**, 1266–1272.

Behm, H. (1985) Hexpotassium(*cyclo*-octahydroxotetracosaoxohexadecaborato) dioxouranate(VI) dodecahyrate, $K_6[UO_2\{B_{16}O_{24}(OH)_8\}]{\cdot}12H_2O$. *Acta Crystallographica*, **C41**, 642–645.

Belov, N.V. (1961) *Crystal Chemistry of Silicates with Large Cations*. Akademia Nauk SSSR, Moscow.

Berlepsch, P., Armbruster, T., Brugger, J., Bykova, E.Y. and Kartashov, P.M. (1999) The crystal structure of vergasovaite $Cu_3O[Mo,S)O_4SO_4]$, and its relation to synthetic $Cu_3O[MoO_4]_2$. *European Journal of Mineralogy*, **11**, 101–110.

Bermanec, V., Armbruster, T., Tiblias, D., Sturman, D. and Kniewald, G. (1994) Tuzlaite, $NaCa[B_5O_8(OH)_2]{\cdot}3H_2O$, a new mineral with a pentaborate sheet structure from the Tuzla salt mine, Bosnia and Hercegovina. *American Mineralogist*, **79**, 562–569.

Bickmore, B.R. (2013) *Structure and Acidity in Aqueous Solutions and Oxide–Water Interfaces*. Structure and Bonding Series. Springer, Berlin.

Bickmore, B.R., Rosso, K.M., Nagy, K.L., Cygan, R.T. and Tadanier, C.J. (2004*a*) *Ab initio* determination of edge surface structures for dioctahedral 2:1 phyllosilicates: implications for acid-base reactivity. *Clays and Clay Minerals*. **51**, 359–371.

Bickmore, B.R., Tadanier, C.J., Rosso, K.M., Monn, W.D. and Eggett, D.L. (2004*b*) Bond-valence methods for pK_a prediction: critical reanalysis and a new approach. *Geochimica et Cosmochimica Acta*, **68**, 2025–2042.

Bickmore, B.R., Rosso, K.M., Tadanier, C.J., Bylaska, E.J. and Doub, D. (2006) Bond-valence methods for pK_a prediction. II. Bond-valence, electrostatic, molecular geometry, and solvation effects. *Geochimica et Cosmochimica Acta*, **70**, 4057–4071.

Bigi, S., Brigatti, M.F. and Capredi, S. (1991) Crystal chemistry of Fe- and Cr-rich warwickite. *American Mineralogist*, **76**, 1380–1388.

Boher, P., Garnier, P., Gavarri, J.R. and Hewat, A.W. (1985) Monoxyde quadratique PbOα (I): Description de la transition structurale ferroélastique. *Journal of Solid State Chemistry*, **57**, 343–350.

Bokii, G.B. and Gorogotskaya, L.I. (1969) Crystal chemical classification of sulfates. *Zhurnal Strukturnoi Khimii*, **10**, 183–185 [in Russian].

Bonazzi, P. and Menchetti, S. (1989) Contribution to the crystal chemistry of the minerals of the ludwigite–vonsenite series. *Neues Jahrbuch für Mineralogie – Monatshefte*, **1989**, 69–83.

Bonazzi, P., Menchetii, S., Sabelli, C. and Trosti-Ferroni, R. (1986) Karlite: crystal structure and chemical composition. *Neues Jahrbuch für Mineralogie – Monatshefte*, **1986**, 253–262.

Borene, J. (1970) Structure cristalline de la parabutlerite. *Bulletin de la Société Française Minéralogie et de Cristallographie*, **93**,185–189.

Bowen, N.L. (1928) *Evolution of Igneous Rocks*. Princeton University Press, Princeton, New Jersey, USA.

Bragg, W.L. (1913) The structure of some crystals as indicated by their diffraction of X-rays. *Proceedings of the Royal Society of London*, **A89**, 248–263.

Bragg, W.L. (1930) The structure of silicates. *Zeitschrift für Kristallographie*, **74**, 237–305.

Brovkin, A.A., Zayakina, N.Y. and Brovkina, V.S. (1975) Crystal structure of strontioborite $Sr[B_8O_{11}(OH)_4]$. *Soviet Physics Crystallography*, **20**, 563–566.

Brown, I.D. (2002) *The Chemical Bond in Inorganic Chemistry. The Bond Valence Model*. Oxford University Press, Oxford, UK.

Brown, I.D. (2009) Recent developments in the methods and applications of the bond valence model. *Chemical Reviews*, **109**, 6858–6919.

Brown, G.E. and Clark, J.R. (1978) Crystal structure of hydrochlorborite, $Ca_2[B_3O_3(OH)_4]OB(OH_3]Cl{\cdot}7H_2O$, a seasonal evaporite mineral. *American Mineralogist*, **63**, 814–823.

Burdett, J.K., Lee, S. and Sha, W.C. (1984) The method of moments and the energy levels of molecules and solids. *Croatica Chemica Acta*, **57**, 1193–1216.

Burns, P.C. (1995) Borate clusters and fundamental building blocks containing four polyhedra: why few clusters are utilized as fundamental building blocks of structures. *The Canadian Mineralogist*, **33**,

1167–1176.

Burns, P.C. (1999) The crystal chemistry of uranium. Pp. 23–90 in: *Uranium: Mineralogy, Geochemistry, and the Environment* (P.C.Burns and R. Finch, editors). Reviews in Mineralogy, **38**. Mineralogical Society of America, Washington DC.

Burns, P.C. (2005) U^{6+} minerals and inorganic compounds: insights into an expanded structural hierarchy of crystal structures. *The Canadian Mineralogist*, **43**, 1839–1894.

Burns, P.C. and Finch, R.J. (1999) Wyartite: crystallographic evidence for the first pentavalent-uranium mineral. *American Mineralogist*, **84**, 1456–1460.

Burns, P.C. and Hawthorne, F.C. (1994*a*) Kaliborite: an example of a crystallographically symmetrical hydrogen bond. *The Canadian Mineralogist*, **32**, 885–894.

Burns, P.C. and Hawthorne, F.C. (1994*b*) Hydrogen bonding in tunellite. *The Canadian Mineralogist*, **32**, 895–902.

Burns, P.C. and Hawthorne, F.C. (1994*c*) Refinement of the structure of hilgardite-1A. *Acta Crystallographica*, **C50**, 653–655.

Burns, P.C. and Hawthorne, F.C. (1995) The crystal structure of sinkankasite, a complex heteropolyhedral sheet mineral. *American Mineralogist*, **80**, 620–627.

Burns, P.C. and Hawthorne, F.C. (1996) Static and dynamic Jahn–Teller effects in Cu^{2+}-oxysalt minerals. *The Canadian Mineralogist*, **34**, 1089–1105.

Burns, P.C., Grice, J.D. and Hawthorne, F.C. (1995*a*) Borate minerals. I. Polyhedral clusters and fundamental building blocks. *The Canadian Mineralogist*, **33**, 1131–1151.

Burns, P.C., Novák, M. and Hawthorne, F.C. (1995*b*) Fluorine-hydroxyl variation in hambergite: A crystal structure study. *The Canadian Mineralogist*, **22**, 1205–1213.

Burns, P.C., Miller, M.L. and Ewing, R.C. (1996) U^{6+} minerals and inorganic phases: a comparison and hierarchy of structures. *The Canadian Mineralogist*, **34**, 845–880.

Burns, P.C., Ewing, R.C. and Hawthorne, F.C. (1997*a*) The crystal chemistry of hexavalent uranium: polyhedron geometries, bond-valence parameters and polymerization of polyhedra. *The Canadian Mineralogist*, **35**, 1551–1570.

Burns, P.C., Finch, R.J., Hawthorne, F.C., Miller, M.L. and Ewing, R.C. (1997*b*) The crystal structure of ianthinite, $[U_2^{4+}(UO_2)_4O_6(OH)_4(H_2O)_4](H_2O)_5$: a possible phase for Pu^{4+} incorporation during the oxidation of spent nuclear fuel. *Journal of Nuclear Materials*, **249**, 199–206.

Burns, P.C., Olson, R.A., Finch, R.J., Hanchar, J.M. and Thibault, Y. (2000) $KNa_3(UO_2)_2(Si_4O_{10})_2(H_2O)_4$, a new compound formed during vapor hydration of an actinide-bearing borosilicate waste glass. *Journal of Nuclear Materials*, **278**, 290–300.

Burns, P.C., Krivovichev, S.V. and Filatov, S.K. (2002) New Cu^{2+} coordination polyhedra in the crystal structure of burnsite, $KCdCu_7O_2(SeO_3)_2Cl_9$. *The Canadian Mineralogist*, **40**, 1587–1595.

Cahill, C.L., Krivovichev, S.V., Burns, P.C., Bekenova, G.K. and Shabanova, T.A. (2001) The crystal structure of mitryaevaite, $Al_5(PO_4)_2[(P,S)O_3(OH,O)]_2F_2(OH)_2(H_2O)_8{\cdot}6.48H_2O$, determined from a microcrystal using synchrotron radiation. *The Canadian Mineralogist*, **39**, 179–186.

Cannillo, E., Dal Negro, A. and Ungaretti, L. (1973) The crystal structure of ezcurrite. *American Mineralogist*, **58**, 110–115.

Cantos, P.M., Jouffret, L.J., Wilson, R.E., Burns, P.C. and Cahill, C.L. (2013) Series of uranyl-4,4′-biphenyldicarboxylates and an occurrence of a cation-cation interaction: Hydrothermal synthesis and in situ Raman studies. *Inorganic Chemistry*, **52**, 9487–9495.

Catti, M., Ferraris, G. and Ivaldi, G. (1979) Refinement of the crystal structure of anapaite, $Ca_2Fe(PO_4)_2(H_2O)_4$. Hydrogen bonding and relationships with the bihydrated phase. *Bulletin de la Société Française Minéralogie et de Cristallographie*, **102**, 314–318.

Chopin, C., Brunet, F., Gebert, W., Medenbach, O. and Tillmanns, E. (1993) Bearthite, $Ca_2Al(PO_4)_2(OH)$, a new mineral from high-pressure terranes of the western Alps. *Schweizerische Mineralogische und Petrographische Mitteilungen*, **73**, 1–9.

Christ, C.L. (1960) Crystal chemistry and systematic classification of hydrous borate minerals. *American Mineralogist*, **45**, 334–340.

Christ, C.L. and Clark, J.R. (1977) A crystal-chemical classification of borate structures with emphasis on hydrated borates. *Physics and Chemistry of Minerals*, **2**, 59–87.

Christ, C.L., Truesdell, A.H. and Erd, R.C. (1967): Borate mineral assemblages in the system $Na_2O–CaO–MgO–B_2O_3–H_2O$. *Geochimica et Cosmochimica Acta*, **31**, 313–337.

Coda, A., Rossi, G., Ungaretti, L. and Carobbi, S.G. (1967) The crystal structure of aminoffite. *Atti della Accademia Nazionale dei Lincei, Classe di Scienze Fisiche, Matematiche e Naturali, Rendiconti, Serie*, **8(43)**, 225–232.

Coda, A., Ungaretti, L. and Guista, A.D. (1974) The crystal structure of leifite, $Na_6[Si_{16}Al_2(BeOH)_2O_{39}]{\cdot}1.5H_2O$. *Acta Crystallographica*, **B30**, 396–401.

Cooper, M.A. and Hawthorne, F.C. (1994) The crystal structure of kombatite, $Pb_{14}(VO_4)_2O_9Cl_4$, a complex heteropolyhedral-sheet mineral. *American Mineralogist*, **79**, 550–554.

Cooper, M.A. and Hawthorne, F.C. (1997) The crystal structure of wicksite. *The Canadian Mineralogist*, **35**, 777–784.

Cooper, M.A. and Hawthorne, F.C. (1998) The crystal structure of blatterite, $Sb^{5+}(Mn^{3+},Fe^{3+})_9(Mn^{2+},Mg)_{35}(BO_3)_{16}O_{32}$, and structural hierarchy in Mn^{3+}-bearing zigzag borates. *The Canadian Mineralogist*, **36**, 1171–1193.

Cooper, M.A. and Hawthorne, F.C. (1999) The structure topology of sidpietersite, $Pb_4^{2+}(S^{6+}O_3S^{2-})O_2(OH)_2$, a novel thiosulphate structure. *The Canadian Mineralogist*, **37**, 1275–1282.

Cooper, M.A. and Hawthorne, F.C. (2003) The crystal structure of vasilyevite, $(Hg_2)_{10}^{2+}O_6I_3(Br,Cl)_3(CO_3)$. *The Canadian Mineralogist*, **41**, 1173–1181.

Cooper, M.A. and Hawthorne, F.C. (2009) The crystal structure of tedhadleyite, $Hg^{2+}Hg_{10}^{1+}O_4I_2(Cl,Br)_2$, from the Clear Creek Claim, San Benito County, California. *Mineralogical Magazine*, **73**, 227–234.

Cooper, M.A., Hawthorne, F.C. and Černý, P. (2009*a*) The crystal structure of ercitite, $Na_2(H_2O)_4[Mn_2^{3+}(OH)_2(PO_4)_2]$, and its relation to bermanite, $Mn^{2+}(H_2O)_4[Mn_2^{3+}(OH)_2(PO_4)_2]$. *The Canadian Mineralogist*, **47**, 173–180.

Cooper, M.A., Hawthorne, F.C. and Moffatt, E. (2009*b*) Steverustite, $Pb_5^{2+}(OH)_5[Cu^{1+}(S^{6+}O_3S^{2-})_3](H_2O)_2$, a new thiosulfate mineral from the Frongoch Mine Dump, Devils Bridge, Ceredigion, Wales: Description and crystal structure. *Mineralogical Magazine*, **73**, 235–250.

Cooper, M.A., Abdu, Y.A., Hawthorne, F.C. and Kampf, A.R. (2013) The crystal structure of comancheite, $Hg_{55}^{2+}N_{24}^{3-}(OH,NH_2)_4(Cl,Br)_{34}$, and crystal-chemical and spectroscopic discrimination of N^{3-} and O^{2-} anions in Hg^{2+} compounds. *Mineralogical Magazine*, **77**, 3217–3237.

Cooper, W.F., Larsen, F.K., Coppens, P. and Giese, R.F. (1973) Electron population analysis of accurate diffraction data. V. Structure and one-center charge refinement of the light-atom mineral kernite, $Na_2B_4O_6(OH)_3{\cdot}3H_2O$. *American Mineralogist*, **58**, 21–31.

Corazza, E. (1974) The crystal structure of kurnakovite: a refinement. *Acta Crystallographica*, **B30**, 2194–2199.

Corazza, E., Menchetti, S. and Sabelli, C. (1974) The crystal structure of biringuccite, $Na_4[B_{10}O_{16}(OH)_2]{\cdot}2H_2O$. *American Mineralogist*, **59**, 1005–1015.

Corbridge, D.E.C. (1985) *Phosphorous. An Outline of its Chemistry, Biochemistry and Technology, 3rd Edition*, Elsevier, Amsterdam.

Cordsen, A. (1978) A crystal structure refinement of libethenite. *The Canadian Mineralogist*, **16**, 153–157.

Cousson, A., Dabos, S., Abazli, H., Nectoux, F., Pagès, M. and Choppin, G. (1984) Crystal structure of a neptunyl cation-cation complex (NpO^{2+}) with mellitic acid: $Na_4(NpO_2)_2Cl_{12}O_{12}{\cdot}8H_2O$. *Journal of the Less-Common Metals*, **99**, 233–240.

Dahmen, T. and Gruehn, R. (1993) Beitrage zum thermischen Verhalten von Sulfaten. IX. Einkristallstrukturverfeinerung der Metall(III)-sulfate $Cr_2(SO_4)_3$ und $Al_2(SO_4)_3$. *Zeitschrift für Kristallographie*, **204**, 57–65.

Dal Negro, A. and Tadini, C. (1974) Refinement of the crystal structure of fluoborite, $Mg_3(F,OH)_3(BO_3)$. *Tschermaks Mineralogische und Petrographische Mitteilungen*, **21**, 94–100.

Dal Negro, A., Martin Pozas, J.M. and Ungaretti, L. (1975) The crystal structure of ameghinite. *American Mineralogist*, **60**, 879–883.

Demartin, F., Gramaccioli, C.M. and Pilati, T. (1992) The importance of accurate crystal structure determination of uranium minerals. II. Soddyite $(UO_2)_2(SiO_4){\cdot}2H2O$. *Acta Crystallographica*, **C48**, 1–4.

Demartin, F., Gramaccioli, C.M. and Campostrini, I. (2010) Pyracmonite, $(NH_4)_3Al(SO_4)_3$, a new ammonium iron sulfate from La Fossa Crater, Vulcano, Aeolian Islands, Italy. *The Canadian Mineralogist*, **48**, 307–313.

Demartin, F., Castellano, C. and Campostrini, I. (2013) Aluminopyracmonite, $(NH_4)_3Fe(SO_4)_3$, a new ammonium aluminium sulfate from La Fossa Crater, Vulcano, Aeolian Islands, Italy. *Mineralogical Magazine* 77, 443–451.

Dowty, E. and Clark, J.R. (1973) Crystal-structure refinements for orthorhombic boracite, $Mg_3ClB_7O_{13}$, and a trigonal, iron-rich analogue. *Zeitschrift für Kristallographie*, **138**, 64–99.

Duribreux, I., Dion, C., Abraham, F. and Saadi, M. (1999) $CsUV_3O_{11}$, a new uranyl vanadate with a layered structure. *Journal of Solid State Chemistry*, **146**, 258–265.

Edwards, J.O. and Ross, V.F. (1960) Structural principles of the hydrated polyborates. *Journal of Inorganic and Nuclear Chemistry*, **15**, 329–337.

Effenberger, H. (1985) $Cu_2O(SO_4)$, Dolerophanite: Refinement of the crystal structure, with a comparison of $[OCu(II)_4]$ tetrahedra in inorganic compounds. *Monatshefte für Chemie*, **116**, 927–931.

Effenberger, H. and Pertlik, F. (1986) Die Kristallstrukturen der Kupfer (II)-oxo-selenite $Cu_2O(SeO_3)$(kubisch und monoklin) und $Cu_4O(SeO_3)_3$ (monoklin und triklin). *Monatshefte für Chemie*, **117**, 887–896.

Effenberger, H. and Zemann, J. (1984) The crystal structure of caratiite. *Mineralogical Magazine*, **48**, 541–546.

Effenberger, H., Pertlik, F. and Zemann, J. (1986) Refinement of the crystal structure of krausite: a

mineral with an interpolyhedral oxygen–oxygen contact shorter than the hydrogen bond. *American Mineralogist*, **71**, 202–205.

Egorov-Tismenko, Y.K., Simonov, M.A. and Belov, N.V. (1980) Crystal structures of calciborite $Ca_2[BO_3BO]_2$ and synthetic calciboraluminate $2CaAl[BO_3] = Ca_2[A!O_3BO]_2$. *Soviet Physics* Doklady, **25**, 226–227.

Evans, H.T. Jr. and Hughes, J.M. (1990) Crystal chemistry of the natural vanadium bronzes. *American Mineralogist*, **75**, 508–521.

Fanfani, L. and Zanazzi, P.F. (1967) Structural similarities of some secondary lead minerals. *Mineralogical Magazine*, **36**, 522–529.

Fanfani, L. and Zanazzi, P.F. (1968) The crystal structure of vauquelinite and the relationships to fornacite. *Zeitschrift für Kristallographie*, **126**, 433–443.

Fanfani, L., Nunzi, A. and Zanazzi, P.F. (1970) The crystal structure of roemerite. *American Mineralogist*, **55**, 78–89.

Fanfani, L., Nunzi, A. and Zanazzi, P.F. (1971) The crystal structure of butlerite. *American Mineralogist*, **56**, 751–757.

Fanfani, L., Nunzi, A., Zanazzi, P.F. and Zanzari, A.R. (1973) The copiapite problem: the crystal structure of a ferrian copiapite. *American Mineralogist*, **58**, 314–322.

Fanfani, L., Nunzi, A., Zanazzi, P.F. and Zanzari, A.R. (1976) Additional data on the crystal structure of montgomeryite. *American Mineralogist*, **61**, 12–14.

Fang, J.H. and Robinson, P.D. (1970) Crystal structures and mineral chemistry of hydrated ferric sulfates. I. The crystal structure of coquimbite. *American Mineralogist*, **55**, 1534–1540.

Filatov, S.K., Semenova, T.F. and Vergasova, L.P. (1992) Types of polymerization of $[OCu_4]^{6+}$ tetrahedra in compounds with 'additional' oxygen atoms. *Proceedings of the USSR Academy of Sciences*, **322**, 536–539 [in Russian].

Finch, R.J., Cooper, M.A., Hawthorne, F.C. and Ewing, R.C. (1999) Refinement of the crystal structure of rutherfordine. *The Canadian Mineralogist*, **37**, 929–938.

Finger, L.W. (1985) Fingerite, $Cu_{11}O_2(VO_4)_6$, new vanadium sublimate from Izalco volcano, El Salvador: crystal structure. *American Mineralogist*, **70**, 197–199.

Fischer, A. (2003) Competitive coordination of the uranyl ion by perchlorate and water – the crystal structures of $UO_2(ClO_4)_2{\cdot}3H_2O$, $UO_2(ClO_4)_2{\cdot}5H_2O$ and redetermination of $UO_2(ClO_4)_2{\cdot}7H_2O$. *Zeitschrift für Anorganische und Allgemeine Chemie*, **629**, 1012–1016.

Foley, J.A., Hughes, J.M and Lange, D. (1997) The atomic arrangement of brackebuschite, redefined as $Pb_2(Mn^{3+},Fe^{3+})(VO_4)_2(OH)$, and comments on Mn^{3+} octahedra. *The Canadian Mineralogist*, **35**, 1027–1033.

Gasperin, M. (1987) Structure du borate d'uranium UB_2O_6. *Acta Crystallographica*, **C43**, 2031–2033.

Ghose, S. and Wan, C. (1977) Aristarainite: $Na_2Mg[B_6O_8(OH)_4]_2{\cdot}4H_2O$: a sheet structure with chains of hexaborate polyanions. *American Mineralogist*, **62**, 979–989.

Ghose, S., Wan, C. and Clark, J.R. (1978) Ulexite, $NaCaB_5O_6(OH)_6{\cdot}5H_2O$: structure refinement, polyanion configuration, hydrogen bonding, and fiber optics. *American Mineralogist*, **63**, 160–171.

Giacovazzo, G., Scordari, F., Todisco, A. and Menchetti, S. (1976) Crystal structure model for metavoltine from Sierra Gorda. *Tschermaks Mineralogische und Petrographische Mitteilungen*, **23**, 155–166.

Giese, R.F. Jr. and Penna, G. (1983) The crystal structure of sulfoborite, $Mg_3SO_4(B(OH)_4)_2(OH)F$. *American Mineralogist*, **68**, 255–261.

Giester, G. and Zemann, J. (1987) The crystal structure of the natrochalcite-type compounds $(Me^+)Cu_2(OH)(ZO_4)_2{\cdot}H_2O$ (Me^+ = Na, K, Rb; Z = S, Se), with special reference to the hydrogen bonds. *Zeitschrift für Kristallographie*, **179**, 431–442.

Giester, G., Mikenda, W. and Pertlik, F. (1996) Kleinite from Terlingua, Brewster County, Texas: investigations by single crystal X-ray diffraction, and vibrational spectroscopy. *Neues Jahrbuch für Mineralogie – Monatshefte*, **1996**, 49–56.

Giuseppetti, G. and Tadini, C. (1983) Structural analysis and refinement of Bolivian creedite, $Ca_3Al_2F_8(OH)_2(SO_4){\cdot}(H_2O)_2$. The role of the hydrogen atoms. *Neues Jahrbuch für Mineralogie – Monatshefte*, **1983**, 69–78.

Giuseppetti, G. and Tadini, C. (1984) The crystal structure of childrenite from Tavistock (SW England), $Ch_{89}Eo_{11}$ term of childrenite–eosphorite series. *Neues Jahrbuch für Mineralogie – Monatshefte*, **1984**, 263–271.

Giuseppetti, G., Mazzi, F., Tadini, C., Larsen, A.O., Asheim, A. and Raade, G. (1990) Berborite polytypes. *Neues Jahrbuch für Mineralogie – Abhandlungen*, **162**, 101–116.

Giuseppetti, G., Tadini, C. and Mattioli, V. (1992) Bertrandite, $Be_4Si_2O_7(OH)_2$, from Val Vigezzo (NO) Italy: The X-ray structural refinement. *Neues Jahrbuch für Mineralogie – Monatshefte*, **1992**, 13–19.

Gorskaya, M.G., Filatov, S.K., Rozhdestvenskaya, I.V. and Vergasova, L.P. (1992) The crystal structure of klyuchevskite, $K_3Cu_3(Fe,Al)O_2(SO_4)_4$, a new mineral from Kamchatka volcanic sublimates. *Mineralogical Magazine*, **56**, 411–416.

Graeber, E.J. and Rosenzweig, A. (1971) The crystal structures of yavapaiite, $KFe(SO_4)_2$, and goldichite,

$KFe(SO_4)_2(H_2O)_4$. *American Mineralogist*, **56**, 1917–1933.

Grice, J.D. (1999) Redetermination of the crystal structure of hanawaltite. *The Canadian Mineralogist*, **37**, 775–778.

Grice, J.D. and Hawthorne, F.C. (1989) Refinement of the crystal structure of leucophanite. *The Canadian Mineralogist*, **27**, 193–197.

Grice, J.D. and Hawthorne, F.C. (2002) New data on meliphanite, $Ca_4(Na,Ca)_4Be_4AlSi_7O_{24}(F,O)_4$. *The Canadian Mineralogist*, **40**, 971–980.

Grice, J.D., Burns, P.C. and Hawthorne, F.C. (1994) Determination of the megastructures of the borate polymorphs pringleite and ruitenbergite. *The Canadian Mineralogist*, **32**, 1–14.

Grice, J.D., Burns, P.C. and Hawthorne, F.C. (1999) Borate minerals II. A hierarchy of structures based on the borate fundamental building block. *The Canadian Mineralogist*, **37**, 731–762.

Groat, L.A. and Hawthorne, F.C. (1986) Structure of ungemachite, $K_3Na_8Fe^{3+}(SO_4)_6(NO_3)_2(H_2O)_6$ a mixed sulfate-nitrate mineral. *American Mineralogist*, **71**, 826–829.

Groat, L.A., Roberts, A.C. and Le Page, Y. (1995) The crystal structure of wattersite, $Hg_4^{1+}Hg^{2+}Cr^{6+}O_6$. *The Canadian Mineralogist*, **33**, 41–46.

Guy, B.B. and Jeffrey, G.A. (1966) The crystal structure of fluellite, $Al_2PO_4F_2(OH)(H_2O)_7$. *American Mineralogist*, **51**, 1579–1592.

Hansen, S., Faelth, L. and Johnson, O. (1984) Bergslagite, a mineral with tetrahedral berylloarsenate sheet anions. *Zeitschrift für Kristallographie*, **166**, 73–80.

Harlow, G.E. and Hawthorne, F.C. (2008) Herderite from Mogok, Myanmar, and comparison with hydroxyl-herderite from Ehrenfriedersdorf, Germany. *American Mineralogist*, **93**, 1545–1549.

Harrison, W.T.A. (2000) Synthetic mansfieldite, $AlAsO_4{\cdot}2H_2O$. *Acta Crystallographica*, **C56**, e421.

Harrison, W.T.A., Nenoff, T.M., Gier, T.E. and Stucky, G.D. (1993) Tetrahedral-atom 3-ring groupings in 1-dimensional inorganic chains: $Be_2AsO_4OH{\cdot}4H_2O$ and $Na_2ZnPO_4OH{\cdot}7H_2O$. *Inorganic Chemistry*, **32**, 2437–2441.

Hassan, I. and Grundy, H.D. (1991) The crystal structure and thermal expansion of tugtupite, $Na_8(Al_2Be_2Si_8O_{24})Cl_2$. *The Canadian Mineralogist*, **29**, 385–390.

Hawthorne, F.C. (1976*a*) The hydrogen positions in scorodite. *Acta Crystallographica*, **B32**, 2891–2892.

Hawthorne, F.C. (1976*b*) Refinement of the crystal structure of adamite. *The Canadian Mineralogist*, **14**, 143–148.

Hawthorne, F.C. (1979) The crystal structure of morinite. *The Canadian Mineralogist*, **17**, 93–102.

Hawthorne, F.C. (1982) The crystal structure of bøggildite. *The Canadian Mineralogist*, **20**, 263–270.

Hawthorne, F.C. (1983*a*) Graphical enumeration of polyhedral clusters. *Acta Crystallographica*, **A39**, 724–736.

Hawthorne, F.C. (1983*b*) The crystal structure of tancoite. *Tschermaks Mineralogische und Petrographische Mitteilungen*, **31**, 121–135.

Hawthorne, F.C. (1984) The crystal structure of stenonite and the classification of the alumino fluoride minerals. *The Canadian Mineralogist*, **22**, 245–251.

Hawthorne, F.C. (1985*a*) Towards a structural classification of minerals: The $^{VI}M^{IV}T_2O_n$ minerals. *American Mineralogist*, **70**, 455–473.

Hawthorne, F.C. (1985*b*) Refinement of the crystal structure of blödite: Structural similarities in the $[^{VI}M(^{IV}T\varphi_4)_2\varphi_n]$ finite-cluster minerals. *The Canadian Mineralogist*, **23**, 669–674.

Hawthorne, F.C. (1986) Structural hierarchy in $^{VI}Mx^{III}T_y\varphi_z$ minerals. *The Canadian Mineralogist*, **24**, 625–642.

Hawthorne, F.C. (1990) Structural hierarchy in $M^{[6]}T^{[4]}\varphi_n$ minerals. *Zeitschrift für Kristallographie*, **192**, 1–52.

Hawthorne, F.C. (1992) The role of OH and H_2O in oxide and oxysalt minerals. *Zeitschrift für Kristallographie*, **201**, 183–206.

Hawthorne, F.C. (1994) Structural aspects of oxide and oxysalt crystals. *Acta Crystallographica*, **B50**, 481–510.

Hawthorne, F.C. (1997) Structural aspects of oxide and oxysalt minerals. Pp. 373–429 in: *European Mineralogical Union Notes in Mineralogy Vol. 1* (S. Merlino, editor). Eötvös University Press, Budapest, Hungary.

Hawthorne, F.C. (1998) Structure and chemistry of phosphate minerals. *Mineralogical Magazine*, **62**, 141–164.

Hawthorne, F.C. (2006) *Landmark Papers: Structure Topology*. Mineralogical Society of Great Britain and Ireland, London.

Hawthorne, F.C. (2012*a*) A bond-topological approach to theoretical mineralogy: crystal structure, chemical composition and chemical reactions. *Physics and Chemistry of Minerals*, **39**, 841–874.

Hawthorne, F.C. (2012*b*) Bond topology and structure-generating functions: Graph-theoretic prediction of chemical composition and structure in polysomatic T–O–T (biopyribole) and H–O–H structures. *Mineralogical Magazine*, **76**, 1053–1080.

Hawthorne, F.C. and Ferguson, R.B. (1975) Refinement of the crystal structure of kröhnkite. *Acta Crystallographica*, **B31**, 1753–1755.

Hawthorne, F.C. and Grice, J.D. (1987) The crystal structure of ehrleite, a tetrahedral sheet structure. *The*

Canadian Mineralogist, **25**, 767–774.

Hawthorne, F.C. and Groat, L.A. (1985) The crystal structure of wroewolfeite, a mineral with $[(Cu_4(OH)_6(SO_4)(H_2O)]$ sheets. *American Mineralogist*, **70**, 1050–1055.

Hawthorne, F.C. and Huminicki, D.M.C. (2002) The crystal chemistry of beryllium. Pp. 333–404 in: *Beryllium: Mineralogy, Petrology, and Geochemistry* (E.S. Grew, editor). Reviews in Mineralogy & Geochemistry, **50**. Mineralogical Society of America and the Geochemical Society, Washington DC.

Hawthorne, F.C. and Schindler, M.S. (2000) Topological enumeration of decorated $[Cu^{2+}\varphi_2]_N$ sheets in hydroxy-hydrated copper-oxysalt minerals. *The Canadian Mineralogist*, **38**, 751–761.

Hawthorne, F.C. and Schindler, M.S. (2008) Understanding the weakly bonded constituents in oxysalt minerals. *Zeitschrift für Kristallographie*, **223**, 41–68.

Hawthorne, F.C. and Schindler, M.S. (2014) Crystallization and Dissolution in Aqueous Solution: A Bond-Valence Approach. Pp. 161–189 in: *Bond Valences* (I.D. Brown and K.R. Poeppelmeier, editors). Springer, Berlin.

Hawthorne, F.C. and Sokolova, E. (2012) The role of H_2O in controlling bond topology: The $^{[6]}Mg(SO_4)(H_2O)_n$ (n = 0–6) structures. *Zeitschrift für Kristallographie*, **227**, 594–603.

Hawthorne, F.C., Groat, L.A., Raudsepp, M. and Ercit, T.S. (1987) Kieserite, Mg(SO4)(H2O), a titanite group mineral. *Neues Jahrbuch für Mineralogie – Abhandlungen*, **157**, 121–132.

Hawthorne, F.C., Groat, L.E. and Eby, R.K. (1989) Antlerite, $Cu_3SO_4(OH)_4$, a heteropolyhedral wallpaper structure. *The Canadian Mineralogist*, **27**, 205–209.

Hawthorne, F.C., Kimata, M., Černý, P., Ball, N., Rossman, G.R. and Grice, J.D. (1991) The crystal chemistry of the milarite-group minerals. *American Mineralogist*, **76**, 1836–1856.

Hawthorne, F.C., Cooper, M. and Sen Gupta, P.K. (1994) The crystal structure of pinchite, $Hg_5Cl_2O_4$. *American Mineralogist*, **79**, 1199–1203.

Hawthorne, F.C., Burns, P.C., Grice, J.D. (1996) The crystal chemistry of boron. Pp. 41–116 in: *Boron: Mineralogy, Petrology, and Geochemistry* (E.S. Grew and L.M. Anovitz, editors). Reviews in Mineralogy, **33**. The Mineralogical Society of America, Washington DC.

Hawthorne, F.C., Krivovichev, S.V. and Burns, P.C. (2000) The crystal chemistry of sulfate minerals. Pp. 1–112 in: *Sulfate Minerals: Crystallography, Geochemistry, and Environmental Significance* (C.N. Alpers, J.L. Jambor, and D.K. Nordstrom, editors). Reviews in Mineralogy & Geochemistry, **40**. The Mineralogical Society of America and the Geochemical Society, Washington DC.

Hayden, l.A. and Burns, P.C. (2002) A novel uranyl sulfate cluster in the structure of $Na_6(UO_2)(SO_4)_4(H_2O)_2$. *Journal of Solid State Chemistry*, **163**, 313–318.

Hazen, R.M. and Finger, L.W. (1986) High-pressure and high-temperature crystal chemistry of beryllium oxide. *Journal of Applied Physics*, **59**, 3728–3733.

Hazen, R.M., Au, A.Y. and Finger, L.W. (1986) High-pressure crystal chemistry of beryl ($Be_3Al_2Si_6O_{18}$) and euclase ($BeAlSiO_4OH$). *American Mineralogist*, **71**, 977–984.

Heller, G. (1970) Darstellung ynd Systematisierungvon Boraten und Polyboraten. *Fortschritte Der Chemischen Forschung*, **15**, 206–280.

Herwig, S. and Hawthorne, F.C. (2006) The topology of hydrogen bonding in minerals of the brandtite, collinsite and fairfieldite groups. *The Canadian Mineralogist*, **44**, 1181–1196.

Hess, H., Keller, P. and Riffel, H. (1988) The crystal structure of chenite, $Pb_4Cu(OH)_6(SO_4)_2$. *Neues Jahrbuch für Mineralogie – Monatshefte*, **1988**, 259–264.

Hesse, K.-F. and Stuempel, G. (1986) Crystal structure of harstigite, $MnCa_6Be_4(SiO_4)_2(Si_2O_7)_2(OH)_2$. *Zeitschrift für Kristallographie*, **177**, 143–148.

Hill, R.J. (1985) Refinement of the structure of orthorhombic PbO (massicot) by Rietveld analysis of neutron powder diffraction data. *Acta Crystallographica*, **C41**, 1281–1283.

Hoyos, M.A., Calderon, T., Vergara, I. and Garcia-Sole, J. (1993) New structural and spectroscopic data for eosphorite. *Mineralogical Magazine*, **57**, 329–336.

Huminicki, D.M.C. and Hawthorne FC (2002*a*) The crystal chemistry of the phosphate minerals. Pp. 123–253 in: *Phosphates* (M.L. Kohn, J. Rakovan and J.M. Hughes, editors). Reviews in Mineralogy and Geochemistry, **48**. Mineralogical Society of America and the Geochemical Society, Washington DC.

Huminicki, D.M.C. and Hawthorne, F.C. (2002*b*) Hydrogen bonding in the crystal structure of seamanite. *The Canadian Mineralogist*, **40**, 923–928.

Ijdo, D.J.W. (1993) $Pb_3U_{11}O_{36}$, a Rietveld refinement of neutron powder diffraction data. *Acta Crystallographica*, **C49**, 654–656.

Ingri, N. (1963): Equilibrium studies of polyanions containing B^{III}, Si^{IV}, Ge^{IV} and V^{V}. *Svensk Kemisk Tidskrift*, **75**, 3–34.

Jackson, J.M. and Burns, P.C. (2001) A re-evaluation of the structure of weeksite, a uranyl silicate framework mineral. *The Canadian Mineralogist*, **39**, 187–195.

Jahn, H.A. and Teller, E. (1937) Stability of polyatomic molecules in degenerate electronic states. *Proceedings of the Royal Society, Series A*, **161**, 220–235.

Jarosch, D. (1985) Kristallstruktur des Leonits; $K_2Mg(SO_4)_2(H_2O)_4$. *Zeitschrift für Kristallographie*, **173**, 75–79.

Kampf, A.R. (1977) Minyulite: its atomic arrangement. *American Mineralogist*, **62**, 256–262.

Kampf, A.R. (1992) Beryllophosphate chains in the structures of fransoletite, parafransoletite, and ehrleite and some general comments on beryllophosphate linkages. *American Mineralogist*, **77**, 848–856.

Kampf, A.R. and Moore, P.B. (1976) The crystal structure of bermanite, a hydrated manganese phosphate. *American Mineralogist*, **61**, 1241–1248.

Kapshukov, I.I., Volkov, Y.F., Moskvitsev, E.P., Lebedev, I.A. and Yakovlev, G.N. (1971) Crystalline-structure of uranyl tetranitrates. *Zhurnal Strukturnoi Khimii*, **12**, 94–98 [in Russian].

Keller, H.L. (1983) Eine neuartige Blei-Sauerstoff-Baugruppe: $Pb_8O_4^{8+}$. *Angewandte Chemie*, **95**, 318–319.

Khan, A.A. and Baur, W.H. (1972) Salt hydrates. VIII. The crystal structures of sodium ammonium orthochromate dihydrate and magnesium diammonium bis(hydrogen ortho phosphate) tetrahydrate and a discussion of the ammonium ion. *Acta Crystallographica*, **B28**, 683–693.

Klaska, K.H. and Jarchow, O. (1977) Die Bestimmung der Kristallstruktur von Trimerit $CaMn_2(BeSiO_4)_3$ und das Trimeritgesetz der Verzwillingung. *Zeitschrift für Kristallographie*, **145**, 46–65.

Kniep, R. and Mootz, D. (1973) Metavariscite - a redetermination of its crystal structure. *Acta Crystallographica*, **B29**, 2292–2294.

Kniep, R., Mootz, D. and Vegas, A. (1977) Variscite. *Acta Crystallographica*, **B33**, 263–265.

Kolitsch, U. and Giester, G. (2000) Elyite, $Pb_4Cu(SO_4)O_2(OH)_4{\cdot}H_2O$: Crystal structure and new data. *American Mineralogist*, **85**, 1816–1821.

Konnert, J.A., Clark, J.R. and Christ, C.L. (1970) Crystal structure of fabianite, $CaB_3O_5(OH)$, and comparison with the structure of its synthetic dimorph. *Zeitschrift für Kristallographie*, **132**, 241–254.

Kostov, I. and Breskovska, V. (1989) *Phosphate, Arsenate and Vanadate Minerals. Crystal Chemistry and Classification*. Kliment Ohridski University Press, Sofia, Bulgaria.

Krivovichev, S.V. (2004) Combinatorial topology of salts of inorganic oxoacids: zero-, one- and two-dimensional units with corner-sharing between coordination polyhedra. *Crystallography Reviews*, **10**, 185–232.

Krivovichev, S.V. (2008) *Structural Crystallography of Inorganic Oxysalts*. International Union of Crystallography Monographs on Crystallography, **22**, Oxford University Press, Oxford, UK.

Krivovichev, S.V. (2009) *Structural Mineralogy and Inorganic Crystal Chemistry*. St. Petersburg University Press, 398 pp.

Krivovichev, S.V. and Burns, P.C. (2000*a*) Crystal chemistry of uranyl molybdates. II. The crystal structure of iriginite. *The Canadian Mineralogist*, **38**, 847–851.

Krivovichev, S.V. and Burns, P.C. (2000*b*) Crystal chemistry of basic lead carbonates. II. Crystal structure of synthetic 'plumbonacrite'. *Mineralogical Magazine*, **64**, 1069–1075.

Krivovichev, S.V. and Burns, P.C. (2001*a*) Crystal chemistry of uranyl molybdates. III. New structural themes in $Na_6[(UO_2)_2O(MoO_4)_4]$, $Na_6[(UO_2)(MoO_4)_4]$ and $K_6[(UO_2)_2O(MoO_4)_4]$. *The Canadian Mineralogist*, **39**, 197–206.

Krivovichev, S.V. and Burns, P.C. (2001*b*) Crystal chemistry of lead oxide chlorides. I. Crystal structures of synthetic mendipite, $Pb_3O_2Cl_2$, and synthetic damaraite, $Pb_3O_2(OH)Cl$. *European Journal of Mineralogy*, **13**, 801–809.

Krivovichev, S.V. and Burns, P.C. (2002*a*) Crystal chemistry of uranyl molybdates. VI. New uranyl molybdate units in the structures of $Cs_4[(UO_2)_3O(MoO_4)_2(MoO_5)]$ and $Cs_6[(UO_2)(MoO_4)_4]$. *The Canadian Mineralogist*, **40**, 201–209.

Krivovichev, S.V. and Burns, P.C. (2002*b*) Crystal chemistry of rubidium uranyl molybdates: crystal structures of $Rb_6[(UO_2)(MoO_4)_4]$, $Rb_6[(UO_2)_2O(MoO_4)_4]$, $Rb_2[(UO_2)(MoO_4)_2]$, $Rb_2[(UO_2)_2(MoO_4)_3]$ and $Rb_2[(UO_2)_6(MoO_4)_7(H_2O)_2]$. *Journal of Solid State Chemistry*, **168**, 245–258.

Krivovichev, S.V. and Burns, P.C. (2003*a*) The first sodium uranyl chromate, $Na_4[(UO_2)(CrO_4)_3]$: synthesis and crystal structure determination. *Zeitschrift für Anorganische und Allgemeine Chemie*, **629**, 1965–1968.

Krivovichev, S.V. and Burns, P.C. (2003*b*) Geometrical isomerism in uranyl chromates. I. Crystal structures of $(UO_2)(CrO_4)(H_2O)_2$, $[(UO_2)(CrO_4)(H_2O)_2](H_2O)$ and $[(UO_2)(CrO_4)(H_2O)_2]_4(H_2O)_9$. *Zeitschrift für Kristallographie*, **218**, 568–574.

Krivovichev, S.V. and Burns, P.C. (2003*c*) Structural topology of potassium uranyl chromates: crystal structures of $K_8[(UO_2)(CrO_4)_4](NO_3)_2$, $K_5[(UO_2)(CrO_4)_3](NO_3)(H_2O)_3$, $K_4[(UO_2)_3(CrO_4)_5](H_2O)_8$ and $K_2[(UO_2)_2(CrO_4)_3(H_2O)_2](H_2O)_4$. *Zeitschrift für Kristallographie*, **218**, 725–752.

Krivovichev, S. and Burns, P.C. (2005) Crystal chemistry of uranyl molybdates. XI. Crystal structures of $Cs_2[(UO_2)(MoO_4)_2]$ and $Cs_2[(UO_2)(MoO_4)_2](H_2O)$. *The Canadian Mineralogist*, **43**, 713–720.

Krivovichev, S.V. and Burns, P.C. (2006) The crystal structure of $Pb_8O_5(OH)_2Cl_4$, a synthetic analogue of

blixite? *The Canadian Mineralogist*, **44**, 515–522.

Krivovichev, S.V. and Filatov, S.K. (1999*a*) Structural principles for minerals and inorganic compounds containing anion-centered tetrahedra. *American Mineralogist*, **84**, 1099–1106.

Krivovichev, S.V. and Filatov, S.K. (1999*b*) Metal arrays in structural units based on anion-centered metal tetrahedra. *Acta Crystallographica*, **B55**, 664–676.

Krivovichev, S.V., Filatov, S.K. and Semenova, T.F. (1998*a*) Types of cationic complexes on the base of oxocentered tetrahedra [OM4] in crystal structures of inorganic compounds. *Russian Chemical Reviews*, **67**, 137–155.

Krivovichev, S.V., Filatov, S.K., Semenova, T.F. and Rozhdestvenskaya, I.V. (1998*b*) Crystal chemistry of inorganic compounds based on chains of oxocentered tetrahedra. I. Crystal structure of chloromenite, $Cu_9O_2(SeO_3)_4Cl_6$. *Zeitschrift für Kristallographie*, **213**, 645–649.

Krivovichev, S.V., Shuvalov, R.R., Semenova, T.F. and Filatov, S.K. (1999) Crystal chemistry of inorganic compounds based on chains of oxocentered tetrahedra III. Crystal structure of georgbokiite, $Cu_5O_2(SeO_3)_2Cl_2$. *Zeitschrift für Kristallographie*, **214**, 135–138.

Krivovichev, S.V., Finch, R.J. and Burns, P.C. (2001) Crystal chemistry of uranyl molybdates. V. Topologically distinct uranyl dimolybdate sheets in the structures of $Na_2[(UO_2)(MoO_4)_2]$ and $K_2[(UO_2)(MoO_4)_2](H_2O)$. *The Canadian Mineralogist*, **40**, 193–200.

Krivovichev, S.V., Filatov, S.K. and Burns, P.C. (2002) The cuprite-like framework of OCu_4 tetrahedra in the crystal structure of synthetic melanothallite, Cu_2OCl_2, and its negative thermal expansion. *The Canadian Mineralogist*, **40**, 1185–1190.

Krivovichev, S.V., Avdontseva, E.Yu. and Burns, P.C. (2004) Synthesis and crystal structure of $Pb_3O_2(SeO_3)$. *Zeitschrift für Anorganische und Allgemeine Chemie*, **630**, 558–562.

Krivovichev, S.V., Filatov, S.K. and Cherepansky, P.N. (2009*a*) The crystal structure of alumoklyuchevskite, $K_3Cu_3AlO_2(SO_4)_4$. *Geology of Ore Deposits* **51**, 656–661.

Krivovichev, S.V., Turner, R.W., Rumsey, M., Siidra, O.I. and Kirk, C.A. (2009*b*) The crystal structure and chemistry of mereheadite. *Mineralogical Magazine*, **73**, 103–117.

Krivovichev, S.V., Filatov, S.K. and Vergasova, L.P. (2013*a*) The crystal structure of ilinskite, $NaCu_5O_2(SeO_3)_2Cl_3$, and review of mixed-ligand CuO_mCl_n coordination geometries in minerals and inorganic compounds. *Mineralogy and Petrology*, **107**, 235–242.

Krivovichev, S.V., Mentré, O., Siidra, O.I., Colmont, M. and Filatov, S.K. (2013*b*) Anion-centered tetrahedra in inorganic compounds. *Chemical Reviews*, **113**, 6459–6535.

Krogh-Moe, J. (1962) The crystal structure of lithium diborate, $Li_20{\cdot}2B_2O_3$. *Acta Crystallographica*, **15**, 190–193.

Krot, N.N. and Grigoriev, M.S. (2004) Cation-cation interaction in crystalline actinide compounds. *Russian Chemical Reviews*, **73**, 89–100.

Lepore, G.O. and Welch, M.M. (2010) The crystal structure of parkinsonite, nominally $Pb_7MoO_9Cl_2$: a naturally occurring Aurivillius phase. *Mineralogical Magazine*, **74**, 269–275.

Li, Y. and Burns, P.C. (2000*a*) Investigations of crystal-chemical variability in lead uranyl oxide hydrates. I. Curite. *The Canadian Mineralogist*, **38**, 727–735.

Li, Y. and Burns, P.C. (2000*b*) Synthesis and crystal structure of a new Pb uranyl oxide hydrate with a framework structure that contains channels. *The Canadian Mineralogist*, **38**, 1433–1441.

Li, Y., Cahill, C.l. and Burns, P.C. (2001*a*) Synthesis, structural characterization, and topological rearrangement of a novel open framework U–O material: $(NH_4)_3(H_2O)_2\{[(UO_2)_{10}O_{10}(OH)][(UO_4)(H_2O)_2]\}$. *Chemistry of Materials*, **13**, 4026–4031.

Li, Y., Krivovichev, S.V. and Burns, P.C. (2001*b*) Crystal chemistry of lead oxide hydroxide nitrates: II. The crystal structure of $Pb_{13}O_8(OH)_6(NO_3)_4$. *Journal of Solid State Chemistry*, **158**, 74–77.

Liebau, F. (1985) *Structural Chemistry of Silicates*. Springer-Verlag, Berlin.

Lima-de-Faria, J. (1978) General chart for inorganic structural units and building units. *Garcia de Orta – Série de Geologia*, **2**, 69–76.

Lima-de-Faria, J. (1983) A proposal for a structural classification of minerals. *Garcia de Orta – Série de Geologia*, **6**, 1–14.

Lima-de-Faria, J. (1994) *Structural Mineralogy*. Kluwer, Dordrecht, The Netherlands.

Lima-de-Faria, J., Hellner, E., Liebau, F., Makovicky, E. and Parthé, E. (1990) Nomenclature of inorganic structure types. *Acta Crystallographica*, **A46**, 1–11.

Locock, A.J. and Burns, P.C. (2002*a*) The crystal structure of triuranyl diphosphate tetrahydrate. *Journal of Solid State Chemistry*, **163**, 275–280.

Locock, A.J. and Burns, P.C. (2002*b*) Structures and synthesis of framework triuranyl diarsenate hydrates. *Journal of Solid State Chemistry*, **176**, 18–26.

Locock, A.J., Burns, P.C. and Flynn, T.M. (2005) The role of water in the structures of synthetic hallimondite, $Pb_2[(UO_2)(AsO_4)_2](H_2O)n$ and synthetic parsonsite, $Pb_2[(UO_2)(PO_4)_2](H_2O)n$, $0 \leqslant n \leqslant 0.5$. *American Mineralogist*, **90**, 240–246.

Loopstra, B.O. and Cordfunke, E.H.P. (1966) On the structure of α-UO_3. *Recueil des Travaux Chimiques des Pays-Bas*, **85**, 135–142.

Lussier, A.J. and Hawthorne, F.C. (2011) Short-range constraints on chemical and structural variations in bavenite. *Mineralogical Magazine*, **75**, 213–239.

Lussier, A.J. and Hawthorne, F.C. (2013) *Structural isomerism in minerals based on octahedral [$^{[6]}M\emptyset_4$] chains*. Geological Association of Canada – Mineralogical Association of Canada Joint Annual Meeting, Program with Abstracts, Volume **36**, 133.

Magarill, S.A., Romanenko, G.V., Pervukhina, N.V., Borisov, S.V. and Palchik, N.A. (2000) Oxocentered polycationic complexes – An alternative approach to crystal-chemical investigation of the structure of natural and synthetic mercury oxosalts. *Journal of Structural Chemistry*, **41**, 96–105.

Matchatski, F. (1928) Zur Frage der Struktur und Konstitution der Feldspate. *Zentralblatt für Mineralogie Abhandlungen A*, **1928**, 97–104.

Mazzi, F., Ungaretti, L., Dal Negro, A., Petersen, O.V. and Rönsbo, J.G. (1979) The crystal structure of semenovite. *American Mineralogist*, **64**, 202–210.

Menchetti, S. and Sabelli, C. (1976) Crystal chemistry of the alunite series: Crystal structure refinement of alunite and synthetic jarosite. *Neues Jahrbuch für Mineralogie – Monatshefte*, **1976**, 406–417.

Menchetti, S., Sabelli, C. and Trosti-Ferroni, R. (1982) Probertite, $CaNa[B_5O_7(OH)_4]\cdot 3H_2O$: a refinement. *Acta Crystallographica*, **B38**, 3072–3075.

Mereiter, K. (1972) Die Kristallstruktur des Voltaits, $K_2Fe^{2+}_5Fe^{3+}_3Al(SO_4)_{12}(H_2O)_{18}$. *Tschermaks Mineralogische und Petrographische Mitteilungen*, **18**, 185–202.

Mereiter, K. (1974) Die Kristallstruktur von Rhomboklas $(H_5O_2)^+(Fe(SO_4)_2(H_2O)_2)$. *Tschermaks Mineralogische und Petrographische Mitteilungen*, **21**, 216–232.

Mereiter, K. (1979) Refinement of the crystal structure of langbeinite $K_2Mg_2(SO_4)_3$. *Neues Jahrbuch für Mineralogie – Monatshefte*, **1979**, 182–188.

Mereiter, K. (1982*a*) The crystal structure of liebigite, $Ca_2UO_2(CO_3)_3\cdot 11H_2O$. *Tschermaks Mineralogische und Petrographische Mitteilungen*, **30**, 277–288.

Mereiter, K. (1982*b*) The crystal structure of walpurgite, $(UO_2)Bi_4O_4(AsO_4)_2\cdot 2H_2O$. *Tschermaks Mineralogische und Petrographische Mitteilungen*, **30**, 129–139.

Mereiter, K. (1986) Crystal structure refinements of two francevillites, $(Ba,Pb)[(UO_2)_2V_2O_8]\cdot 5H_2O$. *Neues Jahrbuch für Mineralogie – Monatshefte*, **1986**, 552–560.

Mereiter, K., Niedermayr, G. and Walter, F. (1994) Uralolite, $Ca_2Be_4(PO_4)_3(OH)\cdot 3.5(H_2O)$ New data and crystal structure. *European Journal of Mineralogy*, **6**, 887–896.

Merlino, S. and Pasero, M. (1992) Crystal chemistry of beryllophosphates: The crystal structure of moraesite, $Be_2(PO_4)(OH)\cdot 4H_2O$. *Zeitschrift für Kristallographie*, **201**, 253–262.

Merlino, S. and Sartori, F. (1969) The crystal structure of lardellerite, $NH_4B_5O_7(OH)_2\cdot 2H_2O$. *Acta Crystallographica*, **B25**, 2264–2270.

Merlino, S. and Sartori, F. (1971) Ammonioborite: new borate polyion and its structure. *Science*, **171**, 377–379.

Metcalf, J. and Gronbaek, H.R. (1976) Crystal structure of sørensenite, $Na_4SnBe_2(Si_3O_9)_2(H_2O)_2$. *Acta Crystallographica*, **B32**, 2553–2556.

Mihalcea, I., Henry, N., Clavier, N., Dacheux, N. and Loiseau, T. (2011) Occurrence of an octanuclear motif of uranyl isophthalate with cation-cation interactions through edge-sharing connection mode. *Inorganic Chemistry*, **50**, 6243–6249.

Mikhailov, Yu.N., Gorbunova, Yu.E., Kokh, l.A., Kuznetsov, V.G., Grevtseva, T.G., Sokol, S.K. and Ellert, G.V. (1977) Synthesis and crystal structure of potassium trisulfatouranylate $K_4(UO_2(SO_4)_3)$. *Koordinatsionnaya Khimiya*, **3**, 508–513.

Mikhailov, Yu.N., Gorbunova, Yu.E., ShiShkina, O.V., Serezhkina, l.B. and Serezhkin, V.N. (2001) Crystal structure of $Cs_2((UO_2)(SeO_4)_2(H_2O))(H_2O)$. *Zhurnal Neorganicheskoi Khimii*, **46**, 1828–1832.

Miller, M.L., Finch, R.J., Burns, P.B. and Ewing, R.C (1996) Description and classification of uranium oxide hydrate sheet anion topologies. *Journal of Materials Research*, **11**, 3048–3056.

Moore, P.B. (1965) The crystal structure of laueite, $MnFe_2(OH)_2(PO_4)_2(H_2O)_6(H_2O)_2$. *American Mineralogist*, **50**, 1884–1892.

Moore, P.B. (1966) The crystal structure of metastrengite and its relationship to strengite and phosphophyllite. *American Mineralogist*, **51**, 168–176.

Moore, P.B. (1970) Crystal chemistry of the basic iron phosphates. *American Mineralogist*, **55**, 135–169.

Moore, P.B. (1973) Pegmatite phosphates: descriptive mineralogy and crystal chemistry. *Mineralogical Record*, **4**, 103–130.

Moore, P.B. (1975) Brianite, $Na_2CaMg[PO_4]_2$: a phosphate analog of merwinite, $Ca_2CaMg[SiO_4]_2$. *American Mineralogist*, **60**, 717–718.

Moore, P.B. and Araki, T. (1972*a*) Wightmanite, $Mg_5(O)(OH)_5[BO_3]\cdot nH_2O$, a natural drainpipe. *Nature Physical Science*, **239**, 25–26.

Moore, P.B. and Araki, T. (1972*b*) Johachidolite, $CaAl[B_3O_7]$, a borate with very dense atomic structure. *Nature Physical Science*, **240**, 63–65.

Moore, P.B. and Araki, T. (1974*a*) Pinakiolite, $Mg_2Mn^{3+}O_2[BO_3]$; warwickite, $Mg(Mg_{0.5}Ti_{0.5})O[BO_3]$; wightmanite, $Mg_5(O)(OH)_5[BO_3]\cdot nH_2O$: crystal chemistry of complex 3A wallpaper structures. *American Mineralogist*, **59**, 985–1004.

Moore, P.B. and Araki, T. (1974*b*) Jahnsite, $CaMnMg_2(H_2O)_8Fe_2(OH)_2(PO_4)_4$. A novel stereo-

isomer of ligands aound octahedral corner-chains. *American Mineralogist*, **59**, 964–973.

Moore, P.B. and Araki, T. (1975) Palermoite, $SrLi_2(Al_4(OH)_4(PO_4)$. Its atomic arrangement and relationship to carminite, $Pb_2(Fe_4(OH)_4(AsO_4)_4)$. *American Mineralogist*, **60**, 460–465.

Moore, P.B. and Araki, T. (1977*a*) Overite, segelerite, and jahnsite: a study in combinatorial polymorphism. *American Mineralogist*, **62**, 692–702.

Moore, P.B. and Araki, T. (1977*b*) Mitridatite, $Ca_6(H_2O)_6(Fe_9O_6(PO_4)_9)(H_2O)_3$. A noteworthy octahedral sheet structure. *Mineralogical Magazine*, **41**, 527–528.

Moore, P.B. and Araki, T. (1983) Surinamite, ca. $Mg_3Al_4Si_3BeO_{16}$: Its crystal structure and relation to sapphirine, ca. $Mg_{2.8}Al_{7.2}Si_{1.2}O_{16}$. *American Mineralogist*, **68**, 8804–8810.

Moore, P.B., Araki, T., Steele, I.M. and Swihart, G.H. (1983) Gainesite, sodium zirconium beryllophosphate: A new mineral and its crystal structure. *American Mineralogist*, **68**, 1022–1028.

Mueller, M.H., Dalley, N.K. and Simonsen, S.H. (1971) Neutron diffraction study of uranyl nitrate dihydrate. *Inorganic Chemistry*, **10**, 323–328.

Nadezhina, T.N., Pushcharovskii, D.Y., Rastsvetaeva, R.K., Voloshin, A.V. and Burshtein, I.F. (1989) Crystal structure of a new natural form of $Be(OH)_2$. *Doklady Akademii Nauk SSSR*, **305**, 95–98 [in Russian].

Niinistö, l., Toivonen, J. and Valkonen, J. (1978) Uranyl (VI) compounds. I. The crystal structure of ammonium uranyl sulfate dihydrate, $(NH4)_2UO_2(SO_4)_2{\cdot}2H_2O$. *Acta Chemica Scandinavica*, **A32**, 647–651.

Obbade, S., Dion, C., Bekaert, E., Yagoubi, S., Saadi, M. and Abraham, F. (2003) Synthesis and crystal structure of new uranyl tungstates $M_2(UO_2)(W_2O_8)$ (M = Na, K), $M_2(UO_2)_2(WO_5)O$ (M = K, Rb), and $Na_{10}(UO_2)_8(W_5O_{20})O_8$. *Journal of Solid State Chemistry*, **172**, 305–318.

Pauling, L. (1929) The principles determining the structures of complex ionic crystals. *Journal of the American Chemical Society*, **51**, 1010–1026.

Peacor, D.R., Rouse, R.C. and Ahn, J.-H. (1987) Crystal structure of tiptopite, a framework beryllophosphate isotypic with basic cancrinite. *American Mineralogist*, **72**, 816–820.

Pekov, I.V., Zelenski, M.E., Yapaskurt, V.O., Polekhovsky, Yu.S. and Murashko, M.N. (2013) Starovaite, $KCu_5O(VO_4)_3$, a new mineral from fumarole sublimates of the Tolbachik volcano, Kamchatka, Russia. *European Journal of Mineralogy*, **25**, 91–96.

Perrin, A. (1976) Structure cristalline du nitrate de dihydroxo diuranyle tétrahydraté. *Acta Crystallographica*, **B32**, 1658–1661.

Pertlik, F. and Zemann, J. (1988) The crystal structure of nabokoite, $Cu_7TeO_4(SO_4)_5{\cdot}KCl$: The first example of a $Te(IV)O_4$ pyramid with exactly tetragonal symmetry. *Mineralogy and Petrology*, **38**, 291–298.

Pilati, T., Demartin, F., Cariati, F., Bruni, S. and Gramaccioli C.M. (1993) Atomic thermal parameters and thermodynamic functions for chrysoberyl ($BeAl_2O_4$) from vibrational spectra and transfer of empirical force fields. *Acta Crystallographica*, **B49**, 216–222.

Piret, P., Deliens, M., Piret-Meunier, J. and Germain, G. (1983) La sayrite, $Pb_2[(UO_2)_5O_6(OH)_2]{\cdot}4H_2O$, nouveau minéral; propriétés et structure cristalline. *Bulletin de la Société Française Minéralogie et de Cristallographie* **106**, 299–304.

Ploetz, K.B. and Muller-Buschbaum, H. (1981) Zur Kristallchemie der Oxoplumbate (II). I. Zur Kenntnis von $Pb_9Al_8O_{21}$. *Zeitschrift für Anorganische und Allgemeine Chemie*, **480**, 149–152.

Pring, A., Gatehouse, B.M. and Birch, W.D. (1990) Francisite, $Cu_3Bi(SeO_3)_2O_2Cl$, a new mineral from Iron Monarch, South Australia: Description and crystal structure. *American Mineralogist*, **75**, 1421–1425.

Pushcharovsky, D.Yu., Lima-de-Faria, J. and Rastsvetaeva, R.K. (1998) Main structural subdivisions and structural formulas of sulfate minerals. *Zeitschrift für Kristallographie*, **213**, 141–150.

Rastsvetaeva, R.K. and Pushcharovskii, D.Yu. (1989) *Crystal chemistry of sulfates.* Itogi Nauki i Tekhniki, Seriya Kristallokhimiya, **Vol. 23**. VINITI, Moscow [in Russian].

Rastsvetaeva, R.K., Rekhlova, O.Yu., Andrianov, V.I. and Malinovskii, Yu.A. (1991) Crystal structure of hsianghualite. *Doklady Akademii Nauk SSSR*, **316**, 624–628 [in Russian].

Razmanova, P., Rumanova, I.M. and Belov, N.V. (1970) Crystal structure of kurnakovite $Mg_2B_6O_{11}{\cdot}15H_2O$ = $2Mg[B_3O_3(OH)_5]{\cdot}5H_2O$. *Soviet Physics Doklady*, **14**, 1139–1142.

Riebe, H.J. and Keller, H.L. (1989) $Pb_{13}O_{10}Br_6$, ein neuer Vertreter der Blei (II)oxidhalogenide. *Zeitschrift für Anorganische und Allgemeine Chemie*, **571**, 139–147.

Roberts, A.C., Cooper, M.A., Hawthorne, F.C., Criddle, A.J., Stanley, C.J., Key, C.L. and Jambor, J.L. (1999) Sidpietersite, $Pb_4^{2+}(S^{6+}O_3S^{2B})O_2(OH)_2$, a new thiosulfate mineral from Tsumeb, Namibia. *The Canadian Mineralogist*, **37**, 1269–1273.

Ross, V.F. and Edwards, J.O. (1967) The structural chemistry of the borates. Pp. 155–207 in *The Chemistry of Boron and its Compounds* (E.L. Muetterties, editor), John Wiley, New York.

Rouse, R.C. and Dunn, P.J. (1985) The structure of thorikosite, a naturally occurring member of the bismuth oxyhalide group. *Journal of Solid State*

Chemistry, **57**, 389–395.

Rouse, R.C., Peacor, D.R. and Metz, G.W. (1989) Sverigeite, a structure containing planar NaO_4 groups and chains of 3- and 4-membered beryllosilicate rings. *American Mineralogist*, **74**, 1343–1350.

Rouse, R.C., Peacor, D.R., Dunn, P.J., Su, S.-C., Chi, P.H. and Yeates, H. (1994) Samfowlerite, a new CaMnZn beryllosilicate mineral from Franklin, New Jersey: Its characterization and crystal structure. *The Canadian Mineralogist*, **32**, 43–53.

Saadi, M., Dion, C. and Abraham, F. (2000) Synthesis and crystal structure of the pentahydrated uranyl orthovanadate $(UO_2)_3(VO_4)_2{\cdot}5H_2O$, precursor for the new $(UO_2)_3(VO_4)_2$ uranyl-vanadate. *Journal of Solid State Chemistry*, **150**, 72–80.

Sabelli, C. and Ferroni, T. (1978) The crystal structure of aluminite. *Acta Crystallographica*, **B34**, 2407–2412.

Sabelli, C. and Trosti-Ferroni, T. (1985) A structural classification of sulfate minerals. *Periodico di Mineralogia*, **54**, 1–46.

Sahl, K. (1975) Zur Kristallstruktur von $4PbO{\cdot}PbSO_4$. *Zeitschrift für Kristallographie*, **132**, 99–117.

Sandomirskii, P.A. and Belov N.V. (1984) *Crystal Chemistry of Mixed Anionic Radicals*. Nauka, Moscow. [in Russian].

Schindler, M. and Hawthorne, F.C. (2001*a*) A bond-valence approach to the structure, chemistry and paragenesis of hydroxy-hydrated oxysalt minerals: I. Theory. *The Canadian Mineralogist*, **39**, 1225–1242.

Schindler, M. and Hawthorne, F.C. (2001*b*) A bond-valence approach to the structure, chemistry and paragenesis of hydroxy-hydrated oxysalt minerals: II. Crystal structure and chemical composition of borate minerals. *The Canadian Mineralogist*, **39**, 1243–1256.

Schindler, M. and Hawthorne, F.C. (2001*c*) A bond-valence approach to the structure, chemistry and paragenesis of hydroxy-hydrated oxysalt minerals: III. Paragenesis of borate minerals. *The Canadian Mineralogist*, **39**, 1257–1274.

Schindler, M. and Hawthorne, F.C. (2004) A bond-valence approach to the uranyl-oxide hydroxy-hydrate minerals: Chemical composition and occurrence. *The Canadian Mineralogist*, **42**, 1601–1627.

Schindler, M. and Hawthorne, F.C. (2008) The stereochemistry and chemical composition of interstitial complexes in uranyl-oxysalt minerals. *The Canadian Mineralogist*, **46**, 467–501.

Schindler, M., Hawthorne, F.C. and Baur, W.H. (2000) A crystal-chemical approach to the composition and occurrence of vanadium minerals. *The Canadian Mineralogist*, **38**, 1443–1456.

Schindler, M., Mutter, A., Hawthorne, F.C. and Putnis, A. (2004*a*) Prediction of crystal morphology of complex uranyl-sheet minerals. I. Theory. *The Canadian Mineralogist*, **42**, 1629–1649.

Schindler, M., Mutter, A., Hawthorne, F.C. and Putnis, A. (2004*b*) Prediction of crystal morphology of complex uranyl-sheet minerals. II. Observation. *The Canadian Mineralogist*, **42**, 1651–1666.

Schindler, M., Huminicki, D.M.C. and Hawthorne, F.C. (2006*a*) Sulfate minerals: I. Bond topology and chemical composition. *The Canadian Mineralogist*, **44**, 1403–1429.

Schindler, M., Mandaliev, P., Hawthorne, F.C. and Putnis, A. (2006*b*) Dissolution of uranyl-oxide-hydroxy-hydrate minerals: I. Curite. *The Canadian Mineralogist*, **44**, 415–431.

Schindler, M., Hawthorne, F.C., Burns, P.C. and Maurice, P.A. (2006*c*) Dissolution of uranyl-oxide-hydroxy-hydrate minerals: II. Becquerelite. *The Canadian Mineralogist*, **44**, 1207–1225.

Schindler, M., Hawthorne, F.C., Halden, N.M., Burns, P.C. and Maurice, P.A. (2007*a*) Dissolution of uranyl-oxide-hydroxy-hydrate minerals: III. Billietite. *The Canadian Mineralogist*, **45**, 945–962.

Schindler, M., Hawthorne, F.C., Burns, P.C. and Maurice, P.A. (2007*b*) Dissolution of uranyl-oxide-hydroxy-hydrate minerals: IV. Fourmarierite and synthetic $Pb_2(H_2O)[(UO_2)_{10}UO_{12}(OH)_6(H_2O)_2]$. *The Canadian Mineralogist*, **45**, 963–981.

Schindler, M., Freund, M., Hawthorne, F.C., Burns, P.C. and Maurice, P.A. (2009) Dissolution of uranophane: an AFM, XPS, SEM and ICP study. *Geochimica et Cosmochimica Acta*, **73**, 2510–2533.

Schindler, M., Hawthorne, F.C., Mandaliev, P., Burns, P.C. and Maurice, P.A. (2011) An integrated study of uranyl mineral dissolution processes: etch pit formation, effects of cations in solution, and secondary precipitation. *Radiochimica Acta* **99**, 79–94.

Scordari, F. (1977) The crystal structure of ferrinatrite, $Na_3(H_2O)_3(Fe(SO_4)_3)$ and its relationship to Maus's salt, $(H_3O)_2K_2(K_{0.5}(H_2O)_{0.5})_6(Fe_3O(H_2O)_3(SO_4)_6)(OH)_2$. *Mineralogical Magazine*, **41**, 375–383.

Scordari, F. (1981*a*) Fibroferrite: a mineral with a $(Fe(OH)(H_2O)_2(SO_4))$ spiral chain and its relationship to $Fe(OH)(SO_4)$, butlerite and parabutlerite. *Tschermaks Mineralogische und Petrographische Mitteilungen*, **28**, 17–29.

Scordari, F. (1981*b*) Sideronatrite: a mineral with a $(Fe_2(SO_4)_4(OH)_2)$ guildite type chain? *Tschermaks Mineralogische und Petrographische Mitteilungen*, **28**, 315–319.

Scordari, F. and Stasi, F. (1990) The crystal structure of euchlorine, $NaKCu_3O(SO_4)_3$. *Neues Jahrbuch für Mineralogie – Monatshefte*, **1990**, 241–253.

Scordari, F., Stasi, F., Schingaro, E. and Comunale, G. (1994) Analysis of the $(Na_{1/3}(H_2O)_{2/3})_{12}$

($NaFe_3^{3+}O(SO_4)_6(H_2O)_3$) compound: Crystal structure, solid-state transformation and its relationship to some analogues. *Zeitschrift für Kristallographie*, **209**, 43–48.

Selway, J.B., Cooper, M.A. and Hawthorne, F.C. (1997) Refinement of the crystal structure of burangaite. *The Canadian Mineralogist*, **35**, 1515–1522.

Semenova, T.F., Rozhdestvenskaya, I.V., Filatov, S.K. and Vergasova, L.P. (1989) Crystal structure of the new mineral ponomarevite, $K_4Cu_4OCl_{10}$. *Doklady Akademii Nauk SSSR*, **304**, 427–430.

Shannon, R.D. and Calvo, C. (1973) Crystal structure of $Cu_5V_2O_{10}$. *Acta Crystallographica*, **B29**, 1338–1345.

Shashkin, D.P., Lur'e, E.A. and Belov, N.V. (1974) Crystal-structure of $Na_2[(UO_2)SiO_4]$. *Kristallografiya*, **19**, 958–963 [in Russian].

Shuvalov, R.R. and Burns, P.C. (2003) A monoclinic polymorph of uranyl dinitrate trihydrate, $[(UO_2)(NO_3)_2(H_2O)_2]\cdot(H_2O)$. *Acta Crystallographica*, **C59**, i71–i73.

Shuvalov, R.R., Vergasova, L.P., Semenova, T.F., Filatov, S.K., Krivovichev, S.V., Siidra, O.I. and Rudashevsky, N.S. (2013) Prewittite, $KPb_{1.5}Cu_6Zn(SeO_3)_2O_2Cl_{10}$, a new mineral from Tolbachik fumaroles, Kamchatka peninsula, Russia: Description and crystal structure. *American Mineralogist*, **98**, 463–469.

Siidra, O.I., Krivovichev, S.V., Armbruster, T. and Depmeier, W. (2007) Crystal chemistry of natural and synthetic lead oxyhalides. Part I. Crystal structure of $Pb_{13}O_{10}Cl_6$. *Geology of Ore Deposits*, **49**, 827–834.

Siidra, O.I., Krivovichev, S.V. and Filatov, S.K. (2008*a*) Minerals and synthetic Pb(II) compounds with oxocentered tetrahedra: review and classification. *Zeitschrift für Kristallographie*, **223**, 114–125.

Siidra, O.I., Krivovichev, S.V., Turner, R.W. and Rumsey, M.S. (2008*b*) Chloroxiphite $Pb_3CuO_2(OH)_2Cl_2$: structure refinement and description in terms of oxocentred OPb_4 tetrahedra. *Mineralogical Magazine*, **72**, 793–798.

Siidra, O.I, Krivovichev, S.V., Turner, R.W., Rumsey, M.S. and Spratt, J. (2013) Crystal chemistry of layered Pb oxychloride minerals with PbO-related structures: Part I. Crystal structure of hereroite, $[Pb_{32}O_{20}(O,\square)](AsO_4)_2[(Si,As,V,Mo)O_4]_2Cl_{10}$. *American Mineralogist*, **98**, 248–255.

Simonov, M.A., Yamanova, N.A., Mzanskaya, E.Y., Egorov¡Tismenko, Y.K. and Belov, N.Y. (1976*a*) Crystal structure of a new natural calcium borate, hexahydroborite $CaB_20_4\cdot6H_2O = Ca[B(OH)]_2\cdot2H_20$. *Soviet Physics Doklady*, **21**, 314–316.

Simonov, M.A., Egorov-Tismenko, Yu.K. and Belov, N.Y. (1976*b*) Refined crystal structure of vimsite $Ca(B_2O_2(OH)_4)$. *Soviet Physics Crystallography*, **21**, 332–333.

Simonov, M.A., Egorov-Tismenko, Y.K. and Belov, N.V. (1977) Accurate crystal structure of uralborite $Ca_2[B_4O_4(OH)_8]$. *Soviet Physics Doklady*, **22**, 277–279.

Simonov, M.A., Kazanskaya, E.Y., Belokoneva, E.L. and Belov, N.Y. (1978) Hydrogen bonds in the crystal structure of nifontovite $Ca_2[B_2O_3(OH)_6]\cdot2H_2O$. *Soviet Physics Doklady*, **23**, 159–161.[1]

Stålhandske, C., Aurivillius, K. and Bertinsson, G.I. (1985) Structure of mercury (I, II) iodide oxide, Hg_2OI. *Acta Crystallographica*, **C41**, 167–168.

Starova, G.L., Filatov, S.K., Fundamenskii, V.S. and Vergasova, L.P. (1991) The crystal structure of fedotovite, $K_2Cu_3O(SO_4)_3$. *Mineralogical Magazine*, **55**, 613–616.

Starova, G.L., Krivovichev, S.V., Fundamenskii, V.S. and Filatov, S.K. (1997) The crystal structure of averievite, $Cu_5O_2(VO_4)_2$.nMX; comparison with related compounds. *Mineralogical Magazine*, **61**, 441–446.

Starova, G.L., Krivovichev, S.V. and Filatov, S.K. (1998) Crystal chemistry of inorganic compounds based on chains of oxocentered tetrahedra: II. Crystal structure of $Cu_4O_2[(As,V)O_4]Cl_1$. *Zeitschrift für Kristallographie*, **213**, 650–653.

Sterns, M., Parise, J.B. and Howard, C.J. (1986) Refinement of the structure of trilead (II) uranate (VI) from neutron powder diffraction data. *Acta Crystallographica*, **42**, 1275–1277.

Street, R.L.T. and Whitaker, A. (1973) The isostructurality of rosslerite and phosphorosslerite. *Zeitschrift für Kristallographie*, **137**, 246–255.

Süsse, P. (1967) Crystal structure of amarantite. *Naturwissenschaften*, **54**, 642–643.

Süsse, P. (1968) Die Kristallstruktur des Botryogens. *Acta Crystallographica*, **B24**, 760–767.

Süsse, P. (1973) Slavikit: Kristallstruktur und chemische Formel. *Neues Jahrbuch für Mineralogie – Monatshefte*, **1973**, 93–95.

Swihart, G.H., Gupta, P.K.S., Schlemper, E.O., Back, M.E. and Gaines, R.V. (1993) The crystal structure of moctezumite $[PbUO_2](TeO_3)_2$. *American Mineralogist*, **78**, 835–839.

Switzer, G., Foshag, W.F., Murata, K.J. and Fahey, J.J. (1953) Re-examination of mosesite. *American Mineralogist*, **38**, 1225–1234.

Sykora, R.E., Mcdaniel, S.M., Wells, D.M. and Albrecht-Schmitt, T.E. (2002) Mixed-metal uranium(VI) iodates: hydrothermal syntheses, structures, and reactivity of $Rb[UO_2(CrO_4)(IO_3)(H_2O)]$, $A_2[UO_2(CrO_4)(IO_3)_2]$ (A = K, Rb, Cs), and

[1] The formula given in the title of this paper is wrong, but is given correctly in the text.

$K_2[UO_2(MoO_4)(IO_3)_2]$. *Inorganic Chemistry*, **41**, 5126–5132.

Sykora, R.E. King, J.E., Illies, A.J. and Albrecht-Schmitt, T.E. (2004) Hydrothermal synthesis, structure, and catalytic properties of $UO_2Sb_2O_4$. *Journal of Solid State Chemistry*, **177**, 1717–1722.

Symanski, J.T. and Groat, L.A. (1997) The crystal structure of deanesmithite, $Hg_2^{1+}Hg_3^{2+}Cr^{6+}O_5S_2$. *The Canadian Mineralogist*, **35**, 765–772.

Tabachenko, V.V., Kovba, L.M. and Serezhkin, V.N. (1983) The crystal structure of molybdatouranylates of magnesium and zinc of composition $M(UO_2)_3(MoO_4)_4(H_2O)_8$ (M = Mg,Zn). *Koordinatsionnaya Khimiya*, **9**, 1568–1571 [in Russian].

Tachez, M., Theobald, F., Watson, K.J. and Mercier, R. (1979) Redetermination de la structure du sulfate de vanadyle pentahydrate $VOSO_4(H_2O)_5$. *Acta Crystallographica*, **B35**, 1545–1550.

Takéuchi, Y. (1952) The crystal structure of magnesium pyroborate. *Acta Crystallographica*, **5**, 574–581.

Takéuchi, Y. and Kudoh, Y. (1975) Szaibélyite, $Mg_2(OH)[B_2O_4(0H)]$: crystal structure, pseudosymmetry, and polymorphism. *American Mineralogist*, **60**, 273–279.

Tennyson, C. (1963) Eine Systematik der Borate auf Kristallchemischer Grundlage. *Fortschritte der Mineralogie*, **41**, 64–91.

Tsirel'son, V.G., Sokolova, Y.V. and Urusov, V.S. (1986) An X-ray diffraction study of the electron-density distribution and electrostatic potential in phenakite Be_2SiO_4. *Geokhimiya*, **8**, 1170–1180 [in Russian].

Tulsky, E.G. and Long, J.R. (2001) Dimensional reduction: A practical formalism for manipulating solid structures. *Chemistry of Materials*, **13**, 1149–1166.

Varaksina, T.V., Fundamenskii, V.S., Filatov, S.K. and Vergasova, L.P. (1990) The crystal structure of kamchatkite, a new naturally occurring oxychloride sulphate of potassium and copper. *Mineralogical Magazine*, **54**, 613–616.

Vasil'ev, V.I., Pervukhina, N.V., Romanenko, G.V., Magarill, S.A. and Borisov, S.V. 1999) New data on the mercury oxide-chloride mineral poyarkovite: The second find, and crystal-structure determination. *The Canadian Mineralogist*, **37**, 119–126.

Voronkov, A.A., Sizova, R.G., Ilyukhin, V.V. and Belov, N.V. (1973) Crystal chemistry of mixed anionic frameworks. I. Alkaline sorosilicates of zirconium and scandium. *Kristallografiya*, **18**, 112–121.

Voronkov, A.A., Ilyukhin, V.V. and Belov, N.V. (1974) Principles of the formation of mixed frameworks and their formula. *Doklady Akademii Nauk SSSR*, **219**, 600–603.

Voronkov, A.A., Ilyukhin, V.V. and Belov, N.V. (1975) Basic microblocks of mixed frameworks. *Koordinatsionnaya Khimiya*, **1(2)**, 244–247.

Wan, C. and Ghose, S. (1977) Hungchaoite, $Mg(H_2O)_5B_4O_5(OH)_4{\cdot}2H_2O$: a hydrogen-bonded molecular complex. *American Mineralogist*, **62**, 1135–1143.

Wan, C., Ghose, S. and Rossman, G.R. (1978) Guildite, a layer structure with a ferric hydroxy-sulphate chain and its optical absorption spectra. *American Mineralogist*, **63**, 478–483.

Wang, X., Huang, J., Liu, l. and Jacobson, A.J. (2002) The novel open-framework uranium silicates $Na_2(UO_2)(Si_4O_{10}){\cdot}2.1(H_2O)$ (USH–1) and $RbNa(UO_2)(Si_2O_6){\cdot}(H_2O)$ (USH–3). *Journal of Materials Chemistry*, **12**, 406–410.

Warner, J.K., Cheetham, A.K., Nord, A.G., von Dreele, R.B. and Yethiraj, M. (1992) Magnetic structure of iron(II) phosphate, sarcopside, $Fe_3(PO_4)_2$. *Journal of Materials Chemistry*, **2**, 191–196.

Weil, M. (2001) Schuetteite, $Hg_3(SO_4)O_2$, a re-investigation. *Acta Crystallographica*, **E57**, 98–100.

Weil, M. (2004) Preparation and Crystal Structure analyses of compounds in the systems $HgO/MXO_4/H_2O$ (M= Co, Zn, Cd; X= S, Se). *Zeitschrift für Anorganische und Allgemeine Chemie*, **630**, 921–927.

Weil, M. (2005) Crystal Structure of the mixed-valent basic mercury nitrate $Hg_2^{I}(NO_3)_2{\cdot}Hg^{II}(OH)(NO_3){\cdot}Hg^{II}(NO_3)_2{\cdot}4Hg^{II}O$ [= $Hg_8O_4(OH)(NO_3)_5$]. *Zeitschrift für Anorganische und Allgemeine Chemie*, **631**, 1346–1348.

Weil, M. and Glaum, R. (2001) Mercury phosphates with the triangular Hg_3^{4+} cluster: $(Hg_3)_3(PO_4)_4$ and $(Hg_3)_2(HgO_2)(PO_4)_2$. *Journal of Solid State Chemistry*, **1579**, 68–75.

Weil, M. and Stoeger, B. (2006) The mercury chromates $Hg_6Cr_2O_9$ and $Hg_6Cr_2O_{10}$ – Preparation and crystal structures, and thermal behaviour of $Hg_6Cr_2O_9$. *Journal of Solid State Chemistry*, **179**, 2479–2486.

Welch, M.D. (2004) Pb-Si ordering in sheet-oxychloride minerals: the super-structure of asisite, nominally $Pb_7SiO_8Cl_2$. *Mineralogical Magazine*, **68**, 247–254.

Welch, M.D., Cooper, M.A., Hawthorne, F.C. and Criddle, A.J. (2000) Symesite, $Pb_{10}(SO_4)O_7Cl_4(H_2O)$, a new PbO-related sheet mineral: description and crystal structure. *American Mineralogist*, **85**, 1526–1533.

Wildner, M. and Giester, G. (1988) Crystal structure refinements of synthetic chalcocyanite ($CuSO_4$) and zincosite ($ZnSO_4$). *Mineralogy and Petrology*, **39**, 201–209.

Williams, S.A., McLean, W.J. and Anthony, J.W. (1970) A study of phoenicochroite – its structure and properties. *American Mineralogist*, **55**, 784–792.

Wilson, R.J. (1979) *Introduction to Graph Theory*. Longman, London.

Wolf, R. and Hoppe, R. (1986) Neues über Oxouranate (VI): Na_4UO_5 und K_4UO_5. *Revue de Chimie Minérale*, **23**, 828–848.

Yakubovich, O.V., Matvienko, E.N., Voloshin, A.V. and Simonov, M.A. (1983) The crystal structure of hingganite-(Yb), $(Y_{0.51}Ln_{0.36}Ca_{0.13})Fe_{0.065}Be(SiO_4)(OH)$. *Kristallografiya*, **28**, 457–460 [in Russian].

Yu, H., Pan, S., Wu, H., Zhao, W., Zhang, F., Li, H. and Yang, Z. (2012) A new congruent-melting oxyborate, $Pb_4O(BO_3)_2$ with optimally aligned BO_3 triangles adopting layered-type arrangement. *Journal of Materials Chemistry*, **22**, 2105–2110.

Zahrobsky, R.F. and Baur, W.H. (1968) On the crystal chemistry of salt hydrates. V. The determination of the crystal structure of $CuSO_4{\cdot}3H_2O$ (bonattite). *Acta Crystallographica*, **B24**, 508–513.

Zelenski, M.E., Zubkova, N.V., Pekov, I.V., Polekhovsky, Yu.S. and Pushcharovsky, D.Yu. (2012) Cupromolybdite, $Cu_3O(MoO_4)_2$, a new fumarolic mineral from the Tolbachik volcano, Kamchatka Peninsula, Russia. *European Journal of Mineralogy*, **24**, 749–757.

Zoltai, T. (1960) Classification of silicates and other minerals with tetrahedral structures. *American Mineralogist*, **45**, 960–973.